ДОКЛАДЫ
АКАДЕМИИ НАУК СССР

SOVIET PHYSICS

"Doklady"

VOLUME 2 NUMBER 2

A Translation

of the

"Physics Section"

of the

Proceedings of the Academy of Sciences of the USSR

(RUSSIAN ORIGINAL VOL. 113, NOS. 1-6)

Published by the
AMERICAN INSTITUTE OF PHYSICS
INCORPORATED

SOVIET PHYSICS
"Doklady"

A translation of the "Physics Section" of the Proceedings of the Academy of Sciences of the USSR.

A publication of the
AMERICAN INSTITUTE OF PHYSICS

Governing Board

ALLEN V. ASTIN
WALTER S. BAIRD
JESSE W. BEAMS
HANS A. BETHE
RAYMOND T. BIRGE
RICHARD H. BOLT
FRANKLIN D. DEXTER
IRVINE C. GARDNER
SAMUEL A. GOUDSMIT
CHARLES KITTEL
HUGH S. KNOWLES
WINSTON E. KOCK
R. BRUCE LINDSAY
WILLIAM F. MEGGERS
WALTER C. MICHELS
R. RONALD PALMER
ROBERT F. PATON
JOSEPH B. PLATT
RALPH A. SAWYER
HENRY D. SMYTH
MARK W. ZEMANSKY

Officers and Staff

FREDERICK SEITZ
Chairman, Governing Board
ELMER HUTCHISSON
Director
HENRY A. BARTON
Associate Director
WALLACE WATERFALL
Executive Secretary
MARK W. ZEMANSKY
Treasurer
THEODORE VORBURGER
Advertising Manager
RUTH F. BRYANS
Publication Manager
KATHRYN SETZE
Assistant Treasurer
ALICE MASTROPIETRO
Circulation Manager
EUGENE H. KONE
Director of Public Relations

American Institute of Physics Advisory Board on Russian Translations

ROBERT T. BEYER, *Chairman*

FREEMAN DYSON, DWIGHT GRAY, MORTON HAMERMESH, VLADIMIR ROJANSKY

Advisory Editor, Soviet Physics—"Doklady": VLADIMIR ROJANSKY, Ramo-Wooldridge Corporation, Los Angeles, California

SOVIET PHYSICS—"Doklady" is a bi-monthly journal published by the American Institute of Physics for the purpose of making available in English reports of current Soviet research in physics as contained in the "Physics Section" of the Proceedings of the Academy of Sciences of the USSR. The Proceedings appears thirty-six times per year and the "Physics Sections" are accumulated and English translations of them are published in six issues per year.

Transliteration of the names of Russian authors follows the system employed by the Library of Congress.

This translating and publishing project was undertaken by the Institute in the conviction that dissemination of the results of research everywhere in the world is invaluable to the advancement of science. The National Science Foundation of the United States encouraged the project initially and is supporting it in large part by a grant. Translation and printing are being handled by Consultants Bureau, Inc.

The American Institute of Physics and its translators propose to translate faithfully all of the scientific material in the "Physics Section" of the Proceedings of the Academy of Sciences of the USSR appearing after January 1, 1956. The views expressed in the translated material, therefore, are intended to be those expressed by the original authors, and not those of the translators nor of the American Institute of Physics.

One volume is published annually. Volume 2 will consist of six issues and will contain all scientific material published in the "Physics Section" of the original Russian journal during the 1957 calendar year.

Subscription Prices:

Per year (6 issues)	
United States and Canada	$25.00
Elsewhere	27.50
Back Numbers	
Single copies	$ 5.00

Subscriptions should be addressed to the American Institute of Physics, 335 East 45th Street, New York 17, New York.

Copyright by American Institute of Physics 1958

SOVIET PHYSICS

"Doklady"

VOLUME 2, NUMBER 2 MARCH-APRIL, 1957

ENERGY AND ANGULAR DISTRIBUTIONS OF FAST PHOTOPROTONS FROM Ni AND Al

E. B. Bazhanov, Iu. M. Volkov, A. P. Komar, Academician of the Academy of Sciences, Ukrainian SSR, L. A. Kul'chitskii, and V. P. Chizhov

In experiments on the photodisintegration of nuclei by quanta of ~ 200-300 Mev [1-6] it has been established that there is a sharp asymmetry in the angular distribution of high energy protons with a peak almost in the direction of the photon beam and a sharp bend in the log-log energy distribution plot at proton energies which are close to half of the maximum bremsstrahlung energy. These effects and the cross sections of the processes can be explained qualitatively as the result of gamma absorption by "quasi-deuterons" in the nucleus [7]. Later experiments which observed n-p coincidences in photodisintegration [8-10] are also in qualitative agreement with the "quasi-deuteron" model.

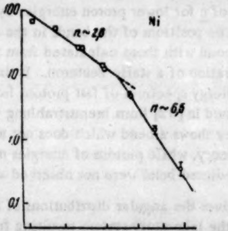

Fig. 1. Energy distribution of photoprotons from Ni. The vertical axis gives the number of protons in a 1 Mev interval per monitor unit, plotted in arbitrary units. Only the statistical errors are indicated.

From experiments thus far performed [11, 12] in which high-energy protons were studied from irradiation of nuclei with gamma rays of ~ 65 Mev maximum it is impossible to come to any definite conclusion regarding the mechanism of the (γ,p) reaction in this region of photon energies.

In the present work a scintillation telescope was used to study the angular and energy distributions of fast photoprotons from Ni and the energy distribution of photoprotons from Al irradiated by a bremsstrahlung spectrum with $E_{\gamma\,\max} = 85 \pm 5$ Mev. The telescope consisted of a thin front CsI(Tl) crystal of 0.026 cm thickness and a back NaI(Tl) crystal of 1.65 cm thickness mounted on Feu-19 M photomultipliers. The pulses of the front counter, which were proportional to dE/dx of a particle, and of the rear counter, which were proportional to E, were analyzed by a five-channel integral analyzer and a five-channel differential analyzer, respectively, with the channel outputs connected to triple coincidence circuits with resolving time $\tau \approx 1 \cdot 10^{-6}$ sec. The third inputs of the circuits received pulses from a double coincidence circuit of the front and rear counters with $\tau \approx 1 \cdot 10^{-7}$ sec, with a switching circuit permitting counting and feeding of these double coincidences to the triple coincidence circuit only while electrons struck the internal synchrotron target. The front counter was calibrated by deuterons from the cyclotron of the Leningrad Physico-Technical Institute; the back counter was calibrated by the light maximum from quanta of a Cs^{137} source. The linearity of the photomultipliers was checked by the ratio between the pulses from the Cs^{137} light maximum and the α-lines of ThC' with different potentials on the photomultipliers. The amplitude-resolving power of the counters for ThC' alpha particles was 10-12%. In order to exclude pulse counts from scattered electrons the bremsstrahlung pulses were extended to 1 msec. At the operating biases on the discriminators the number of coincidence counts per monitor unit remained unchanged within the limits of statistical error during a six-fold intensity change. This indicated that the telescopes were insensitive to pulses from scattered electrons. The energy windows of the five-channel differential analyzer for pulses from the back counter were arranged for each channel to count protons in a range $\Delta E/E \approx 20\%$. Corresponding biases were applied to the front counter. The proton energies were given both by the photomultiplier voltages and by copper absorbers. For a definite photomulitplier voltage 5 proton counts were taken, which were converted to unit energy integral per monitor unit. The next 5 counts were taken at a different photomultiplier voltage; the converted counts corresponding to identical average proton energies in these two measurements were in good agreement. Good agreement of the corresponding converted counts was also obtained for proton energies that were varied with the aid of absorbers, thus indicating accurate calibration and functioning of the telescope.

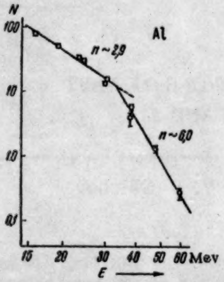

Fig. 2. Energy distribution of photoprotons from Al. The vertical axis gives the number of protons in a 1 Mev interval per monitor unit, in arbitrary units. Only the statistical errors are indicated.

The proton energy losses in the absorbers and front crystal were computed from the data of [13]. The calculations of proton energy losses in copper are in good agreement with calculations from the range-energy curves of protons in copper given in [14].

Figures 1 and 2 give the energy distributions of protons emerging at 90° to the beam (in the laboratory system) from Ni and Al, in the usual log-log plot. The vertical axes give the proton counts per unit energy interval (1 Mev) per monitor unit, in arbitrary relative units. It is seen that the proton energy distribution has the same form in both elements: $f(E_p) \sim E_p^{-n}$, where the value of $\underline{n}$ for the portion of the proton spectrum above 33 Mev exceeds the value of $\underline{n}$ for lower proton energies by a factor larger than 2. The positions of the bends in the energy spectrum correspond with those calculated from the theory of photodisintegration of a static deuteron. It should be noted that the energy spectrum of fast protons from Al which was obtained in [12] from bremsstrahlung with $E_{\gamma\,max} \approx 65$ Mev shows a bend which does not agree well with this theory, while protons of energies near the theoretically predicted bend were not observed at all.

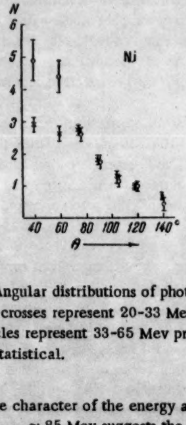

Fig. 3. Angular distributions of photoprotons from Ni. The crosses represent 20-33 Mev protons; the open circles represent 33-65 Mev protons. The errors are statistical.

Figure 3 gives the angular distributions of fast protons from Ni in the laboratory system resulting from bremsstrahlung with $E_{\gamma\,max} = 85 \pm 5$ Mev, in the two proton ranges: 20-33 and 33-65 Mev. In the plot the points at 120° to the beam were set equal to each other. It is seen that the degree of asymmetry in the angular distribution rises with increased proton energy.

The character of the energy and angular distributions obtained for fast photoprotons produced by bremsstrahlung with $E_{\gamma\,max} \approx 85$ Mev suggests the correctness of the "quasi-deuteron" model in this range of photon energies.

LITERATURE CITED

[1] C. Levinthal and A. Silverman, Phys. Rev. 82, 822 (1951).

[2] D. Walker, Phys. Rev. 81, 634 (1951); 84, 149 (1951).

[3] I. C. Keck, Phys. Rev. 85, 410 (1952).

[4] I. Rosengren and I. M. Dudley, Phys. Rev. 89, 603 (1953).

[5] I. W. Weil and B. D. McDaniel, Phys. Rev. 90, 380 (1953).

[6] B. T. Feld, R.D. Godbole et al., Phys. Rev. 94, 1000 (1954).

[7] I. S. Levinger, Phys. Rev. 84, 43 (1951).

[8] M. Q. Barton and I. H. Smith, Phys. Rev. 95, 573 (1954).

[9] H. Myers, A. C. Odian, P. C. Stein, and A. Wattenberg, Phys. Rev. 95, 576 (1954).

[10] A. C. Odian, P. C. Stein, A. Wattenberg, and B. T. Feld, Phys. Rev. 102, 837 (1956).

[11] S. Johansson, Phys. Rev. 97, 434 (1955).

[12] M. M. Hoffman and A. G. Cameron, Phys. Rev. 92, 1184 (1953).

[13] J. Lindhard and M. Scharff, Kgl. Danske Widensk. Selsk. Mat. f. Medd. 27, 15 (1953).

[14] Experimental Nuclear Physics, Segre, Editor, Vol. II (Foreign Lit. Press, 1955) p. 182 (Russian translation).

Received November 23, 1956

Leningrad Physico-Technical Institute,
USSR Academy of Sciences

FERMION FIELDS AND SPINORS IN INFINITE-DIMENSIONAL SPACE

Iu. A. Gol'dfand

(Presented by Academician I. E. Tamm November 21, 1956)

The development of functional methods in quantum field theory has enabled us to reduce the problem of determining the propagation function of a system of interacting particles to that of determining the propagation function of a fermion moving in any field of bosons, followed by functional integration over this external field [1-3]. In practice however this procedure encounters very serious mathematical difficulties and thus far no real success has been achieved in this way. The present note considers a new aspect of the problem which reveals a somewhat unexpected relationship between the theory of fermion fields and the theory of spinors in infinite-dimensional space.

We shall refer specifically to quantum electrodynamics although all results can be extended directly to any variant of meson theory.

Let us write the operator of a quantized electron-positron field $\psi(x)$ in the interaction representation:

$$\psi(x) = \sum u_n(x) a_n, \tag{1}$$

where $u_n(x)$ is a complete orthonormal system of solutions of the Dirac equation and a_n, depending on the sign of the energy, are either electron-annihilation operators or positron-creation operators which satisfy the usual commutation rules:

$$[a_m, a_n]_+ = \delta_{mn}. \tag{2}$$

We introduce the quantities $\Gamma_{n\alpha}$ ($\alpha = 1, 2$):

$$\Gamma_{n1} = a_n + a_n^+, \quad \Gamma_{n2} = \frac{1}{i}(a_n - a_n^+). \tag{3}$$

Using (2) it is easy to establish the correctness of the commutation rules:

$$\Gamma_{m\alpha}\Gamma_{n\beta} + \Gamma_{n\beta}\Gamma_{m\alpha} = 2\delta_{mn}\delta_{\alpha\beta}. \tag{4}$$

For brevity we shall hereinafter sometimes designate complex subscripts such as $n\alpha$ by a single letter: A, B, etc.

The relations in (4) enable us to use the Γ_A to obtain a spinor representation of the group of rotations of infinite-dimensional Euclidean space E_∞, that is, the group of linear transformations of the variables $\underline{x}$ which leave invariant the quadratic form Σx_A^2. The operators of infinitely small rotations ("moments") in this representation are

$$M_{AB} = \frac{1}{4i}(\Gamma_A\Gamma_B - \Gamma_B\Gamma_A), \tag{5}$$

and the spinors are the state vectors of the field Ψ. This definition of the spinors is the direction extension to infinite-dimensional space of Cartan's definition of spinors in Euclidean space of $\underline{n}$ dimensions [4]. This relationship is especially clear in the concept of occupation numbers.

By using the operators of (5) we can represent any rotation S in the form

$$S = \exp\left\{ i \sum S_{AB} M_{AB} \right\}, \tag{6}$$

where S_{AB} is any antisymmetric real matrix.

Let us consider the relation between the vector representations of rotations of space E_∞. In order to determine the vector transformation corresponding to rotation S we note that Γ_A must be transformed like a vector of space E_∞, that is, the following relation must be satisfied:

$$S^{-1} \Gamma_A S = \sum V_{AB} \Gamma_B, \tag{7}$$

where V_{AB} is the matrix of an orthogonal transformation of space E_∞. Conversely, if the transformation V is given the corresponding transformation S is

$$S = \exp\left\{ \frac{i}{2} \sum (\ln V)_{AB} M_{AB} \right\}. \tag{8}$$

We shall show that the motion of an electron in an external electromagnetic field $A_\mu(x)$ can be described by a rotation of E_∞ of the form of (6). The general solution of the Schroedinger equation can be constructed if we know the operator $S(t, t_0)$ which satisfies

$$i \frac{\partial S(t, t_0)}{\partial t} = H(t) S(t, t_0) \tag{9}$$

and the initial condition

$$S(t_0, t_0) = I.$$

The Hamiltonian H(t) in our case is

$$H(t) = \frac{e}{2} \int [\bar{\psi}(x), \gamma_\mu \psi(x)] A_\mu(x) d^3x.$$

Using (1), (3), and (5) we transform H(t) to

$$H(t) = -\sum \operatorname{Im} \{ \varepsilon_{\alpha\beta} W_{mn}(t) \} M_{m\alpha, n\beta}, \tag{10}$$

where

$$W_{mn}(t) = \frac{e}{2} \int \bar{u}_m(x) \gamma_\mu u_n(x) A_\mu(x) d^3x,$$

with the matrix

$$\| \varepsilon_{\alpha\beta} \| = \begin{pmatrix} 1 & i \\ -i & 1 \end{pmatrix}.$$

It is seen from (10) that H(t) as a linear combination of operators (5) is the operator of an infinitesimal rotation of space E_∞. Therefore the operator $S(t, t_0)$ will be a finite rotation of the same space and can thus be represented in the form of (6).

The relations between the spinor and vector representations are found in the field theory in the form of relations between the interaction representation and the Heisenberg representation. This can be seen from the familiar equation

$$\psi_H(x) = S^{-1}(t, t_0)\,\psi(x)\,S(t, t_0)$$

where $\psi_H(x)$ is a field operator in the Heisenberg representation. $\psi(x)$ is a linear combination of the Γ_A, which in view of (7) can be subjected to the linear transformation V. The Relation (8) shows how by solving the Heisenberg equations of motion for $\psi_H(x)$ we can construct the operator $S(t, t_0)$.

The relation established between motion of an electron in an external field $A_\mu(x)$ and rotations of space E_∞ enables us to indicate a new procedure for solving the general problems of quantum field theory. Instead of determining the propagation function of an electron moving in any external field $A_\mu(x)$, that is, obtaining a general solution of the Dirac equation with any field, we can turn to the investigation of relatively simple things – orthogonal transformations of space E_∞. Of course there are difficulties in this procedure associated with the fact that not every rotation S can be obtained through (9) and (10). By varying the field $A_\mu(x)$ in these relations, using every possible method, we obtain only a certain class of such rotations. The problem of describing this class thus arises. One of the simplest conditions satisfied by the rotations S which are obtained in this way is the fact that they all commute with the charge operators Q. To be sure, this is only a necessary but far from sufficient condition.

In addition, we can pass from functional integration over the field $A_\mu(x)$ to integration over some subset of elements of the rotation group of space E_∞.

We note in conclusion that the considered relation of the theory of fermion fields and the theory of spinors in space E_∞ depends only on the commutation Relations (2) which are characteristic of Fermi statistics. Therefore our procedure can be extended without difficulty to any variation of the theory of fermion fields such as the theory of quasi-fields [5] and can also be applied to problems of statistical physics.

LITERATURE CITED

[1] E. S. Fradkin, Doklady Akad. Nauk SSSR 98, 1, 47 (1954).

[2] N. N. Bogoliubov, Doklady Akad. Nauk SSSR 99, 2, 225 (1954).

[3] S. F. Edwards and R. E. Peierls, Proc. Roy. Soc. A, 224, 24 (1954).

[4] E. Cartan, Theory of Spinors (Foreign Lit. Press, 1947) (Russian translation).

[5] Iu. A. Gol'dfand, J. Exptl.-Theoret. Phys. (USSR) 28, 2, 140 (1955).

Received November 16, 1956

P. N. Lebedev Physics Institute,
USSR Academy of Sciences

ON THE DIVISION OF THE CATHODE SPOT

I. G. Kesaev

(Presented by Academician L. A. Artsimovich November 15, 1956)

Detailed studies of the cathode spot of a low pressure mercury arc have shown that during its existence the spot is continually being divided. Under the ordinary conditions of irregular spot motion on the cathode the dividing process is to a large degree obscured and only the final result can be observed, which is the appearance of two or a larger number of emission centers moving at a considerable distance from each other when these points are sufficiently stable. A convenient and at the same time simple method of observing the division of a spot is the photographing of the spot trace during its orderly motion in a magnetic field tangent to the cathode. Such photographs have made it possible to establish certain laws for spot division and to associate these with the ability of the latter to exhibit directed motion in a magnetic field.

Figure 1 shows a group of photographs, enlarged 5×, of a cathode spot track in inhomogeneous magnetic field on a thin mercury film covering a copper plate. The field was generated by an electromagnet with parallel pole pieces placed below the plate and separated by a 1 cm gap. The equilibrium pressure of the mercury vapor in the discharge space corresponded to a temperature of 20-22°. In this experimental arrangement the spot tries to move along the axis of symmetry of the field in the region of maximum field strength, which under the conditions of Fig. 1 was about 520 oersteds. The individual photographs of the group differ in the current strength, which increases from the top to the bottom photograph. An examination of these and similar photographs leads to the following conclusions.

1. The branchings of the bright band in the photographs are always found to be turned in the direction of the spot motion, which is of the so-called "retrograde" type. They are the tracks of independent moving spots that were formed by splitting of the parent cathode spot.

2. After the division the emission centers are separated with the appearance of being pushed apart; some of them quickly disintegrate while others acquire the entire arc current.

3. As the current increases the character of the division becomes complicated by an increasing number of branchings which have a considerable lifetime and which themselves undergo division. As a result the number of simultaneously active spots increases with the current, with an average of 8 amperes per spot. Nevertheless, even with the minimum current which can give a stable arc spot division occurs, but may remain unobserved because of the rapid disintegration of the branches.

4. The branchings can be divided into the symmetrical and the unsymmetrical. In the first instance the two branches form equal angles with the axis of symmetry of the field; this corresponds to splitting of the spot into two approximately equal parts. In unsymmetrical splitting the smaller current is associated with the larger angle and usually with the shorter lifetime.

5. As the spots diverge the angle between the branches is reduced; in symmetric splitting sooner or later the branches become parallel at an equilibrium separation l_e.

6. To each given current and field there corresponds a completely definite l_e which increases as the current increases and as the field strength is reduced.

7. The initial angle of divergence of branches in a very weak field approaches π, that is, the spots are pushed apart in diametrically opposite directions. As the field strength increases the angle is reduced.

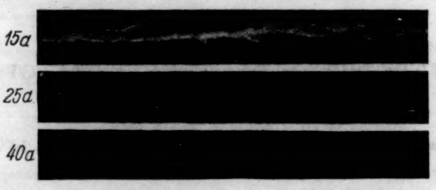

Fig. 1. Photographs of the trace of a cathode spot in a tangential magnetic field (520 oersteds).

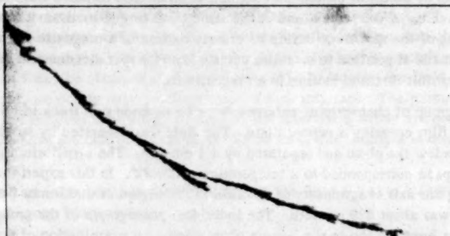

Fig. 2. Photograph of the trace of a cathode spot beginning its motion toward the axis of symmetry of the field, which is indicated by the dashed line.

8. The magnetic field exercises an appreciable stabilizing effect on the cathode spot. This is visible in Fig. 2 where during the spot motion toward the axis of symmetry the more stable branchings are those in the direction of field increase; this is the cause of the additional deflection of the entire ensemble in the direction of the axis of symmetry.

9. Spot division also occurs in the absence of an external magnetic field, which introduces into the process only the quantitative changes indicated in the preceding items and also causes directed motion of the entire ensemble of spots thus facilitating observation.

10. The intervals between successive acts of spot division are distributed close to the most probable interval of about 10^{-5} sec, which corresponds to a splitting frequency of about 10^5 per second.

11. The division of the cathode spot is one of the causes of the random spot motion on the cathode surface which is observed in the absence of an external magnetic field.

All of the observations enumerated above can be explained and arranged in an orderly system by applying to the individual parts of the cathode spot the principle of the field maximum which was discussed in an earlier article for the simple case of motion of a single spot in an external magnetic field [1]. According to this principle the direction of motion of the spot at each point of its trajectory must coincide with the direction of the sharpest increase, on the spot boundary, of the total magnetic field, which is a combination of the external field

H and the intrinsic field H_i of the current that intersects the cathode within the confines of the spot. Passing to the case of the motion of two or more spots in the field H_w of an electromagnet, H_i must be taken to mean the field of the independent current i associated with a particular spot while the external field with respect to this spot is the sum of the fields of the remaining currents H_k and of the vector field H_w. This problem is in general associated with the solution of a set of simultaneous equations; this is especially complicated by the uncontrollable redistribution of the current among the individual emission centers. However, a number of important conclusions can be drawn even without solving this complicated problem if we limit ourselves to a definite direction of motion for a given current distribution or a definite trajectory in the special case of symmetrical splitting.

The simplest case is that of two commensurable and sufficiently distant currents acted on only by their mutual field ($H_w = 0$). It is easily seen that by the field maximum principle the two currents must move apart along the straight line connecting them. The addition of an external electromagnetic field induces an additional displacement of each current but even in this case the mutual field of the currents continues to push them part (which is not to be associated with any force).

A consistent solution of the problem of spot division in an external field is impossible without a specific model of the spot. In the present short note it is sufficient to assume that a spot has the shape of a line moving in the direction of its normal and undergoing division in the transverse direction [2]. The application of the maximum field principle to the further motion of independent currents leads to the following conclusions.

The direction of motion of each current for a given arrangement depends on the ratio of the inhomogeneities $\left(\frac{\partial H}{\partial x}\right)$ and $\left(\frac{\partial H}{\partial y}\right)$ of the external field in the plane of the cathode, and of the quantities $\left(\frac{H_y}{H}\right)\left(\frac{0.2i}{r^2}\right)$ and $\left(\frac{H_x}{H}\right)\left(\frac{0.2i}{r^2}\right)$, which represent the asymmetry of addition of the fields H and $H_i = \frac{0.2i}{r}$ along the x and y axes, where r is the effective radius of interaction of an independent spot with the external magnetic field. This quantity, according to an estimate made in the earlier article [1] from the study of the trajectory of a single spot in an electromagnetic field, is between $3 \cdot 10^{-2}$ and $9 \cdot 10^{-2}$ cm for currents from 3 to 15 amperes.

The inhomogeneity of the external field itself forces the spot to move in the direction of increasing field strength, whereas the asymmetry of superposition of the fields causes the so-called "retrograde" motion as well as the mutual repulsion of the currents. Applying these ideas to the experimental conditions of Fig. 1 we can easily explain the observations enumerated in items 2, 4, 5, 6, and 7. An especially valuable possibility of checking the theory quantitatively is provided by the determination of the equilibrium distance l_e between the branches in symmetrical spot division. According to our interpretation l_e must be regarded as twice the distance x from the axis of symmetry of the field at which the repulsive effect of the mutual field $H_y = 0.2i/2x$ of the currents is compensated by the effect of the electromagnetic field inhomogeneity $\partial H_w/\partial x$ which forces the currents to move toward the axis of the symmetry (for sufficiently large x the inhomogeneity of the mutual field can be neglected). It thus follows that l_e can be determined from the equation

$$\frac{\partial H_w}{\partial x} - \frac{H_y}{H_w}\frac{0.2i}{r^2} = 0,$$

which for the field distribution H_w used in the experiments leads to the approximate formula

$$l_e = \frac{0.4}{H_w r}\, i.$$

By determining l_e according to the data obtained from the photographs of Fig. 1 and similar photographs we were able to estimate the values of the radius r, which were between 10^{-1} and $4 \cdot 10^{-1}$ cm. These values of r are quite close to those obtained in the previous article from the study of the trajectory of a single spot in a magnetic field. Thus the values of r obtained from experimental studies of spot motion and division are approximately the same.

The results given above show that the independent emission centers formed by spot division move apart under the influence of the magnetic fields of the associated currents. This interaction can only be increased at small distances; hence it can be concluded that the most important cause of cathode spot division at low pressures is the intrinsic magnetic field of the arc localized within the spot and causing repulsion of its individual parts. This repulsive action of the field is not associated with forces of interaction between the individual separate currents, but is based on improvement of the conditions for emission on the periphery of the cathode spot.

Our conclusion regarding the tendency of a cathode spot toward continual division or spontaneous disintegration in the magnetic field of the arc may at first seem to contradict the fact that a stable cathode spot exists. This apparent contradiction disappears if we remember a number of additional stabilizing factors. It is noteworthy that the repulsive action of the field produced by the asymmetrical addition of the external and intrinsic fields must diminish with reduced size of the detached portion of the spot. On the other hand considerable importance must be attached to the continuous current redistribution, as a result of which the decay of one of the spots leads to the recovery of the other and to the return of the lost fraction of the current. Under these conditions the instability of the small emission centers is equivalent to the existence of an insurmountable barrier for them around the spot which thus prevents the complete disintegration of the spot.

These phenomena give rise to the concept of parallel processes of continuous division and restoration of the cathode spot.

LITERATURE CITED

[1] I. G. Kesaev, Doklady Akad. Nauk SSSR 112, 4, 619 (1957).

[2] K. D. Froome, Proc. Phys. Soc. (B) 62, 805 (1949).

Received November 9, 1956

V. I. Lenina All-Union Institute of Electrical Engineering

TERNARY FISSION OF URANIUM BY FAST PARTICLES

N. A. Perfilov, V. P. Shamov, and O. V. Lozhkin

(Presented by Academician L. A. Artsimovich December 15, 1956)

1. Experimental Data. In examining plates impregnated with uranium and irradiated with 660-Mev protons a few cases of uranium fission were detected which were accompanied by the emission of a particle of charge $Z \geq 4$. Among these was a plane ternary fork whose photomicrograph is given in Fig. 1. The tracks of all three particles of the fork from their external appearance (grain density and the presence of δ-nuclei on two tracks) must belong to multicharged particles, two of these to the fission fragments of a heavy nucleus, while the third in the intensity of its blackening considerably exceeds alpha particle tracks.

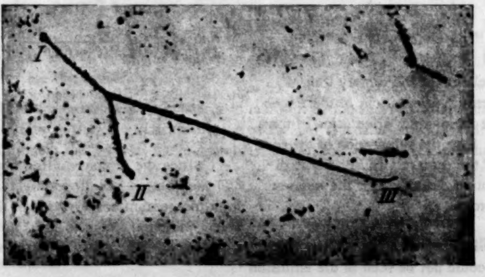

Fig. 1. Photomicrograph of uranium fission with the emission of a multicharged particle. I and II are heavy fragments; $Z_{I,II} = 41$ (range $l_I = l_{II} = 12\mu$); III is the light nucleus, $Z_{III} = 9.8 \pm 1$ (range $l_{III} = 42\mu$).

In the experiment we used the especially fine-grained P-9 emulsion with ~ 35 Mev sensitivity threshold for protons and with good differentiating capacity for particles of different nature.

The blackening along all three tracks was measured photometrically with a $5 \times 0.8\mu^2$ slit in the object plane. We measured the total blackening $P = \frac{I_{ph} - I_c}{I_{ph}}$, where I_{ph} is the output current of the photomultiplier when the slit is alongside the track and I_c is the current when the slit is on the track.

The measurements of total blackening along track III (from the end of its range) are given in Fig. 2. For comparison we also give the results of photometry of nitrogen ion tracks.

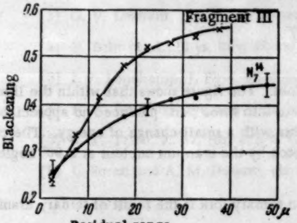

Fig. 2. Dependence of total blackening $P = \frac{I_{ph} - I_c}{I_{ph}}$ on range for fragment III and N_7^{14} ions.

From the slope of the curve P = f(R) we are able, as was shown by O. V. Lozhkin [1], to determine Z. For the particle producing track III we obtained the charge $Z_{III} = 9.8 \pm 1$. The average blackening of tracks I and II was 0.350 and 0.400 , respectively. In the same emulsion the average blackening for tracks of binary fission fragments and alpha particles was 0.380 and 0.220, respectively.

A comparison shows that tracks I and II were produced by multicharged ions of the type of fission fragments. Since the ranges of particles I and II are equal we shall assume these particles to be of the same kind. Assuming $Z_{III} = 10$ we obtain $Z_I = Z_{II} = 41$.

2. Calculation for the ternary fork. As already mentioned, the fork was coplanar and the trajectory of the incident proton was also in the plane of the fork. Using range-energy relations [2, 3] we estimated the kinetic energy and momenta of the two heavy fragments and of the third (and lighter) particle. The solid lines in Fig. 3 show the momentum scheme of the ternary fork. The direction of motion of the primary proton coincides with the x axis in Fig. 3 and is given with an accuracy of 3-4° by the experimental conditions.

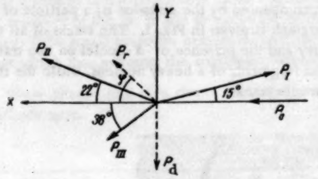

Fig. 3. Momentum scheme of the ternary fork. P_I and P_{II} are the momentum orientations of the fission fragments; P_{III} is the momentum orientation of the light fragment Ne^{20}_{10} ; P_r is the orientation of the resultant momentum of the ternary fork; P_d is the direction of the momentum deficit; P_0 is the momentum of the incident proton.

For the magnitude and direction of the resultant momentum P_r of the triple fork the scheme of Fig. 3 gives the following equations:

$$P_r = \sqrt{(\Sigma P_x)^2 + (\Sigma P_y)^2} = 1820\ \frac{\text{Mev}}{c},$$

$$\tan\varphi = \frac{\Sigma P_y}{\Sigma P_x} = \frac{1290}{1280} \approx 1, \quad \varphi = 45°.$$

Since the fission resulted from a collision with a 660-Mev proton and the momentum is P_0 = 1290 Mev/c, from momentum conservation of the entire system (incident proton and ternary fork) we can obtain the magnitude and direction of the momentum deficit. We subsequently assumed that the lost momentum belonged to a proton whose track could not be seen in the emulsion *:

$$\mathbf{P}_d = \mathbf{P}_0 - \mathbf{P}_r,$$

$$P_d = \sqrt{P_0^2 - 2P_0P_r \cos 45° \cdot + P_r^2} = 1300\ \frac{\text{Mev}}{c},$$

$$\theta = \arcsin \frac{P_r \sin 45°}{P_d} = 270°.$$

The orientations of P_r and P_d are shown in Fig. 3 by dashed lines. The figure shows that within the limits of possible experimental errors the collision which divided the nucleus into three parts produced no appreciable change of the initial momentum with regard to its magnitude and thus with a small change of energy. The change of initial energy corresponds to elastic scattering of the incident proton by the uranium nucleus at a 90° angle (ΔE ~ 8 Mev).

On the basis of this analysis it can be concluded that the given ternary fork is the result of ternary uranium fission with small initial excitation energy.

---

* It can also be assumed that the lost or deficit momentum is carried off not by one but by a few particles of the same mass or by one heavier particle, but such a view leads to a number of inconsistencies when applied to the fork under consideration.

Here, however, we encounter a new difficulty. In the collision of a 660-Mev proton with a uranium nucleus the probability of elastic or near-elastic scattering at 90° is very small. It is also known that at small excitation energies (in the interaction of slow neutrons with uranium nuclei) ternary fission is a very improbable process [4-6]. In consideration of the above we assumed that in the present case of collision between a proton of such high energy and a uranium nucleus ternary fission could occur with appreciable probability only through a noncentral impact with the transfer of considerable angular momentum.

We attempt below to give a qualitative picture of the possible mechanism of ternary fission by fast particles. Because of the existence of a large quadrupole moment the uranium nucleus must be considerably elongated. The elongation of the uranium nucleus enables us to assume both a central and (with considerably greater probability) a noncentral impact. For the more probable process it must be assumed that the primary interaction of the fast proton and the uranium nucleus was a noncentral elastic collision. As a result of this impact the uranium nucleus had to receive, in addition to kinetic energy, a certain angular momentum $M_n = P_r \Delta r$. From conservation of angular momentum the uranium nucleus had to scatter the acquired angular momentum M_n. When the acquired angular momentum is large (in a strong noncentral collision) the nucleus cannot get rid of it by noncentral emission of light particles (especially if we consider that the initial excitation energy is either zero for elastic impact or insignificant, for a practically elastic impact).

In our case it is reasonable to assume that the removal of the angular momentum is brought about by the noncentral emission of a light Ne_{10}^{20} fragment.

Let us consider the energy side of the process. If the nucleus was able to emit a light Ne_{10}^{20} fragment with momentum $P_{\mathrm{Ne}_{10}^{20}} = 1800$ Mev/c its initial excitation energy had to be $E_0 \geq 100$ Mev. By what processes can a uranium nucleus liberate this amount of energy ?

The energy liberated through the mass defect in uranium fission into two fragments of unequal masses ($A_1 = 20$; $A_2 = 218$) is one-half of the indicated value of E_0. But if it is assumed that simultaneously with the emission of a light fragment the residual nucleus divides in half, the energy liberated through this ternary fission is 240 Mev. The experimentally observed energy of two heavy fragments and a light fragment (in the center of mass system) is 210 Mev, which corresponds to the energy liberated in ternary fission.

Thus it is possible to explain the observed triple fork by assuming a very specific process of nuclear reaction. For a more or less rigorous explanation of such processes it is necessary to study all cases of uranium fission with multicharged particles.

The authors are greatly indebted to I. M. Shmushkevich for participating in discussions of the results.

LITERATURE CITED

[1] O. V. Lozhkin, J. Exptl.-Theoret. Phys. (USSR) 32, 1 (1957).

[2] N. Bohr et al., Phys. Rev. 58, 839 (1940).

[3] J. P. Lonchamp, J. Phys. Radium 14, 89 (1953).

[4] N. A. Perfilov, Doctoral Dissertation, Radium Inst., Acad. Sci. USSR, 1947.

[5] S. T. Tsien, Z. W. Ho, and R. Chastel, J. Phys. Radium 8, 165 (1947).

[6] L. Rosen and A. M. Hudson, Phys. Rev. 78, 5, 533 (1950).

Received October 4, 1956

Radium Institute, USSR Academy of Sciences

THE OBSERVATION OF FERROMAGNETIC DOMAIN STRUCTURE BY MEANS OF PHOTOELECTRONS

G. V. Spivak, T. N. Dombrovskaia, and N. N. Sedov

(Presented by Academician M. A. Leontovich November 3, 1956)

This article describes an electron-optical method of depicting the domain structure of a ferromagnet by means of photoelectrons focused by magnetic optics. The advantage of this method is that it enables us to obtain an excellent image, with high contrast, of the magnetic microfields on the surfaces of ferromagnetic polycrystals and single crystals. This work continues previous experiments conducted in our laboratory [1-4] on the electron-optical visualization of magnetic microfields.

The fundamental idea of our earlier work [1-4] and of the present article was that domain fields can be seen directly if we cause an interaction between an electron beam and a cathode electron lens, with the magnetic fields to be studied inserted into the plane of the cathode as magnetic "microlenses." These "microlenses" produce chromatic and spherical aberration of the immersion optics, as a result of which the "microlenses" can be visualized on a fluorescent screen.

Thus by our method the "defects" of immersion optics which result from magnetic microfields on the cathode are used to depict them. We mention two characteristics of our method: 1) it is possible to depict all of the domains and their boundaries appearing on a plane surface; 2) it is possible to control the contrast and resolution of the electron-optical pattern by varying the parameters of the immersion optics and the properties of the electron beam.

We have previously compared our method with electron-optical methods of visualizing magnetic microfields which were proposed by other authors [1, 2, 3].

The requirements that must be met by an electron-optical system based on the use of a cathode lens are as follows: 1) high sensitivity to the magnetic fields which are to be visualized, thus insuring the required contrast; and 2) high resolution of the magnetic microstructure. Both of these requirements are better satisfied by the method which employs photoelectrons than by two other methods which we have previously proposed [2, 3].

A simple device was used for the qualitative electron-optical visualization of domain structure and other microfields of cobalt; this was a glass model of a photoelectron emission microscope with continuous evacuation (Fig. 1). The photoelectron source in the microscope was an antimony-cesium cathode backed by the ferromagnetic object under investigation. The locally distributed magnetic field of the backing penetrates the semiconducting photocathode and forms a picture of the magnetic field on the fluorescent screen. The focusing system is a short-focus iron-encased magnetic lens. The source of illumination is an electric incandescent lamp. When the sensitive coating of the ferromagnet is sufficiently thin the image is highly modulated by the local microfields of the domains. A field of 6-8 kv was applied to the cathode-anode system (cathode-sample). The magnetic field of the lens used both for focusing and magnetization of the sample was 400-600 oersteds. The vacuum in which the image was formed was of the order of $5 \cdot 10^{-7}$ mm Hg; it was produced by a rotary fore-vacuum pump and an oil vapor diffusion pump (TsVL-100). For freezing of the oil vapor liquid nitrogen was used.

With this apparatus we obtained images of domains on the hexagonal surface of a cobalt single crystal as well as on the polished surface of polycrystalline cobalt. Figure 2a is a picture of the domain structure. The magnetic field of the focusing and magnetizing lens was applied perpendicular to the hexagonal surface of the cobalt single crystal (60 ×). Figure 2b is a photoelectronic image of the same portion of the cobalt single crystal with the direction of the magnetic field reversed (60 ×). As is shown by an examination of these two photographs (see the parts indicated by arrows), when the direction of the magnetizing field is reversed the contrast of the electron-optical image is also reversed. Figure 2c is a picture of domains of figures of the same hexagonal surface of the cobalt single crystal, obtained by the powder figure method [5].

Figure 3a is a photograph of local magnetic microfields obtained in the photoelectronic microscope on the polished surface of polycrystalline cobalt. The photograph obtained by using a ferromagnetic powder on polycrystalline cobalt is shown in Fig. 3b.

We thus see that photoelectron emission can be used to obtain electron-optical pictures of local magnetic microfields distributed in the plane of an object.

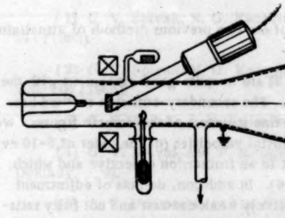

Fig. 1. Design of the photoelectron microscope.

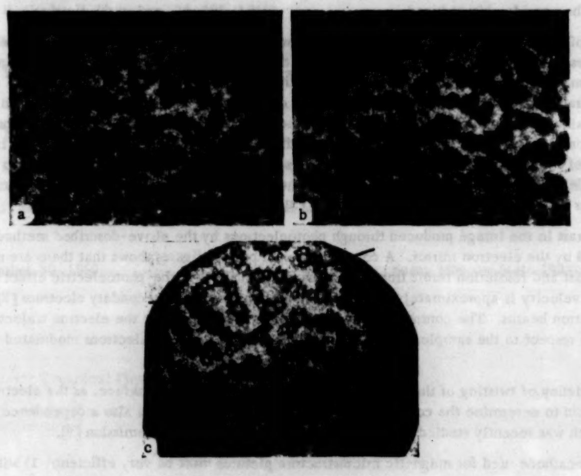

Fig. 2. 60 ×.

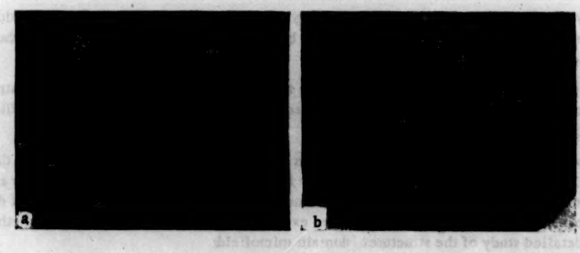

Fig. 3. 60 ×.

which are comparable in quality with powder figures and which are also considerably better than those which we obtained previously [2, 3].

Let us compare with the present method the status and prospects of our two previous methods of visualizing magnetic microfields [2, 3].

The images obtained by using a secondary-emission microscope [2] are in quite good agreement with the powder method but are inferior to the latter in the resolution of details. The secondary-emission method has thus far not produced sufficiently good electron-optical contrast for the fine structure of the domain figures. We believe that the cause for this is the use of secondary electrons of high initial velocities (of the order of 5-10 ev), which results in the geometric and chromatic aberration that is inherent in an immersion objective and which becomes more pronounced as the initial electron velocity is increased [6]. In addition, defects of adjustment lead to first order aberration. These circumstances determined the relatively weak contrast and not fully satisfactory resolution of the electron-optical image. An important characteristic of the secondary emission method is the fact that the surface is not lacking in sensitivity, quite large emission can be produced and the indicated aberration can be considerably reduced.

The use of an electron mirror [3] for the visualization of magnetic microfields immediately enabled us to obtain images with considerably better contrast than those produced by secondary electrons and with relatively high effective magnification (200 ×). The use of electrons which are stopped on the surface of the ferromagnetic sample considerably improved both the resolving power of the optical system and the contrast in the picture. But the picture obtained with an electron mirror possesses the characteristic that the reflection of the electrons takes place on a concave surface which does not coincide with the surface of the sample, so that the image is distorted. This distortion of the electron-optical image hinders the interpretation of the image and thus to a certain extent limits the possibilities of the mirror method. The mechanism of the formation of an electron image of magnetic inhomogeneities by an electron mirror is discussed in [3].

The contrast in the image produced through photoelectrons by the above-described method is not inferior to that obtained by the electron mirror. A comparison with powder figures shows that there are no distortions. The good contrast and resolution result from a number of factors: 1) in the photoelectric effect slow electrons are used whose velocity is approximately one order lower than that of the secondary electrons [2]; 2) there are no oblique electron beams. The contrast of the picture must depend both on the electron trajectories that are "external" with respect to the sample and on the work function of the photoelectrons modulated by the magnetic field [7].

The efficiency of twisting of the electron trajectories on the cathode surface, as the electrons enter the vacuum, is known to determine the contrast [2, 4]. Theoretically [8] there is also a dependence of the work function on H, which was recently studied at different temperatures and in cold emission [9].

The photocathode used for magnetic microstructure pictures must be very efficient: 1) with regard to electron emission to insure the required screen brightness; 2) in uniformity of emission and 3) of small thickness so that the magnetic field of the ferromagnetic backing will enter the vacuum for an appreciable distance.

Uniformity of emission is associated with the roughness of the cathode. As recent observations have shown [10], the roughness of an antimony-cesium cathode can be made quite small without affecting the uniformity required for depicting the magnetic microstructure.

Electron-optical methods of visualizing magnetic fields [1-4] give brighter and better contrasted images than the magneto-optical method which employs the Kerr effect, where visual observation is difficult [11] and the photographing requires a considerable exposure.

Considerable success has recently been attained in the study of ferromagnetic domains by the use of the powder method [12]. But it must be mentioned that the inertia of the powder particles and their size when viewed with an optical microscope impose a definite limit to further penetration into the microworld of domain structures by the use of the powder method. It is therefore expedient to develop electron-optical methods in addition for the required detailed study of the structure of domain microfields.

LITERATURE CITED

[1] G. V. Spivak, N. G. Kanavina, I. S. Sbitnikova, and I. N. Chernyshev, Doklady Akad. Nauk SSSR 92, 541 (1953).

[2] G. V. Spivak, N. G. Kanavina, I. S. Sbitnikova, and T. N. Dombrovskaia, Doklady Akad. Nauk SSSR 105, 706 (1955).

[3] G. V. Spivak, I. N. Prilezhaeva, and V. K. Azovtsev, Doklady Akad. Nauk SSSR 105, 965 (1955).

[4] G. V. Spivak and T. N. Dombrovskaia, Doklady Akad. Nauk SSSR 106, 39 (1956) [Soviet Physics – Doklady, p. 9].

[5] S. V. Vonsovskii and Ia. S.Shur, Ferromagnetism, 1948.

[6] Electron Microscopy, A. A. Lebedev, Editor, 1954, Ch. VI.

[7] A. B. Cardwell, Phys. Rev. 76, 125 (1949).

[8] S. V. Vonsovskii and A. V. Sokolov, Doklady Akad. Nauk SSSR 76, 2 (1951).

[9] G. V. Spivak and A. Gel'berg, Doklady Akad. Nauk SSSR 94, 455 (1954).

[10] A. I. Frimer and L. I. Gerasimova, J. Tech. Phys. (USSR) 26, 726 (1956).*

[11] H. J. Williams, F. Forster, and E. A. Wood, Phys. Rev. 82, 120 (1951).

[12] L. F. Bates and D. H. Martin, Proc. Phys. Soc., London, 88, 537 (1955); 99, 145 (1956); L. F. Bates, Research 8, 462 (1955); M. Jamamoto and T. Iwata, Sci. Rep. Res. Inst. Tohoku Univ. A-5, 5, 433 (1953); L. V. Kirenskii and V. D. Dylgerov, Metal Physics and Metallography (USSR) 3, 216 (1956).

Received October 30, 1956

M. V. Lomonosov Moscow State University

---

* [Soviet Physics – Technical Physics, p. 705].

ON OBTAINING TIME CORRELATION FUNCTIONS FOR STATISTICAL SYSTEMS WITH LONG-RANGE INTERACTIONS FOR PERIODS UP TO THE MEAN FREE TIME

V. V. Tolmachev

(Presented by Academician N. N. Bogoliubov September 19, 1956)

In a recent article [1] we derived a chain of equations for the determination of symmetrical distribution functions:

$$\frac{\partial F_s(x_1t_1, \ldots, x_st_s)}{\partial t_k} = [H(x_k);\ F_s(x_1t_1, \ldots, x_st_s)]_{x_k} + \frac{1}{v}\int_{\Omega} [\Phi(|q_k - q|);\ F_{s+1}(x_1t_1, \ldots, x_st_sxt_k)]_{x_k}\, dx. \tag{1}$$

As "initial" conditions we take

$$F_s(x_1t_1, \ldots, x_st_s) = \sum_{(m_1, \ldots, m_l)} \frac{v^{s-l}}{l!} \frac{1}{m_1! \ldots m_l!} \sum_{(T)} \hat{T} \left\{ \prod_{i=1}^{m_1} \delta(x_i - x_1) \prod_{i=m_1+1}^{m_1+m_2} \delta(x_i - x_{m_1+1}) \ldots \prod_{i=m_1+\ldots+m_{l-1}+1}^{s} \delta(x_i - x_{m_1+\ldots+m_{l-1}+1}) \right\} F_l(tx_1,\ x_{m_1+1}, \ldots, x_{m_1+\ldots+m_{l-1}+1}). \tag{2}$$

The functions $F_l(tx_1, x_{m_1+1}, \ldots, x_{m_1+\ldots+m_{l-1}+1})$ in the right-hand side of (2) are the ordinary distribution functions of N. N. Bogoliubov [2]. The summation $\sum_{(m_1, \ldots, m_l)}$ is performed over all sets of integers $m_1, \ldots, m_l$; the summation $\sum_{(T)}$ is performed over all $s!$ permutations of s symbols. In (1) and (2) we have assumed that the usual transition to the limit is satisfied: $N \to \infty$, $V \to \infty$, $v = \frac{V}{N} = \text{const}$.

In order to obtain the solution of (1) and (2) for a plasma in statistical equilibrium without external fields we make the following substitutions in (1): $H(x_k)$ for $T(p_k)$ and $\Phi(|q_k - q|)$ for $v\,\psi(|q_k - q|)$.

The solution of (1) and (2) will be sought in the form of a power series in the specific volume v:

$$F_s = F_s^{(0)} + vF_s^{(1)} + \cdots; \tag{3}$$

we also make use of the expansion of the ordinary distribution functions which was obtained in [2] for a plasma in statistical equilibrium without external fields.

It is easily seen that the zeroth order approximation will be

$$F_s^{(0)}(x_1t_1, \ldots, x_st_s) = \prod_{(1<i<s)} f(p_i). \tag{4}$$

The first approximation will be sought in the form

$$F_s^{(1)}(x_1t_1,\ldots,x_st_s)=\sum_{(1\leqslant i<j\leqslant s)} g(x_it_i,\ x_jt_j)\prod_{\substack{(1\leqslant l\leqslant s)\\(l\neq i,\ l\neq j)}} f(p_l), \tag{5}$$

where $g(x_it_i,\ x_jt_j)$ is a symmetrical function with respect to the permutation of its arguments; it is also homogeneous in space and time, that is,

$$g(x_1t_1,\ x_2t_2)=g(q_1-q_2,\ t_1-t_2,\ p_1,\ p_2). \tag{6}$$

We obtain

$$g(q,\ t,\ p_1,\ p_2)=g\left(q-\frac{p_1}{m}t,\ p_1,p_2\right)+$$

$$+\int\limits_0^t\int\limits_\Omega K(q-q',\ t-t',\ p_1)\,g(-q',\ -t',\ p_2,p')\,dq'dp'dt', \tag{7}$$

where

$$q=q_1-q_2,\quad t=t_1-t_2, \tag{8}$$

$$K(q,\ t,\ p)=-\sum_{(1\leqslant\alpha\leqslant3)}\frac{p^\alpha}{m\theta}\,\frac{e^{-\frac{p^2}{2m\theta}}}{(2\pi m\theta)^{3/2}}\,\frac{\partial\psi\left(\left|q-\frac{p}{m}t\right|\right)}{\partial q^\alpha}, \tag{9}$$

$$g(q,\ p_1,\ p_2)=g(q,\ 0,\ p_1,\ p_2). \tag{10}$$

We perform a Fourier transformation in the variables $\underline{q}$:

$$g(q,\ t,\ p_1,\ p_2)=\frac{1}{(2\pi)^3}\int e^{ikq}r(k,t,p_1,p_2)\,dk; \tag{11}$$

then from (7)

$$r(k,\ t,\ p_1,\ p_2)=e^{-i\frac{kp_1}{m}t}\,g(|k|,\ p_1,\ p_2)+$$

$$+\int\limits_0^t\int\limits_\Omega K(k,\ t-t',\ p_1)\,r(-k,\ -t',\ p_2,\ p')\,dp'dt', \tag{12}$$

where (13)

$$K(k,\ t,\ p)=-i\frac{kp}{m\theta}\,\frac{e^{-\frac{p^2}{2m\theta}-i\frac{kp}{m}t}}{(2\pi m\theta)^{3/2}}\,\nu(|k|); \tag{14}$$

$$\nu(|k|)=\int e^{-ikq}\psi(|q|)\,dq; \tag{15}$$

$$g(|k|,\ p_1,\ p_2)=f(p_1)\,\delta(p_1-p_2)+g(|k|)\,f(p_1)\,f(p_2);$$

$$g(|k|)=\int e^{-ikq}g(|q|)\,dq. \tag{16}$$

From the space and time homogeneity of $g(x_1t_1,\ x_2t_2)$

$$r(k,\ t,\ p_1,\ p_2)=r(-k,\ -t,\ p_2,\ p_1). \tag{17}$$

We note that the problem of solving (12) and (17) is equivalent to solving

$$r(k, t, p_1, p_2) = e^{-i\frac{kp_1}{m}t} g(|k|, p_1, p_2) + \\ + \int_0^t \int K(k, t-t', p_1)\, r(k, t', p', p_2)\, dp'dt', \tag{18}$$

which also satisfies Condition (17). Equation (18) was obtained from (12) by replacing $r(-k, -t, p_2, p')$ with $r(k, t'\ p', p_2)$ in the integral term. We now use a convenient division of the problem of (18) and (17): we can seek the solution of (18) only in the region $t > 0$ and then use (17) for a continuation of this solution into the region $t < 0$. An operational method can conveniently be used to solve (18) for $t > 0$. We introduce the following notation for the Laplace transformations:

$$R(k, z, p_1, p_2) = \int_0^\infty r(k, t, p_1, p_2)\, e^{-zt}\, dt \qquad (\operatorname{Re} z > 0), \tag{19}$$

$$K(k, z, p_1) = \int_0^\infty K(k, t, p_1)\, e^{-zt}\, dt \qquad (\operatorname{Re} z > 0), \tag{20}$$

$$F(k, z, p_1, p_2) = \int_0^\infty e^{-i\frac{kp_1}{m}t - zt} g(|k|, p_1, p_2)\, dt \qquad (\operatorname{Re} z > 0). \tag{21}$$

For $R(k, z, p_1, p_2)$ we have

$$R(k, z, p_1, p_2) = F(k, z, p_1, p_2) + K(k, z, p_1) \frac{\int F(k, z, p_1, p_2)\, dp_1}{1 - \int K(k, z, p_1)\, dp_1}. \tag{22}$$

Using (13) and (15), after some calculation we obtain a quite complicated expression for $R(k, z, p_1, p_2)$, which we shall not give for lack of space.

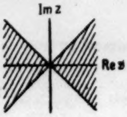

Fig. 1.

From the inverse Laplace transformation we obtain

$$r(k, t, p_1, p_2) = \frac{1}{2\pi i} \int_{\sigma - i\infty}^{\sigma + i\infty} R(k, z, p_1, p_2)\, e^{zt}\, dz \quad (t > 0), \tag{23}$$

$$r(k, t, p_1, p_2) = r(-k, -t, p_2, p_1) \qquad (t < 0) \tag{24}$$

Equations (23) and (24) in principle give the solution in first approximation.

We shall say a few words regarding the analytical nature of $R(k, z, p_1, p_2)$. The only singularities of $R(k, z, p_1, p_2)$ at finite points of the z plane are poles at the points $z = -ikp_1/n$, $z = -ikp_2/m$ and at the roots of the dispersion equation

$$1 + \frac{\nu(|k|)}{\theta} - \frac{\nu(|k|)}{\theta} z \int_0^\infty e^{-zt - \theta k^2 t^2/2m}\, dt = 0.$$

For $\lambda \gg 1$, $|k| \ll 1/r_D$ the roots of (25) can be written approximately as (see [3]):

$$z_1 \simeq i\omega_0 \left(1 + \frac{3}{2} r_D^2 k^2\right) - \sqrt{\frac{\pi}{8}}\, \omega_0 \frac{1}{k^3 r_D^3} e^{-1/2r_D^2 k^2}, \tag{26}$$

$$z_2 \simeq -i\omega_0\left(1+\frac{3}{2}r_D^2k^2\right)-\sqrt{\frac{\pi}{8}}\,\omega_0\,\frac{1}{k^3r_D^3}\,e^{-1/2r_D^2k^2}, \tag{27}$$

where $\omega_0 = \sqrt{4\pi e^2/vm}$ is the plasma frequency; $r_D = \sqrt{\theta v/4\pi e^2}$ is the Debye radius, e is the electron charge; $\theta = kT$. For large $|z|$ the function $R(k, z, p_1, p_2)$ behaves as follows: as z goes to infinity inside the shaded region of Fig. 1, the function becomes infinite, but when z becomes infinite outside of this region the function vanishes. It is of interest to use the solution in (23) and (24) to obtain formulas for the function

$$g_1(q_1, t_1, q_2, t_2)=\iint g(x_1t_1, x_2t_2)\,dp_1dp_2. \tag{28}$$

After some calculation we have

$$g_1(q_1, t_1, q_2, t_2)=\frac{1}{(2\pi)^3}\int e^{ikq}\,r_1(k, t)\,dk, \tag{29}$$

$$r_1(k, t)=\frac{1}{2\pi i}\int\limits_{\sigma-i\infty}^{\sigma+i\infty}R_1(k, z)\,e^{zt}\,dz \quad (t>0), \tag{30}$$

$$r_1, (k, t)=r_1(-k, -t) \quad (t<0), \tag{31}$$

$$R_1(k, z)=\frac{(1+g(|k|))\int\limits_0^\infty e^{-zt-\theta k^2t^2/2m}\,dt}{1+\frac{\nu(|k|)}{\theta}-\frac{\nu(|k|)}{\theta}\,z\int\limits_0^\infty e^{-zt-\theta k^2t^2/2m}\,dt}. \tag{32}$$

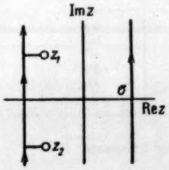

Fig. 2.

In order to obtain the asymptotic integral of (30) for large t it is necessary, in using the familiar method of asymptotic approximations of such integrals, to move the path of integration to the left so that the poles of $R_1(k, z)$ will be to the right of the path (Fig. 2). Then

$$r_1(k, t)\cong \operatorname*{res}_{z=z_1} R_1(k, z)\,e^{zt}+\operatorname*{res}_{z=z_2} R_1(k, z)\,e^{zt}. \tag{33}$$

By calculating the residues we obtain

$$r_1(k, t)\cong(1+g(|k|))\,e^{-\gamma t}\cos\omega_0 t, \tag{34}$$

where γ is the Landau logarithmic decrement $\gamma=\sqrt{\frac{\pi}{8}}\,\omega_0\,\frac{1}{k^3r_D^3}\,e^{-1/2k^2r_D^2}$. In order to determine the behavior of $r_1(k, t)$ for small t we turn directly to the equation for $r_1(k, t)$:

$$r_1(k, t)=e^{-\theta k^2t^2/2m}\,(1+g(|k|))-\frac{k^2\nu(|k|)}{m}\int\limits_0^t(t-t')\,e^{-\theta(t-t')^2k^2/2m}\,r_1(k, t')\,dt', \tag{35}$$

which is obtained from (18) by integrating over the momenta p_1, p_2. Replacing the exponential factors by 1 for small t and solving the resulting equation we obtain

$$r_1(k, t)\cong(1+g(|k|))\cos\omega_0 t. \tag{36}$$

From a comparison of (36) and (34) we conclude that (34) clearly gives a good idea of the behavior of the solution for all t.

It must be emphasized that since we have used the expansion (3) directly in powers of $\underline{v}$ Eq. (34) is valid for times smaller than the mean free time.

In conclusion the author takes this opportunity to express his deep appreciation to Academician N. N. Bogoliubov for valuable discussions of this work, which was performed under his direct supervision.

LITERATURE CITED

[1] V. V. Tolmachev, Doklady Akad. Nauk SSSR 105, 439 (1955).

[2] N. N. Bogoliubov, Dynamical Problems in Statistical Physics (Moscow, 1946).

[3] L. D. Landau, J. Exptl.-Theoret. Phys. (USSR) 16, 574 (1946).

Received September 12, 1956

THE MEASUREMENT OF TOTAL CROSS SECTIONS σ_t FOR 14.8-MEV NEUTRONS BY (n,α) COINCIDENCES [1]

M. M. Khaletskii

(Presented by Academician V. N. Kondrat'ev November 13, 1956)

The recording of monoenergetic alpha particles from the reaction $D^2(T, n)He^4$ enables us to use a coincidence scheme to isolate in space a narrow neutron beam from this reaction. The use of a neutron beam correlated with alpha particles for measuring the cross section σ_t provides the possibility of eliminating the background (of other neutrons, especially neutrons from the $D^2(D, n)He^3$ reaction, and from other causes).

TABLE 1

Element	Number of nuclei per cm^3, n·10^{22}	Total cross sections σ_t in barns (our measurements)	σ_t in barns [2]	σ_t in barns (Goodman [3])
Li	4.59	1.24 ± 0.06*	1.45 ± 0.03	—
Be	12	1.46 ± 0.03*	1.53 ± 0.03	1.4 ± 0.1
C	7.72	1.18 ± 0.12	1.32 ± 0.02	1.20 ± 0.04
Mg	4.31	1.83 ± 0.05*	1.75 ± 0.03	1.8 ± 0.2
Al	5.81	1.75 ± 0.08	1.73 ± 0.03	1.8 ± 0.1
Fe	8.5	2.51 ± 0.06	2.60 ± 0.05	2.4 ± 0.2
Cu	8.38	2.66 ± 0.07	2.96 ± 0.06	2.5 ± 0.1
Pd	6.7	4.0 ± 0.1	—	—
Cd	4.61	4.12 ± 0.06	4.44 ± 0.09	—
Sn	3.51	4.05 ± 0.07	4.68 ± 0.09	4.0 ± 0.4
Pb	3.29	5.28 ± 0.15	5.48 ± 0.11	5.1 ± 0.4
Bi	2.82	5.33 ± 0.08	5.46 ± 0.11	5.2 ± 0.5
U	4.73	5.64 ± 0.1	5.87 ± 0.12	

* Measured by G. A. Ovsiannikov.

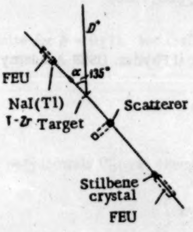

Fig. 1. Scheme of measurement of the cross section σ_t.

In the present work a thick T-Zr target (Fig. 1) was used. The target was struck by a beam of magnetically isolated deuterons of energy E_d = 160 kev. Alpha particles emitted by the target were recorded by a NaI(Tl) crystal of thickness d = 0.5 mm with an FEU-19 photomultiplier. The window of the alpha counter formed the solid angle $\omega_\alpha = 1.8 \cdot 10^{-3}$ sterad with the target. At a distance of 75 cm on the other side of the target the neutron counter was placed, consisting of stilbene crystal 34 mm in diameter and an FEU-19.

The neutron detector was placed in the beam of "correlated" neutrons with accuracy ± 0.5°; for this purpose the alpha counter was rotated by single degrees first through the angle φ (in the horizontal plane) and then through the angle θ (in the vertical plane) and in each

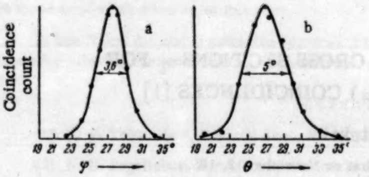

Fig. 2. Direction of the neutron beam correlated with alpha particles. Stilbene neutron counter, d = 34 mm at r = 75 cm from the target; a) the counter was rotated through the angle φ around the target; b) the counter was rotated through the angle θ.

position the (n, α) coincidence count was taken for the same alpha particle count (Fig. 2).

Between the target and the neutron counter at 26 cm from the target a special device was used to shift cylindrical scatterers in and out of the neutron beam. These scatterers measured 25 mm in diameter and 25 mm in length. The total cross sections σ_t were measured by taking the count of (n, α) coincidences with and without the presence of the scatterers. From the attenuation of the count of (n, α) coincidences $T = e^{-n\sigma_t d}$, where n is the number of nuclei in 1 cm^3, σ_t was determined. The coincidence scheme had a resolution of $\tau = 5 \cdot 10^{-8}$ sec. The coincidence counting rate was ~ 30 pulses per second; at the same time that the coincidences were registered the neutrons and alpha particles were counted by channels. The neutron yield from the target was known from the alpha particle count.

The measurements of σ_t are given in Table 1; the data of Coon et al. [2] and of Goodman [3], obtained by a different method are also given for 14-Mev neutrons.

The described method of measuring neutron cross sections can be extended to neutrons from the $D^2(T, n)He^4$ reaction for $E_n \gg 14$ Mev and for $E_n < 14$ Mev (independently of whether the $D^2(T, n)He^4$ reaction for higher deuteron energies remains a source of monochromatic neutrons [4, 5] or whether two neutron groups result) and for neutrons from the reaction $D^2(D, n)He^3$ [1, 6] and $p(T, n)He^3$.

LITERATURE CITED

[1] M. M. Khaletskii, Coincidence Schemes for the Measurement of Total Neutron Cross Sections, Report of Inst. Chem. Phys. Acad. Sci. USSR, March 13, 1953.

[2] J. H. Coon, E. R. Graves, and H. H. Barshall, Phys. Rev. 88, 562 (1952).

[3] S. Goodman, Phys. Rev. 88, 686 (1952).

[4] C. H. Johnson and A. Galonsky, Phys. Rev. 100, 1252 (A) (1955).

[5] R. M. Eisberg, Phys. Rev. 102, 1104 (1956).

[6] W. Franzen, P. Huber, and L. Schellenberg, Z. Naturforsch. 10a, 820 (1955).

Received November 2, 1956

Institute of Chemical Physics, USSR Academy of Sciences

THE ANGULAR AND LATERAL DISTRIBUTION FUNCTIONS OF PARTICLES IN A CASCADE SHOWER MAXIMUM

V. V. Guzhavin and I. P. Ivanenko

(Presented by Academician D. V. Skobeltsyn December 4, 1956)

The one-dimensional development of an electron-photon cascade can be considered a completely solved problem. The method of functional transformations [1] and the method of moments [2] provide a quite accurate description of the linear development of an average shower in light and heavy matter.

The situation is entirely different with regard to the three-dimensional development of a cascade shower. Thus far an analytic expression for the lateral distribution * has not been obtained because of the extreme complexity of the initial equations; an analytic expression was obtained for the angular distribution only by neglecting ionization losses [1]. A number of writers have calculated angular and lateral distributions numerically for various special cases ([3], for example) but these calculations are so complicated that thus far even an approximate scheme of calculation has not been published.

We believe that a very promising method of solving the problem of the angular and lateral distribution of shower particles is the method of moments. In [4, 5] an angular and lateral distribution function for any depth was obtained by the method of moments. In these articles the distribution functions were constructed from the moments through graphical selection of an arbitrary function whose first few moments agreed with the exact moments. The authors of [4, 5] also neglected the pole of the lateral distribution function; therefore they were unable to plot this function in the neighborhood of zero.

A simple method can be shown for calculating the angular and lateral distribution functions in a cascade shower maximum from known moments.

An analysis of the equations for the angular and lateral distribution functions easily shows that these functions depend on $\bar{r}$ and $\bar{\theta}$ only in the combinations $x_\theta = \frac{E\theta}{E_s}$ $x_r = \frac{Er}{E_s}$, where $E_s = 21$ Mev. It appears that the differential angular distribution function

$$P(E_0, E, \theta, t) = P_{\text{lin}}(E_0, E, t)\, P(s, x_\theta) \tag{1}$$

remains finite for $\theta = 0$ [1]. We shall approximate $P(1, x_\theta)$ by the sum of polynomials $V_n(\alpha x)$:

$$P(1, x_\theta) = e^{-\alpha x_\theta} \sum_{n=0}^{k/2-1} a_n V_n(\alpha x_\theta). \tag{2}$$

The polynomials $V_n(\alpha x)$ except for a normalization constant are determined from the condition

$$\int\limits_0^\infty x^{2n'+1} e^{-\alpha x} V_n(\alpha x)\, dx = 0 \quad \text{for} \quad n' < n. \tag{3}$$

---

* Everywhere in this article by an angular distribution function we mean a function integrated over a plane perpendicular to the shower axis; by a lateral distribution function we mean a function integrated over the angles.

The explicit expressions are

$$V_0(y) = \alpha; \quad V_1(y) = \frac{\alpha}{2}(-2 + y); \quad V_2(y) = \frac{\alpha}{8}(8 - 7y + y^2);$$
$$V_3(y) = \frac{\alpha}{48}(-48 + 57y - 15y^2 + y^3).$$

The polynomials which are orthogonal to $V_n(y)$ are determined from

$$\int_0^\infty e^{-\alpha x} V_n(\alpha x) V_{n'}^+(\alpha x)\, dx = \delta_{nn'}. \tag{4}$$

The explicit expressions are

$$V_0^+(y) = y; \quad V_1^+(y) = -y + \frac{y^3}{3!}; \quad V_2^+(y) = y - 2\frac{y^3}{3!} + \frac{y^5}{5!};$$
$$V_3^+(y) = -y + 3\frac{y^3}{3!} - 3\frac{y^5}{5!} + \frac{y^7}{7!}.$$

By using the polynomials $V_n^+(y)$ it is easy to obtain the following expressions for the coefficients a_n:

$$a_n = \int_0^\infty V_n^+(\alpha x) P(1, x_0)\, dx; \tag{5}$$

$$a_0 = 1; \quad a_1 = -\frac{3!}{\alpha^2}\left(1 - \alpha^2 \frac{\overline{\theta^2}}{3!}\right), \quad a_2 = \frac{5!}{\alpha^4}\left(1 - 3\alpha^2 \frac{\overline{\theta^2}}{3!} + \alpha^4 \frac{\overline{\theta^4}}{5!}\right);$$
$$a_3 = -\frac{7!}{\alpha^6}\left(1 - 3\alpha^2 \frac{\overline{\theta^2}}{3!} + 3\alpha^4 \frac{\overline{\theta^4}}{5!} - \alpha^6 \frac{\overline{\theta^6}}{7!}\right).$$

TABLE 1 *

x_θ	$P(1, x_\theta)$			x_θ	$P(1, x_\theta)$		
	$k=6$	$k=4$	from (4)		$k=6$	$k=4$	from (4)
0	9.84	10.42	9.3	1.6	$6.06 \cdot 10^{-2}$	$5.75 \cdot 10^{-2}$	$6.00 \cdot 10^{-2}$
0.2	5.30	5.49	5.3	1.8	3.10	3.03	2,90
0.4	2.85	2.89	2.78	2.0	1.56	1.56	1.46
0.6	1.51	1.51	1.52	2.2	$7.76 \cdot 10^{-3}$	$8.31 \cdot 10^{-3}$	$7.13 \cdot 10^{-3}$
0.8	$8.6 \cdot 10^{-1}$	$7.93 \cdot 10^{-1}$	$8.20 \cdot 10^{-1}$	2.4	3.76	4.32	3.56
1.0	4.28	4.14	4.46	2.6	1.76	2.24	1.74
1.2	2.25	2.16	2.32	2.8	$7.92 \cdot 10^{-4}$	1.15	$8.29 \cdot 10^{-4}$
1.4	1.17	1.12	1.18	3.0	3.28	$6.02 \cdot 10^{-4}$	3.92

---

* In calculating $P(1, x_\theta)$ and $P(1, x_r)$ we used the numerical values of the moments given in [4, 5].

Thus the coefficients a_n are expressed simply in terms of moments of the angular distribution function. The coefficient α is obtained from the following condition: we require that the k-th moment of the weighting function $e^{-\alpha x}$ equal the k-th moment of the sought distribution function, i. e., we determine α from the condition

$$\int_0^\infty e^{-\alpha x} x^k \, dx \Big/ \int_0^\infty e^{-\alpha x} \, dx = \overline{\theta^k}. \tag{6}$$

The calculated values of $P(1, x_\theta)$ are given in Table 1. The first column contains the values of $P(1, x_\theta)$ calculated from (2) with k = 6, i. e., by using the first three even moments; the second column contains the values calculated with k = 4; the third column contains the values given in [4]. An analysis of Table 1 shows that the proposed method of approximating $P(1, x_\theta)$ even with k = 4, that is, using the first two even moments, enables us to obtain $P(1, x_\theta)$ very accurately over a wide range of values of x_θ. We note that a comparison of the values of $P(1, x_\theta)$ for k = 6 and k = 4 enables us to determine the limits of applicability of approximation (2) for a given value of k.

In order to obtain an approximate formula for the integral lateral distribution function

$$N(E_0, E, r, t) = N \lim (E_0, E, t)\, N(s, x_r)$$

in the shower maximum we proceed as follows. In [3, 6, 7] it was shown that for r → 0, $N(s, x_r)$ is proportional to r^{s-2}. We represent $N(s, x_r)$ in the shower maximum by

$$N(1, x_r) = \frac{1}{x_r} P(1, x_r). \tag{7}$$

We note that the moments of $N(E_0, E, r, t)$ and $P(1, x_r)$ are related by $\overline{r^n} = \left(\frac{E_s}{E}\right)^n \overline{x_p^n}$.

We approximate the function $P(1, x_r)$ by a sum of polynomials $R_n(\alpha x)$:

$$P(1, x_r) = e^{-\alpha x_r^{1/2}} \sum_{n=0}^{k/2-1} a_n R_n(\alpha x_r). \tag{8}$$

The polynomials $R_n(\alpha x)$ are determined from the condition

$$\int_0^\infty x^{2n'} e^{-\alpha x^{1/2}} R_n(\alpha x)\, dx = 0 \quad \text{for} \quad n' < n.$$

The explicit expressions are:

$$R_0(y) = \frac{\alpha^2}{2}; \quad R_1 = \frac{\alpha^2}{8640}(-6 + \alpha^2 x);$$

$$R_2(y) = \frac{\alpha^2}{1.8835 \cdot 10^9}(1092 - 242\,\alpha^2 x + 3\alpha^4 x^2).$$

The polynomials which are orthogonal to $R_n(y)$ are determined from (6) with the weighting function $e^{-\alpha x^{1/2}}$ instead of $e^{-\alpha x}$. The explicit expressions are:

$$R_0^+(y) = 1; \; R_1^+(y) = -120 + \alpha^4 x^2; \; R_2^+(y) = 6.854 \cdot 10^5 - 8.736 \cdot 10^3 \alpha^4 x^2 + \alpha^8 x^4.$$

Using (5) we can obtain the following expressions for the coefficients a_n:

$$a_0 = 1; \quad a_1 = -120 + \alpha^4 \overline{x_p^2}; \quad a_2 = 6.854 \cdot 10^5 - 8.736 \cdot 10^3 \alpha^4 \overline{x_p^2} + \alpha^8 \overline{x_p^4}.$$

The coefficient α in (8) is determined from the condition

$$\int_0^\infty e^{-\alpha x^{1/2}} x^k \, dx \Bigg/ \int_0^\infty e^{-\alpha x^{1/2}} \, dx = \overline{x^k_p}.$$

The calculated values of $P(1, x_r)$ are given in Table 2. The first column contains the values of $P(1, x_r)$ calculated from (8) with $k = 6$; the second column contains the values with $k = 4$; the third column contains the values given in [5]. An analysis of Table 2 shows that the proposed method of approximation even for $k = 4$, that is, using two even moments, enables us to obtain very accurate values of $P(1, x_r)$ for a wide range of values of x_r. As in the case of the angular distribution a comparison of the data for $k = 6$ and $k = 4$ enables us to determine the limits of applicability of approximation (8) for a given value of k.

TABLE 2 *

x_r	$\frac{x_r}{E} P(1, x_r)$			x_r	$\frac{x_r}{E} P(1, x_r)$		
	$k=6$	$k=4$	from [5]		$k=6$	$k=4$	from [5]
0	10.77	11.18	—	0.15	1.80	—	—
0.0001	10.28	—	—	0.2	1.36	1.35	1.62
0.0002	10.09	—	—	0.6	$2,93 \cdot 10^{-1}$	—	$3.16 \cdot 10^{-1}$
0.0005	9.72	—	—	1.0	1.01	$9,91 \cdot 10^{-2}$	1,03
0.001	9.31	—	—	1.4	$4.24 \cdot 10^{-2}$	—	$4,11 \cdot 10^{-2}$
0,002	8.77	—	—	1,8	1.99	—	1.86
0.005	7.78	—	—	2.2	1.01	—	$9.34 \cdot 10^{-3}$
0.010	6.80	—	—	2.6	$5.46 \cdot 10^{-3}$	—	5.12
0.015	6.13	—	—	3.0	3.06	$3.13 \cdot 10^{-3}$	3.02
0.02	5.62	—	—	4.0	$8.45 \cdot 10^{-4}$	$8.88 \cdot 10^{-4}$	1.09
0.04	4.47	—	—	5.0	2.72	2.93	—
0.06	3.48	—	—	6.0	1.01	1.07	—
0.1	2.50	—	—	7.0	$3.89 \cdot 10^{-5}$	$4.25 \cdot 10^{-5}$	—

---

* In [5] the differential function $P(1, x_r)$ was calculated in the interval $0.2 < x_r < 6$. Therefore, in order to obtain the integral function, we assumed that the function $P(1, x_r)$ of [5] is proportional to e^{-x_r}/x_r in the interval $(6, \infty)$. We note that the correction obtained in this manner changes the last number of the corresponding column by 40% but that it has a smaller effect on the remaining numbers.

We expect that this method will enable us to obtain the angular and lateral distribution functions which allow for ionization losses. The calculations are in progress.

The authors are indebted to N. S. Strunina for assistance with the calculations.

LITERATURE CITED

[1] S. Z. Belen'kii, Shower Processes in Cosmic Rays (1948) [Soviet Physics – J.E.T.P., p. 115].

[2] I. P. Ivanenko, J. Exptl.-Theoret. Phys. (USSR) 31, 86 (1956); Doklady Akad. Nauk SSSR 107, 819 (1956) [Soviet Physics – Doklady, p. 231].

[3] J. Nishimura and K. Kamata, Progr. Theor. Phys. 5, 899 (1950).

[4] L. Eyges and S. Fernbach, Phys. Rev. 82, 287 (1951).

[5] S. Fernbach, Phys. Rev. 82, 288 (1951).

[6] I. Ia. Pomeranchuk, J. Exptl.-Theoret. Phys. (USSR) 14, 1252 (1944).

[7] A. B. Migdal, J. Exptl.-Theoret. Phys. (USSR) 15, 313 (1945).

Received November 24, 1956

M. V. Lomonosov Moscow State University

(n,α) REACTIONS OF 14-MEV NEUTRONS WITH CADMIUM

B. G. Dzantiev, V. N. Levkovskii, and A. D. Malievskii

(Presented by Academician V. N. Kondrat'ev November 23, 1956)

The interaction between cadmium and slow neutrons has been studied in great detail but the reactions between cadmium and fast neutrons have been investigated very little. We know only that Ag^{106}, Ag^{108}, Ag^{110}, Ag^{111}, and Ag^{112} are obtained from (n, p) reactions with the corresponding cadmium isotopes; this was established in 1937-1938 [1]. There have been no further investigations of these reactions nor measurements of their thresholds and cross sections. Thus far no (n, α) reaction has been observed for a cadmium isotope.

The present paper results from an investigation of (n,α) reactions in cadmium leading to the production of palladium isotopes. At the same time we determined the cross section for the production of Pd^{109} from silver in a (n, p) reaction. In view of the existence of a large number of stable cadmium isotopes the identification of the reaction products was possible only through the use of radiochemical methods.

Cd(n, α)Pd reactions and the identification of reaction products. Metallic cadmium and its salts were irradiated with ~ 4-Mev (d, d), 14-Mev (t, d) neutrons and fission neutrons. The radioactive palladium was separated from the target with a carrier by precipitation with dimethylglyoxime in an acid medium. In order to obtain samples free of contamination with radioactive silver isotopes from the (n, p) reaction the precipitate of palladium dimethylglyoximate was dissolved in concentrated nitric acid and doubly precipitated with an AgCl carrier, after which the palladium was again precipitated with dimethylglyoxime. Experiments with radioactive Pd^{109} and Ag^{110} introduced into unirradiated samples showed that the losses of radioactive palladium by the method of separation which was employed do not exceed 3-5 % and that the precipitates of palladium dimethylglyoximate do not contain radioactive silver contamination.

The radiochemically pure samples prepared in this manner were either used for measurement of their activity by a Geiger counter or were dissolved, after which at definite intervals of time silver (AgCl) was precipitated from the solution in order to identify the palladium isotopes from the daughter products.

After irradiation with 4-Mev neutrons no radioactivity was observed in the palladium fraction. After irradiation with fission neutrons 14-hour palladium radioactivity was observed. After irradiation with 14-Mev neutrons the palladium fraction revealed three radioactive components with the half-lives 22± 1 min, 5.5± 0.2 hours and 14.0± 0.5 hours, with initial radioactivity ratios (26.4± 0.8): (0.40± 0.04): 1.0.

TABLE 1

Period of irradiation	Irradiated compound	Radioactivity, pulses per min: obtained graphically			Radioactivity, pulses per min: allowing for decay during period of irradiation			Relative radioactivity		
		14 hr	5.5 hr	22min	14 hr	5.5 hr	22min	14 hr	5.5 hr	22 min
2 hr	$CdSO_4$	10200	4100	77700	10700	4650	280000	1.00	0.435	26.2
2 ″	$CdSO_4$	6170	2630	45600	6480	2900	160000	1.00	0.462	24.8
20 min	$CdSO_4$	1900	6850	40300	1900	870	53000	1.00	0.457	27.9
20 ″	$CdCl_2$	3230	1080	59600	3230	1100	79000	1.00	0.341	24.5
5 ″	$CdSO_4$	1080	430	25700	1080	430	27500	1.00	0.400	25.4
5 ″	$CdSO_4$	1140	420	28200	1140	420	30200	1.00	0.368	26.5
5 ″	$Cd(NO_3)_2$	750	320	19100	750	320	24400	1.00	0.426	27.2
5 ″	$Cd(NO_3)_2$	910	290	23100	910	290	24700	1.00	0.320	27.1

Table 1 gives the results of a graphical analysis of the decay curves of palladium samples precipitated from different cadmium targets. The radioactivity was measured by a standard cylindrical Geiger counter of 44.5 mg/cm² wall thickness; the thickness of the active samples was ~ 2 mg/cm².

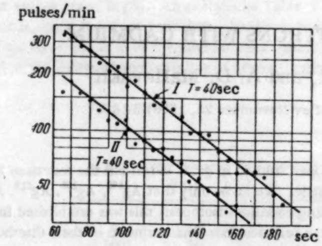

Fig. 1. Radioactivity decay curves of silver rapidly precipitated from a palladium fraction a few hours after irradiation. The radioactivity was measured with an end-window counter of ~ 3 mg/cm² window thickness.

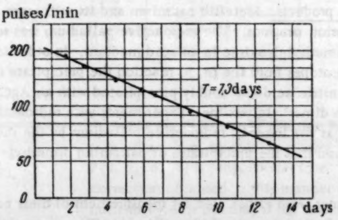

Fig. 2. Radioactivity decay curve of silver precipitated from a palladium fraction rapidly removed from a cadmium target.

TABLE 2

Radiation	Half-thickness $d_{1/2}$, mg/cm²	E, Mev	Correction for absorption in counter wall
Pd 14 hr.	42	1.06	0.45
Pd 5.5 hr.	100	2.29	0.72
Pd 22 min.	110	2.50	0.74
Ag 7.5 days	40	1.02	0.44
Cu 10 min.	140	3.13	0.80

The table shows that the radioactivity ratios are well reproduced for different targets and different periods of irradiation; this shows that the observed radioactivities result from the interaction of cadmium with neutrons.

In order to be able to assign these radioactivities to definite palladium isotopes in addition to the half-lives we determined their aluminum half-thicknesses and also investigated the daughter silver which is the decay product.

Figures 1, 2, and 3 give the radioactivity measurements for samples of silver separated from palladium fractions after different periods of time following irradiation.

Table 2 contains absorption measurements for palladium with T = 14 hrs, 5.5 hrs, and 22 minutes and silver with T = 7.5 days. The table also gives absorption data for Cu^{62} emission which were used in calculating the reaction cross sections (see below). The third column of the table gives the values of the maximum beta ray energies calculated from the empirical relation $E = 2.12 \cdot 10^{-2} d_{1/2} + 0.17$ [2].

It follows from Figs. 1, 2, and 3 and Table 2 that palladium with T = 14 hrs which emits beta particles of $E \approx 1$ Mev is transformed into Ag with T = 40 sec and soft emission, and palladium with T = 22 min emitting beta rays with $E \approx 2.5$ Mev is transformed into Ag with T = 7.5 days and $E \approx 1$ Mev; this is in good agreement with the known decay schemes of Pd^{109} and Pd^{111}.

Thus the 14-hr and 22-min periods must certainly be attributed to the Pd^{109} and Pd^{111} isotopes which result from the previously unobserved reactions $Cd^{112}(n,\alpha)Pd^{109}$ and $Cd^{114}(n,\alpha)Pd^{111}$.

The 5.5-hr half-life in view of the available data on radioactive palladium isotopes must evidently belong to the little-studied isomer Pd^{111m}, which according to [3] resulted from the (d, p) reaction and possesses T = 5.5 hrs and a beta ray maximum of 2.25 Mev. The results of our experiments are not in contradiction with these findings. The correctness of the half-life was confirmed by measuring the integral curve of palladium radioactivity through a 1.5 mm aluminum filter which completely cut off the Pd^{109} emission. The result is a clear T = 5.7 hr (Fig. 4) belonging to hard beta emission. The absorption measurements showed that the energy peak of this emission is ~ 2.3 Mev (Table 2). It was also shown that a possible source of palladium with T = 5.5 hrs is Ag^{111} with T = 7.5 days; a period close to this was detected in AgCl samples doubly precipitated from palladium fractions a few hours after irradiation, that is, after sufficient time for the complete decay of Pd^{111} with T = 22 min.

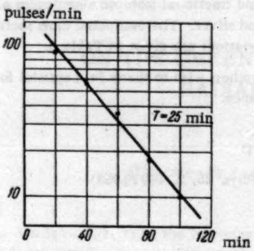

Fig. 3. A curve showing the diminution of silver radioactivity with T = 7.5 days as a function of the time of precipitation from a short-lived palladium fraction; every 20 minutes a carrier was used to remove the radioactive silver which had accumulated during that period from a palladium fraction rapidly separated from the cadmium target.

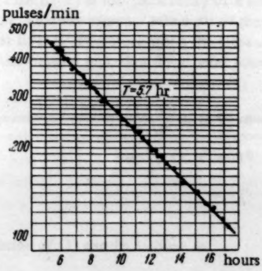

Fig. 4. Decay of palladium radioactivity, obtained with a 1.5 mm aluminum filter which completely absorbs Pd^{109} beta emission.

TABLE 4

Irradiated compound	Weight of target in g	Initial radioactivity with allowance for decay during irradiation		$\frac{I_{Pd}}{I_T}\cdot 10^3$
		Pd^{109}	teflon	
Cd	12.8	4400	361000	1.22
Cd	12.8	4900	393000	1.25
Cd	12.8	3880	358000	1.08
Cd	12.8	3480	258000	1.35
Cd	12.8	5150	390000	1.32
Cd	12.8	5200	410000	1.27
Cd	12.8	3450	276000	1.25
Cd	12.8	3920	335000	1.17
$AgNO_3$	8.0	14800	189000	6.6
$AgNO_3$	8.0	16400	169500	8.2
$AgNO_3$	8.0	20900	228500	7.8

Measurement of the cross sections of the reactions $Cd^{112}(n, \alpha)Pd^{109}$, $Cd^{114}(n, \alpha)Pd^{111}$, $Cd^{114}(n, \alpha)Pd^{111m}$, and $Ag^{109}(n, p)Pd^{109}$ with 14-Mev neutrons. The absolute cross sections of the reactions Cd(n, α)Pd and Ag(n, p)Pd were estimated by comparing the yield of these reactions with the yield of $Cu^{63}(n, 2n)Cu^{62}$, whose cross section for 14-Mev neutrons is $0.5\cdot 10^{-24}$ cm² [4, 5].

Since for prolonged irradiation a copper detector is unsuitable due to the short half-life of Cu^{62} (T = 10 min) the yields of the reactions Cd(n, α), Ag(n, p), and $Cu^{63}(n, 2n)$ were not compared directly but through a fluorine monitor using the reaction $F^{19}(n, 2n)F^{18}$ (threshold ~ 11 Mev; T = 112 min.). The indicators used were standard plates of teflon, which is polymerized tetrafluoroethylene containing 76 % fluorine.

TABLE 3

Weight of copper plate in g	Initial radioactivity of $Cu^{62}\cdot 10^{-5}$ (T = 10 min)	Radioactivity per g Cu, $I_{Cu}\cdot 10^{-5}$	Radioactivity of teflon. $I_T\cdot 10^{-5}$	$\alpha = \frac{I_T}{I_{Cu}}\cdot 10^3$
0.1850	5.05	2.73	1.0	3.66
0.2051	5.25	2.56	0.9	3.52
0.1880	5.31	2.83	1.1	3.88
0.1836	5.84	3.18	1.2	3.78
0.1906	3.83	1.48	0.6	4.05
0.1710	2.48	1.45	0.5	3.66

Table 3 gives the data for the calibration of the fluorine indicator when a neutron beam simultaneously irradiated for 15 sec the standard (22× 64 mm²) teflon plates and thin copper foils of the same dimensions. From the ratio of the initial radioactivities of F^{18} and Cu^{62} measured for identical geometry we obtained the coefficient α which relates the beta yield of $Cu^{63}(n, 2n)$ to the radioactivity of teflon.

Table 4 gives the ratios of the radioactivities of teflon plates and Pd^{109} samples precipitated from cadmium targets (22 × 64 mm² Cd plates) and silver targets ($AgNO_3$ in a thin 22× 64× 3 mm³ container) irradiated simultaneously with 14-Mev neutrons for 1 hr. The samples formed a 90° angle with the direction of the beam. The constancy of the neutron flux was controlled continuously with a boron counter. All radioactivities were measured under identical geometry by standard cylindrical Geiger counters of 44.5 mg/cm² wall thickness. The thickness of the Pd samples did not exceed 2 mg/cm².

The cross sections of $Cd^{112}(n,\alpha)Pd^{109}$, $Cd^{114}(n,\alpha)Pd^{111}$, $Cd^{114}(n, \alpha)Pd^{111m}$, and $Ag^{109}(n, p)Pd^{109}$ were computed

TABLE 5

Reaction	Cross section in millibarns
$Cd^{114}(n, \alpha)Pd^{111}$	0.51 ± 0.13
$Cd^{114}(n, \alpha)Pd^{111m}$	0.13 ± 0.04
$Cd^{112}(n, \alpha)Pd^{109}$	1.35 ± 0.27
$Ag^{109}(n, p)Pd^{109}$	10.5 ± 2.0

from the data in Tables 1, 2, 3, and 4 and from the known half-lives and fractional isotopic abundances of natural cadmium and silver. The computed cross sections and standard deviations are given in Table 5.

The authors wish to thank Iu. Lapitskii for very much assistance.

LITERATURE CITED

[1] M. Hollander, I. Perlman, and G. T. Seaborg, Rev. Mod. Phys. 25, 2, 469 (1953).

[2] E. Broda, Modern Radiochemistry (1953) p. 122.

[3] C. L. McGinnis, Phys. Rev. 87, 202 (1952).

[4] J. E. Brolley, J. L. Fowler, and L. K. Schlacks, Phys. Rev. 88, 618 (1952).

[5] S. G. Forbes, Phys. Rev. 88, 1309 (1952).

[6] E. B. Paul and R. L. Clarke, Can. J. Phys. 31, 267 (1953).

Received November 20, 1956

Institute for Chemical Physics, USSR Academy of Sciences

ON THE GREEN'S FUNCTION IN THE THEORY OF RADIANT ENERGY TRANSFER

B. B. Kadomtsev

(Presented by Academician M. A. Leontovich September 27, 1956)

1. Let $I(\nu, \vec{\omega}, \mathbf{r}, t)$ be the intensity of a beam of radiation of frequency ν in the direction $\vec{\omega}$ at the point $\mathbf{r}$. This beam satisfies the transfer equation

$$\left\{\frac{1}{c}\frac{\partial}{\partial t} + (\vec{\omega}\nabla) + \alpha(\nu, \mathbf{r}) + \sigma(\nu, \mathbf{r})\right\} I(\nu, \vec{\omega}, \mathbf{r}, t) - \\ - \int\limits_{\nu', \vec{\omega}'} p(\nu, \nu'; \cos\theta; \mathbf{r})\, \sigma(\nu', \mathbf{r})\, I(\nu', \vec{\omega}', \mathbf{r}, t) = j(\nu', \vec{\omega}', \mathbf{r}, t), \qquad (1)$$

where c is the velocity of light; $\alpha(\nu, \mathbf{r})$ is the true absorption coefficient; $\sigma(\nu, \mathbf{r})$ is the scattering coefficient; $p(\nu, \nu', \cos\theta; \mathbf{r})$ is the probability of a scattered beam of frequency ν' at angle θ with frequency change $\nu - \nu'$; $j(\nu, \vec{\omega}, \mathbf{r}, t)$ is the source. When all of these quantities are given and are independent of the radiation intensity Eq. (1) is linear. Therefore when the Green's function $G(\nu, \vec{\omega}, \mathbf{r}, t; \nu_0, \vec{\omega}_0, \mathbf{r}_0, t_0)$ is introduced, that is, the solution of the transfer equation for a point source:

$$\left\{\frac{1}{c}\frac{\partial}{\partial t} + (\omega\nabla) + \alpha(\nu, \mathbf{r}) + \sigma(\nu, \mathbf{r})\right\} G(\nu, \omega, \mathbf{r}\ t; \nu_0, \omega_0, \mathbf{r}_0, t_0) - \\ - \int p(\nu, \nu'; \cos\theta; \mathbf{r})\, \sigma(\nu', \mathbf{r})\, G(\nu', \vec{\omega}', \mathbf{r}, t; \nu_0, \vec{\omega}, \mathbf{r}_0, t_0)\, d\nu' d\vec{\omega}' = \\ = \delta(\nu - \nu_0)\, \delta(\vec{\omega} - \omega_0)\, \delta(\mathbf{r} - \mathbf{r}_0)\, \delta(t - t_0), \qquad (2)$$

any solution of (1) can be written as

$$I(\nu, \vec{\omega}, \mathbf{r}, t) = \int G(\nu, \vec{\omega}, \mathbf{r}, t; \nu', \vec{\omega}', \mathbf{r}', t')\, j(\nu', \vec{\omega}, \mathbf{r}', t')\, d\nu'\, d\vec{\omega}' d\mathbf{r}'\, dt'. \qquad (3)$$

Equations (1) and (2) must be supplemented by suitable boundary conditions.

As an initial condition it is reasonable to assume

$$I(\nu, \omega, \mathbf{r}, t) = 0 \quad \text{for} \quad t = -\infty. \qquad (4)$$

We assume as a boundary condition that our medium can be surrounded by a convex surface which encloses all radiation sources. Then on the boundary S the following condition will be satisfied:

$$I(\nu, \vec{\omega}, \mathbf{r}, t) = 0 \quad \text{for} \quad \mathbf{r} \in S, \quad \mathbf{n}\vec{\omega} < 0, \qquad (5)$$

where $\mathbf{n}$ is the outward normal to S at the point $\mathbf{r}$.

In addition to (1) we introduce the conjugate equation for a certain function $I^*(\nu, \vec{\omega}, \mathbf{r}, t)$:

$$\left\{-\frac{1}{c}\frac{\partial}{\partial t}-(\vec{\omega}\vec{\nabla})+\alpha(\nu,\mathbf{r})+\sigma(\nu,\mathbf{r})\right\} I^*(\nu,\vec{\omega},\mathbf{r},t)-$$
$$-\int I^*(\nu',\vec{\omega},\mathbf{r},t)\,\sigma(\nu,\mathbf{r})p(\nu',\nu;\cos\theta;\mathbf{r})\,d\nu'\,d\vec{\omega}'=i(\nu,\vec{\omega},\mathbf{r},t), \tag{6}$$

where we shall assume that I* satisfies the boundary conditions which are conjugate to (4) and (5):

$$\begin{aligned} I^*(\nu,\vec{\omega},\mathbf{r},t)&=0 \quad \text{for} \quad t=+\infty;\\ I^*(\nu,\vec{\omega},\mathbf{r},t)&=0 \quad \text{for} \quad \mathbf{r}\in S,\quad \mathbf{n}\vec{\omega}>0. \end{aligned} \tag{7}$$

We now write (1) as LI = j, where L is an integro-differential operator whose action is defined by (1). Equation (6) has the form L*I* = i, where L* is the operator conjugate to L. The conjugate operators and conjugate boundary conditions are uniquely defined by

$$\int (I^*LI-IL^*I^*)\,d\nu\,d\vec{\omega}\,d\mathbf{r}\,dt\equiv 0, \tag{8}$$

which is integrated over all angles, frequencies, time, and the space bounded by the surface S.

We substitute in (8) $I(\nu,\vec{\omega},\mathbf{r},t)=G(\nu,\vec{\omega},\mathbf{r},t;\nu_0,\vec{\omega}_0,\mathbf{r}_0,t_0)$ and $I^*(\nu,\vec{\omega},\mathbf{r},t)=G^*(\nu,\vec{\omega},\mathbf{r},t;\nu',\vec{\omega}',\mathbf{r}',t')$, where G* is the Green's function for (6). From the rule for integration of the δ-function we obtain

$$G(\nu',\vec{\omega}',\mathbf{r}',t';\nu_0,\vec{\omega}_0,\mathbf{r}_0,t_0)=G^*(\nu_0,\vec{\omega}_0,\mathbf{r}_0,t_0;\nu',\vec{\omega}',\mathbf{r}',t'). \tag{9}$$

This relation shows that the following reciprocity theorem holds: the Green's function satisfies the conjugate equation for a point source with the conjugate boundary conditions.

Hence we can understand the meaning of the conjugate Condition (7): when on S there is a source which emits radiation into outer space there is no radiation inside S. In addition the reciprocity theorem enables us to determine the physical meaning of the conjugate equation.

Indeed any solution of (6) can according to (9) be written as

$$I^*(\nu,\vec{\omega},\mathbf{r},t)=\int i(\nu',\vec{\omega}',\mathbf{r}',t')\,G(\nu',\vec{\omega}',\mathbf{r}',t';\nu,\vec{\omega},\mathbf{r},t)\,d\nu'\,d\vec{\omega}'\,d\mathbf{r}'\,dt', \tag{10}$$

whence we see that I* is a linear functional of the radiation intensity regarded as a function of the coordinates of the point source.

This means that the conjugate equation can be used successfully in problems where it is required to determine some properties of the radiation as a function of the parameters of a point source. (We note that similar conjugate equations are extensively used in neutron physics in connection with similar physical processes [1, 2]).

2. We assume that σ is independent of frequency and that the scattering probability satisfies the symmetry condition $p(\nu,\nu';\cos\theta)=p(\nu',\nu;\cos\theta)$. Then if in the conjugate equation for G

$$\left\{-\frac{1}{c}\frac{\partial}{\partial t}-(\vec{\omega}\vec{\nabla})+\alpha(\nu,\mathbf{r})+\sigma(\nu,\mathbf{r})\right\} G(\nu_0,\vec{\omega}_0,\mathbf{r}_0,t_0;\nu,\vec{\omega},\mathbf{r},t)-$$
$$-\int G(\nu_0,\vec{\omega}_0,\mathbf{r}_0,t_0;\nu',\vec{\omega}',\mathbf{r},t)\,p(\nu',\nu;\cos\theta)\,\sigma(\nu,\mathbf{r})\,d\nu'\,d\vec{\omega}'=$$
$$=\delta(\nu-\nu_0)\,\delta(\vec{\omega}-\vec{\omega}_0)\,\delta(\mathbf{r}-\mathbf{r}_0)\,\delta(t-t_0) \tag{11}$$

the directions of $\vec{\omega}$ and $\vec{\omega}_0$ are reversed and t and t_0 are interchanged it coincides with the direct equation. The coupled boundary conditions then are transformed into (4) and (5). In other words in this case we have the optical reversibility:

$$G(\nu, \vec{\omega}, \mathbf{r}, t; \nu_0, \vec{\omega}_0, \mathbf{r}_0, t_0) = G(\nu_0, -\vec{\omega}_0, \mathbf{r}_0, t; \nu, -\vec{\omega}, \mathbf{r}, t_0). \tag{12}$$

The preceding is also valid for polarized light, because the angular scattering matrix is symmetrical [3]. Thus optical reversibility is a special case of the general reciprocity.

3. There are problems in which it is required to determine the intensity of radiation in only a part of the medium bounded by some surface S_1. For such problems we wish to obtain the boundary conditions on S_1. We shall assume that the source for I differs from zero only inside S_1.

We introduce the auxiliary Green's function $\Gamma(\nu, \vec{\omega}, \mathbf{r}, t; \nu', \vec{\omega}', \mathbf{r}', t')$ for the region between the outer surface S and the inner surface S_1 with the additional condition that the region inside of S_1 is replaced by a black body. Γ satisfies the Conditions (5) and (7) for S and also

$$\Gamma(\nu, \vec{\omega}, \mathbf{r}, t; \nu' \vec{\omega}', \mathbf{r}', t') = 0 \quad \text{for} \quad \begin{cases} \mathbf{r} \in S_1, \ \mathbf{n}_1 \vec{\omega} > 0; \\ \mathbf{r}' \in S, \ \mathbf{n}_1' \vec{\omega}' < 0, \end{cases}$$

where $\mathbf{n}_1$ is the outward normal to S_1 at the point r and $\mathbf{n}_1'$ at the point r'.

We shall use the Relation (8) for the region between S_1 and S. Substituting $I^*(\nu, \vec{\omega}, \mathbf{r}, t) = \Gamma(\nu, \vec{\omega}, \mathbf{r}, t; \nu', \vec{\omega}', \mathbf{r}', t')$ we obtain .

$$I(\nu, \vec{\omega}, \mathbf{r}, t)\big|_{\mathbf{r} \in S_1, \vec{\omega}\mathbf{n}_1 < 0} =$$

$$= \oint\limits_{S_1} \int\limits_{\vec{\omega}'\mathbf{n}_1' > 0} (\mathbf{n}_1' \vec{\omega}) \Gamma(\nu, \vec{\omega}, \mathbf{r}, t; \nu', \vec{\omega}', \mathbf{r}', t') I(\nu', \vec{\omega}', \mathbf{r}', t')\, dS_1\, d\nu'\, d\omega'\, dt', \tag{13}$$

where $\mathbf{n}_1'$ is the outward normal at the point r' where we integrate. This is the desired boundary condition. It enables us to determine the incoming radiation from the outgoing radiation and is therefore altogether sufficient for a complete solution of the transfer equation within S_1.

In the same manner we obtain the conjugate boundary condition on S_1:

$$I^*(\nu, \vec{\omega}, \mathbf{r}, t)\big|_{\mathbf{r} \in S_1, \vec{\omega}\mathbf{n}_1 > 0} =$$

$$= -\oint\limits_{S_1} \int\limits_{\vec{\omega}'\mathbf{n}_1' < 0} (\mathbf{n}_1' \vec{\omega}') \Gamma(\nu', \vec{\omega}', \mathbf{r}', t'; \nu, \vec{\omega}, \mathbf{r}, t) I^*(\nu', \vec{\omega}', \mathbf{r}', t')\, dS_1\, d\nu'\, d\vec{\omega}'\, dt'. \tag{14}$$

It follows from (13) and (14) that (8) is also valid for the region bounded by S_1.

I am very grateful to Professor D. I. Blokhintsev for discussions and a number of suggestions.

Note added in proof. After this article had already been sent to press article [4] appeared in which the reciprocity Relation (9) was derived from the theory of Markov chains.

LITERATURE CITED

[1] A. Weinberg, Am. J. Phys. 20, 401 (1952).

[2] L. N. Usachev, Reactor Design and Theory (in Russian), Geneva Conference on the Peaceful Uses of Atomic Energy (1955) p. 251.

[3] S. Chandrasekhar, The Transfer of Radiant Energy (Foreign Lit. Press, 1953) (Russian translation).

[4] A. M. Biberman and B. A. Vekslenko, J. Exptl.-Theoret. Phys. (USSR) 31, 341 (1956) [Soviet Physics – J.E.T.P., p. 440].

Received September 27, 1956

ON THE APPLICATION OF THE VARIATIONAL PRINCIPLE TO THE ISING MODEL OF AN ANTIFERROMAGNETIC SUBSTANCE

I. A. Kvasnikov

(Presented by Academician N. N. Bogoliubov December 4, 1956)

An Ising antiferromagnetic material is described by the Hamiltonian

$$E = \frac{1}{2}\sum_{ij}^{N} e(i-j)\,\sigma_i\sigma_j - h\sum_{i=1}^{N}\sigma_i, \tag{1}$$

where i and j are the numerical designations of lattice sites; σ_i has the values ± 1; $e(i-j)$ are quantities which characterize the interaction of the i-th and j-th spins; h is the external magnetic field multiplied by the Bohr magneton. This model, which is very crude for an antiferromagnetic, can more reasonably be applied to a description of order-disorder processes in binary alloys [1]. The free energy of the alloy which is associated with order $F_A = -\Theta \ln Z_A$, can be calculated if we know the statistical sum of the system (1). Indeed for the function Z_A we can obtain the expression

$$Z_A = \exp\left\{-\frac{1}{\Theta}\left[\frac{NM}{2}(\mu_1-\mu_2) + \right.\right.$$
$$\left.\left. + \frac{N}{8}\sum_i \left(e^{11}(i-j) + e^{22}(i-j) + 2e^{12}(i-j)\right)\right]\right\} Z_{Is}(h, \{e(i-j)\}), \tag{2}$$

where the exchange integrals $e(i-j)$ and the magnetic field h are related to the interaction energies of alloy atoms $e^{11}(i-j)$, $e^{22}(i-j)$, and $e^{12}(i-j)$ as follows:

$$\begin{gathered} e(i-j) = \frac{e^{11}(i-j) + e^{22}(i-j) - 2e^{12}(i-j)}{4}, \\ h = \frac{1}{4}\left[2(\mu_1-\mu_2) - \sum_i \left(e^{11}(i-j) - e^{22}(i-j)\right)\right], \end{gathered} \tag{3}$$

and the Ising sum of the states is given by (5).

In this model the magnetization M is a given function which determines the fractional composition of the alloy,

$$N_1 = \frac{N}{2}(1+M), \quad N_2 = N - N_1 = \frac{N}{2}(1-M),$$

and the external magnetic field is a function of the temperature Θ. The unknown quantity $(\mu_1 - \mu_2)$ is eliminated from (2) by the use of the equation

$$\frac{1}{N}\frac{\partial \ln Z_{Is}}{\partial H} = M, \tag{4}$$

where

$$Z_{Is} = \sum_{\sigma_1 \ldots \sigma_N} \exp\left\{-\frac{1}{2}\sum_{ij} E(i-j)\,\sigma_i\sigma_j + H\sum_i \sigma_i\right\},$$

$$E(i-j) = \frac{e(i-j)}{\Theta}, \quad H = \frac{h}{\Theta}. \tag{5}$$

The determination of the sum (5) also represents problems in the thermodynamics of an adsorbed monolayer or cellular gas [1] (in this model it is assumed that each of the cells into which the gas volume is divided can contain not more than one particle, and the interaction potential of two atoms is a power function of the distance between them).

We assume as in an earlier note [2] that the lower limit of the statistical sum (5) $Z_{\text{inf}} \leq Z$ obtained by using Bogoliubov's variational principle as an approximate expression for the statistical sum of our problem. We shall assume for simplicity that the system can be divided into two sublattices, an even and an odd one, so that the nearest neighbors of an atom in one lattice are atoms of the other lattice. We introduce

$$E_0 = -(h-u_1)\sum_{\text{even}} \sigma_i - (h-u_2)\sum_{\text{odd}} \sigma_i; \quad E_1 = E - E_0. \tag{6}$$

The quantities u_1 and u_2 are conveniently replaced by other variational parameters:

$$y - x = u_1, \quad y + x = u_2. \tag{7}$$

Then after some simple transformations we can obtain the following expression for the lower limit of the sum (5) of the states: *

$$Z_{\text{inf}}^{1/N} = 2\,[\text{ch}(Y-X+H)\,\text{ch}(Y+X-H)]^{1/2}\exp\left\{-\frac{\Theta}{2\Theta_0}Y^2 + \frac{\Theta}{2\Theta_n}X^2\right\}, \tag{8}$$

with the functions $X = x/\Theta$ and $Y = y/\Theta$ determined by the equations

$$\text{th}(Y-X+H) = \frac{\Theta}{\Theta_0}Y + \frac{\Theta}{\Theta_n}X, \tag{9}$$

$$\text{th}(Y+X-H) = \frac{\Theta}{\Theta_0}Y - \frac{\Theta}{\Theta_n}X.$$

Θ_0 and Θ_n are constants that depend on the properties of a given lattice:

$$\Theta_0 = \frac{2}{N}\sum_{\text{even-odd}} e(i-j) - \frac{2}{N}\sum_{\text{even-even}} e(i-j),$$

$$\Theta_n = \frac{2}{N}\sum_{\text{even-odd}} e(i-j) + \frac{2}{N}\sum_{\text{even-even}} e(i-j) = \frac{1}{N}\sum_{ij} e(i-j). \tag{10}$$

If we assume that only nearest neighbors interact, that is, $e(i-j) = e \cdot a_{ij}$, then

$$\Theta_0 = \Theta_n = ce. \tag{11}$$

We shall assume that the system possesses the property $\Theta_0 > 0$.

---

* ['ch' ≡ 'cosh'; 'th' ≡ 'tanh' – editor's note.]

We note that the magnetization calculated from (4) can be written as

$$M = \frac{\Theta}{\Theta_n} X. \tag{12}$$

Eliminating X from (9) we obtain relations for M which agree with the equations of the theory of the internal molecular field [3]. The general solution of (9) can only be obtained numerically.

When $\Theta \sim 0$ for the state sum (8) it is possible to obtain the approximate formula

$$Z^{1/N} \simeq 2\left[\operatorname{ch}\frac{\Theta_0 + h}{\Theta}\operatorname{ch}\frac{\Theta_0 - h}{\Theta}\right]^{1/2} \exp\left\{-\frac{\Theta_0}{2\Theta}\right\}, \tag{13}$$

which when (11) is assumed agrees with the expression that follows from (5) directly at low temperatures. For temperatures such that $\Theta < \Theta_0$ but $h/\Theta \ll 1$ the equations of (9) can be written as

$$\operatorname{th} Y = \frac{\Theta}{\Theta_0} Y, \quad H - X = \frac{\Theta}{\Theta_n} X \operatorname{ch}^2 Y. \tag{14}$$

The temperature Θ_0 at which Y vanishes is the Curie point. In the neighborhood of Θ_0 the expression for the magnetic susceptibility is

$$\chi = \frac{\mu^2}{\Theta_n + \Theta\left[1 + 3\left(\frac{\Theta}{\Theta_0}\right)^2 \frac{\Theta_0 - \Theta}{\Theta_0}\right]}. \tag{15}$$

Using the expression for the mean energy calculated for a particle:

$$\overline{E} = -\frac{\Theta}{\Theta_n} hX - \frac{1}{2}\frac{\Theta^2}{\Theta_0} Y^2 + \frac{1}{2}\frac{\Theta^2}{\Theta_n} X^2, \tag{16}$$

the specific heat can be obtained in units of the Boltzmann constant to the right of the Curie point for $\Theta \to \Theta_0$:

$$c = \frac{3}{2} - h^3\left[\frac{1}{\Theta_0(\Theta_0 + \Theta_n)} - \frac{\Theta_0 - \Theta_n}{(\Theta_0 + \Theta_n)^2}\right]. \tag{17}$$

In the paramagnetic region $\Theta > \Theta_0$ we have Y = 0; therefore the analytic form of (8) and (9) agrees except for the sign of Θ_n with the corresponding expressions for an Ising ferromagnetic [2], (6) and (7) . Noting that the condition $h/\Theta \ll 1$ is satisfied for all practical fields we can use (12), (9), and (16) to obtain expressions for the magnetic susceptibility and specific heat:

$$\chi = \frac{\mu^2}{\Theta + \Theta_n}. \tag{18}$$

$$c = \frac{\Theta h^2}{(\Theta_n + \Theta)^2}. \tag{19}$$

Comparing (19) and (17) we note that the specific heat at the point $\Theta = \Theta_0$ shows a discontinuity which in the absence of an external field amounts to $^3/_2$.

For a binary alloy the mean energy is defined by

$$\overline{E} = \frac{1}{8}\sum_i \{e^{11}(i-j) + e^{22}(i-j) + 2e^{12}(i-j)\} - \frac{M\Theta^2}{2}\frac{\partial}{\partial\Theta}\frac{\mu_1 - \mu_2}{\Theta} + {} \\ + \Theta^2 M \frac{\partial H}{\partial\Theta} - \frac{\Theta^2}{2\Theta_0} Y^2 + \frac{\Theta^2}{2\Theta_n} X^2. \tag{20}$$

In the paramagnetic region $\Theta > \Theta_0$ the energy of the alloy is found to be independent of temperature.

In the antiferromagnetic region solutions such as (14), (15), and (17) cannot be obtained since the "magnetic field" $\underline{h}$ is not a small quantity (as in the problems of an adsorbed monolayer and cellular gas); therefore (9) must be solved numerically. An exception is provided by a 50% alloy when M = 0. Then, as can be seen from (12) and (9), H = X = 0, and (14) is correct. Defining long-range order by the expression

$$\xi = \frac{e^{Y} - e^{-Y}}{e^{Y} + e^{-Y}} = \operatorname{th} Y,$$

we obtain from (20) and (14) the relations for the energy of the alloy:

$$E = E_0 - \frac{\Theta_0}{2}\xi^2, \qquad \operatorname{th}\frac{\Theta_0}{\Theta}\xi = \xi,$$

which agree with the Bragg-Williams equations, the first equation having been essentially a theoretical assumption.

In conclusion I wish to express my sincere thanks to Academician N. N. Bogoliubov who suggested the subject of this note.

LITERATURE CITED

[1] C. F. Newell and E. W. Montroll, Rev. Mod. Phys. 25, 353 (1953); P. W. Kasteleijn, Physica 22, 397 (1956); R. Peierls, Proc. Cambr. Phil. Soc. 32, 471 (1936).

[2] I. A. Kvasnikov, Doklady Akad. Nauk SSSR 110, 5, 755 (1956).

[3] T. H. Van Vleck, J. Chem. Phys. 9, 369 (1941).

Received June 26, 1956

M. V. Lomonosov Moscow State University

ON THE PROBABILITY OF ELECTRON CAPTURE BY NEUTRAL ATOMS IN TRIPLE COLLISIONS

Iu. S. Saiasov

(Presented by Academician V. N. Kondrat'ev November 27, 1956)

Electron capture by neutral atoms or molecules in the presence of a third (heavy) particle which acquires the excess energy play an important part in many phenomena (ionization during combustion, gas discharge, the ionosphere). However we have at present no information, either theoretical or experimental, regarding the probability of this process which is even qualitatively correct. Recently there have been published some quite accurate measurements of the cross section of the reverse process [1], which is the detaching of an electron from a negative atomic hydrogen ion in collision with a hydrogen molecule: $H^- + H_2 = H + H_2 + e$, measured by irradiating hydrogen with a monoenergetic H^- beam. In the present note we calculate the electron capture coefficient α cm^6/sec in the process $e + H + H_2 = H^- + H_2$ from the cross sections for $H^- + H_2 = H + H_2 + e$.

In equilibrium the total numbers of collisions of the two kinds are equal, giving

$$\alpha\,(e)\,(H)\,(H_2) = \alpha^{*}\,(H^-)\,(H_2) \tag{1}$$

(the densities of H^- and H are assumed to be small compared with the density of H_2). From (1), knowing the ionization coefficient α^{*}, we can calculate α:

$$\alpha = \alpha^{*}\frac{(H^-)}{(e)\,(H)} = \alpha^{*}K\,(T), \tag{2}$$

where $K(T) = \frac{(2\pi)^{3/2}}{4}\,\frac{h^3}{(mkT)^{3/2}}\,e^{\Delta E/kT} = 3.25\cdot 10^{-21}\,\theta^{-3/2}e^{8.7/\theta}$ is the equilibrium constant of $H^- \rightleftharpoons H + e$ ([2], p. 332); $\Delta E = 0.747$ ev is the ionization energy of H^-; m is the electron mass; $\theta = T\,°K/1000$; $h = 1.05\cdot 10^{-27}$ erg-sec.

The magnitude of α^{*} can be determined from the data of [1] as follows. It follows from very general considerations that the ionization cross section on the assumption that the effective collision time is a/v (a is the effective diameter and v is relative velocity of the colliding particles) is much greater than the transition time between electronic states of a system with energy difference ΔE, which is $2\pi h/\Delta E$, will be described by the formula [3]

$$\sigma = \sigma_0 e^{-c\Delta Ea/2\pi hv}, \qquad c \sim 1. \tag{3}$$

The data of [1] for H^- energies from 6.8 to 75 ev can actually be represented with sufficient accuracy by the empirical formula

$$\sigma = 1.67\cdot 10^{-16}e^{-5.7\cdot 10^{6}/v},$$

where $\exp(-5.7\cdot 10^6/v)$ is of reasonable magnitude since for $\Delta E = 0.747$ ev $\Delta Ea/2\pi hv = 2\cdot 10^6/v$. The coefficient α^{*} cm^3/sec is the evident result of averaging σv over the Maxwellian distribution of the velocities of H^- and H_2:

$$\alpha^{*} = \sigma_0 v_T \frac{4}{\sqrt{\pi}} \int_0^{\infty} e^{-\varkappa/c - c^2} c^3 dc, \tag{4}$$

where $v_T = (2kT/\mu)^{1/2}$; $\mu = {}^2/_3 m_H$ is the reduced mass of H^- and H_2; $c = v/v_T$; $\kappa = 5.7 \cdot 10^6/v_T$. For $\kappa \gg 1$, which is assumed hereinafter, the integral of (4) is easily calculated by the method of steepest descent. The function $-(\kappa/c + c^2)$ has a maximum at $c_m = (\kappa/2)^{1/3}$ and the principle role is played by the region of values of c close to c_m, i. e., we can use the expansion $\kappa/c + c^2 = 3(\kappa/2)^{2/3} + 6(c - c_m)^2 + \ldots$. Hence we easily obtain *

$$\alpha^{*} = \sigma_0 v_T \frac{1}{\sqrt{3}} \varkappa e^{-3(\varkappa/2)^{2/3}} = 5.50 \cdot 10^{-10} e^{-9.6/\theta^{1/3}}. \tag{5}$$

The final expression for the capture coefficient α is therefore

$$\alpha = 1.8 \cdot 10^{-30} \theta^{3/2} e^{-0.6/\theta^{1/3} + 8.7/\theta} \text{ cm}^6/\text{sec}$$

We present a table of values of α:

θ	1	1.5	2	2.5	3	3.5
α	$0.74 \cdot 10^{-30}$	$1.08 \cdot 10^{-31}$	$2.5 \cdot 10^{-32}$	$1.34 \cdot 10^{-32}$	$0.78 \cdot 10^{-32}$	$0.61 \cdot 10^{-32}$

These values of α give a preliminary idea of the orders of magnitude of the electron capture coefficient for various atoms and molecules with the participation of a third particle in the indicated temperature range. It must be noted that the values of α obtained here are much greater than those determined by the approximate formula given in [6], p. 39:

$$\alpha \sim \sigma_H \sigma_{H_2} a \lambda v_{el} \sim 10^{-34} - 10^{-35} \text{ cm}^6/\text{sec}$$

where σ_H and σ_{H_2} are the geometric cross sections of H and H_2; a is of the order 10^{-8} cm, $\lambda \sim 10^{-2}$ is the probability of electron energy transfer to H_2 molecules; $v_{el} \sim 10^7$ cm/sec is the electron velocity at $T \sim 1000°K$.

I wish to thank Professor A. S. Kompaneits for a discussion of the results.

LITERATURE CITED

[1] E. E. Muschlitz, T. L. Bailey, and J. H. Simons, J. Chem. Phys. 24, 1202 (1956).

[2] L. D. Landau and E. M. Lifshits, Statistical Physics (1951).

[3] H. S. Massey and E. H. Burhop, Electronic and Ionic Impact Phenomena (Oxford, 1952), p. 515.

[4] L. Landau, Physik Z. Sovietunion 2, 46 (1932).

[5] Collection, Problems of Modern Physics 1954, No. 1.

[6] H. S. Massey, Negative Ions (Oxford, 1938).

Received November 22, 1956

Institute for Chemical Physics, USSR Academy of Sciences

---

* It is known that a formula similar to (5) is obtained for the probability of thermonuclear reactions (see [5], for example).

THE OPTICAL CONTACT BETWEEN MICA AND GLASS

E. S. Trekhov

(Presented by Academician P. A. Rebinder December 12, 1955)

Glass-glass and mica-mica contacts have been thoroughly studied [2, 3]. The contact between a cleavage surface of mica and a polished glass surface was an object of attention a long time ago [1]. But the possibility of optical contact ("adhesion") of mica and glass was denied [4].

We have established that optical contact with glass can be made by sufficiently thin (about 5μ) mica leaves which are placed in contact immediately after cleavage in air. The condition of the polished glass surface strongly affects not only the character of the contact but its very possibility. The greatest success in making the contacts results when the glass surfaces are purified in a high-frequency (corona) glow discharge and after purification are in contact for not less than 15 minutes with air.

A contact between mica and glass never produces large surfaces of firm contact. It should be noted that a mica leaf which is freshly cleaved and placed on a glass surface that has just been subjected to an electric discharge does not form an optical contact even under high pressure [5]. When such a leaf slides along a glass surface the two surfaces are strongly and irregularly locked together. This is similar to what happens when very rough surfaces slip along each other [6]. The mica surface is heavily scratched in the process.

All of the mica-glass contacts observed by the author can be divided into two types.

The first type consists of optical contacts with large contact surfaces. The boundary of the contact break in the microregion is usually rectilinear; when observed in reflected monochromatic light the interference ring width is constant. From the character of the interference pattern the contact boundary cannot easily be distinguished from that which is observed in mica cleavage. This is evidence of highly constant molecular forces of adhesion between the surfaces in contact. Such a contact can be called homogeneous. Figure 1 shows the characteristic appearance of the interference pattern in homogeneous contacts. This photograph gives an idea of the shape of the contact boundary.

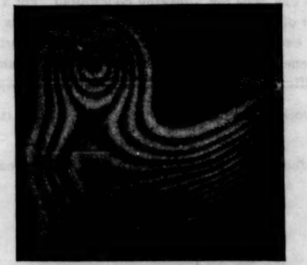

Fig. 1. A part of an optical contact boundary between mica and glass. Homogeneous contact. Instant of formation of the membrane spot λ = 0.53μ. 40 ×.

The second type of contact is characterized by an irregular shape of boundary, varying curvature of the separated leaf and varying interference ring width. This type of contact, which we have called inhomogeneous, is found more frequently than homogeneous contact. In this case the contact is made with great difficulty. This is evidence of the fact that the strength of the contact forces varies greatly from point to point on the contact surface; in my opinion this corresponds to a microheterogeneous structure of the glass surface.

By varying the process of purification of the glass surfaces it is possible to vary the type of contact with mica. Thus, for example, purification with alcohol, distilled water, (corona) glow discharge followed by exposure to air for 15-20 min. usually resulted in the first type of contact. Treatment with a strong flame or corona discharge followed by immediate placing in contact resulted in the second type if any.*

As in the case of mica-mica contacts we established the degree of restoration of a mica-glass contact. As was to be expected, in the case of an inhomogeneous contact the slightest separating force made it impossible to reestablish the contact after separation. When the separating wedge is withdrawn the curvature of the mica leaf is very strongly reduced, and the interference bands spread, become distorted or disappear entirely without optical contact. The transition from the contact region to the region of separation remains at its previous location. The contact can be restored only to a very small extent and only with strong external pressure on the mica.

For homogeneous contact the results were exactly opposite. Optical contact was often completely restored by simple reduction of the separating force. The separation boundary could be repeatedly moved on the contact surface without greatly charging the interference ring width or curvature of the leaf. This shows that neither macro- nor microchanges occurred in the contact region.

When the separation boundary was shifted in the region of homogeneous contact we observed an interesting "memory" effect of the contiguous surfaces; there was not simply a restoration of the contact but its identical reproduction in all stages of separation and contact. It was striking that it was almost impossible to distinguish the topography of the contact surface before beginning separation and after returning the separation boundary to its previous location.

TABLE 1

Calculation of membrane spots $f = k\frac{Pa^2}{Eh^3}$

f is the depth of curvature(in numbers of rings), a is the diameter of a spot (in arbitrary units) Mica-glass. Experiment No. 86-87

Photo No.	f	a	$\frac{f}{a^2}$
18	6.5	13.0	0.038
18	2.5	8.0	0.039
10	2.5	8.0	0.039
10	0.5	3.5	0.041
19	6.0	12.5	0.038
19	16.0	21.0	0.036

$$\left(\frac{f}{a^2}\right)_{\text{av}} = (38.0 \pm 0.7) \cdot 10^{-3}.$$

The so-called "membrane spots" are an interesting formation on the mica-glass contact surface. These are gas bubbles with the bounding mica film stretched like a thin elastic membrane. The membrane spots observed in homogeneous contact have regular round shapes — and a constant interference ring width. A heterogeneous contact region is speckled with membrane spots of various sizes, partly of irregular shape and with varying interference ring width even within a single spot. It was of interest to determine whether the membrane spots are purely air bubbles or are formed by some kind of unevenness or dirt particles. An investigation of the cross sectional shape of a spot confirmed its similarity to the shape of a circular membrane fastened along its edge with a load concentrated at its center. The calculated and experimental shapes of the cross sections [7] are in good agreement. This enabled us to perform a number of calculations.

Using the familiar formula for the sagging of a thin circular membrane due to a load concentrated at its center we can draw the following conclusions. For a homogeneous contact the ratio of the square of the visible diameter of "membrane spots" to the depth (sag) is constant (see Table 1). For a heterogeneous contact these ratios differ even for two neighboring spots; this is certain evidence of the inhomogeneity of the contact surface. A homogeneous contact form is evidently always associated with a high degree of purity of a surface which was also in sufficiently prolonged contact with the atmosphere.

Calculation shows that for a homogeneous contact the work of formation of a unit of spot surface is constant, which is in good agreement with all other facts.

The work of separation of an optical contact was measured by the method described in [2]. The calculation used the formula

$$Q = \frac{1}{24}\frac{Ey^2h^3}{x^4},$$

---

* According to the author's observations, confirmed by an oral communication of E. P. Osmolovskii, this method of purification results in very strong adhesion of glass and a polished steel surface in air.

where E is the flexural modulus of curvature; h is the thickness of the leaf; y is the sag at distance x from the zero ring.

The work of separation under our conditions was 13 ergs/cm^2 for the initial separation of the mica-glass boundary and changed only slightly. After prolonged action of a separating strain the boundary is displaced, the separating force is reduced and the work of separation is fixed at 9 ergs/cm^2. The spread of values which was insignificant for a quantity of this kind, amounted to as much as 50% of the measured value.

I consider it a duty to thank Associate Academician I. V. Obreimov for suggesting the research and for directing it.

LITERATURE CITED

[1] N. K. Adam Physics and Chemistry of Surfaces (1947).

[2] I. W. Obreimov, Proc. Roy. Soc. (A) 127, 290 (1930).

[3] E. S. Trekhov, Dissertation, Moscow Inst. of Eng. Physics, 1954.

[4] V. D. Kuzentsov, Physics of Solids (USSR) 5 (1950).

[5] V. V. Karasev and G. I. Izmailova, J. Tech. Phys. (USSR) 24, 5, 871 (1954).

[6] A. Strong, Techniques of Physical Experiments (1952) (Russian translation).

[7] L. D. Landau and E. M. Lifshits, Mechanics of Continuous Media (1954).

Received December 10, 1955

Moscow Institute of Engineering Physics

DETERMINATION OF DIFFERENTIAL ELASTIC SCATTERING CROSS SECTIONS FOR 14.8-MEV NEUTRONS BY (n,α) COINCIDENCES [1]

M. M. Khaletskii

(Presented by Academician V. N. Kondrat'ev November 13, 1956)

The neutron source was the $D^2(T, n)He^4$ reaction. The alpha particles emitted by the source at 135° to the deuteron beam were recorded by an FEU-19 photomultiplier with a thin NaI(Tl) crystal. After emerging from the target the neutrons correlated with the alpha particles traversed a narrow channel bored through a shield of iron of thickness d_1= 260 mm (Fig. 1). The shield reduced the count of random (n, α) coincidences. Immediately behind the shield were cylindrical scatterers of 25 mm diameter and length d = 22 mm to 25 mm. During the measurements the scatterers were shifted in and out of the neutron beam by a special device. Neutrons were recorded by a toroidal liquid scintillation counter. The torus was made of a thin-walled glass tube (inside diameter 20 mm). The average diameter of the torus was 18 cm. The torus contained a 2% solution of terphenyl in m-xylene. The scintillation torus was placed in an aluminum reflector: the narrow base of the reflector was turned toward the cathode of the FEU-19. For variation of the angle θ at which neutron scattering was being investigated the torus was shifted with respect tothe scatterer.

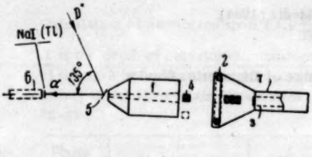

Fig. 1. Scheme of measurement of σ(θ): 1) Fe shield; 2) scintillation torus; 3) FEU-19; 4) scatterer; 5) target; 6) alpha counter; 7) reflector.

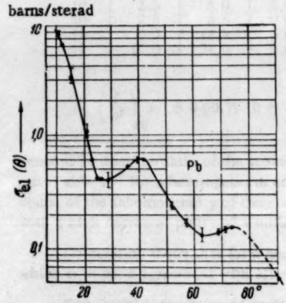

Fig. 2. Measured cross sections σ (θ) for Pb. Errors are shown only for points at which several measurements were made.

The resolving time of the concidence circuit was $\tau = 2 \cdot 10^{-8}$ sec; simultaneously with the concidences the circuit recorded alpha particles and neutrons in channels. In the neutron channel circuit the pulse cutoff corresponded to the neutron threshold of $E_n \approx 11.5$ Mev. Variation of the time of flight of neutrons by shifting of the torus with respect to the scatterer was corrected by inserting suitable sections of coaxial cable into the alpha channel.

The cross section σ(θ) was measured by counting: 1) (n, α) coincidences with a scatterer (N_p); 2) (n, α) coincidences without a scatterer (Φ-background); 3) neutrons striking the torus from the target at a given position (N_n). For measurement of N_n the neutron counter was rotated around the target on the iron shield side.

The investigation showed that the background of the coincidence count was 90 ± 10% caused by the fact that the cathode of the FEU-19 counts 14-Mev neutrons. Special experiments showed that attenuation of the background in the presence of a scatterer follows the law $\Phi e^{-n\sigma_t d}$, where σ_t is the total neutron cross section for E_n = 14 Mev and n is the number of nuclei in 1 cm³ of the scatterer.

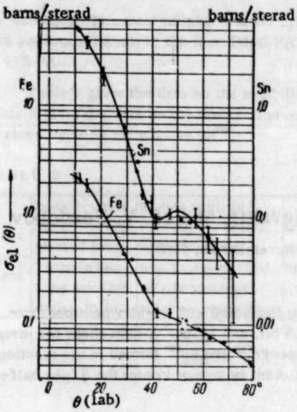

Fig. 3. Measured cross sections σ (θ) for Sn and Fe.

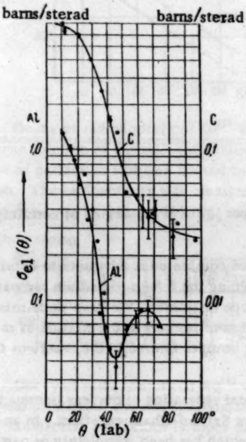

Fig. 4. Measured cross sections σ (θ) for Al and C.

The cross sections σ (θ) were calculated from the formula

$$\sigma(\theta) = \frac{N_p - \Phi e^{-n\sigma_t d}}{aN_n}\,\frac{r^2}{r_\theta^2}\cdot \Pi\,(\theta).$$

(This formula is correct on the assumption that the diameter of the scatterer d ≪ r.) Here r is the scatterer-torus separation; r_0 is the distance from the torus to the center of the target; $a = k_1 k_2 n \omega_\alpha d$; k_1 is the fraction of "correlated" neutrons which strike the scatterer; k_2 is the ratio of the alpha flux (per sterad) with the alpha counter forming the angle $\varphi_\alpha = 135°$ to the deuteron beam in the lab system, to the alpha flux in the c.m. system at the corresponding angle $\varphi_{c.m.}$; ω_α is the solid angle of the alpha counter with respect to the target.

The correction Π(θ) accounts for absorption of direct neutrons and neutrons scattered elastically at angle θ in scatterer volume v:

$$\Pi\,(\theta) \sim \int e^{-x/\lambda} e^{-r(\theta)/\lambda}\,dv \qquad \left(\lambda = \frac{1}{n\sigma_t}\right).$$

Π(θ) was calculated approximately by replacing r(θ) with $r_{av}(\theta)$ on the assumption that $r_{av}(\theta) < \lambda$, where $r_{av}(\theta)$ is the average neutron path in the volume v for scattering at angle θ.

During the measurements the coincidence counting rate was ~ 1 impulse/sec; the background Φ was 30 to 50% of the total count depending on the angle θ and the material of the scatterer. For reduction of the background Φ a Pb rod was inserted into the reflector (Fig. 1) (the procedure has now been improved by the fact that scintillations in the torus are registered simultaneously by two FEU-19's).

The cross sections σ(θ) measured for Pb, Sn, Fe, Al, and C are given in Figs. 2-4. Whenever measurements were repeated a few times Figs. 2-4 show the errors. The statistical error of a single measurement was ~15%. Our measurements agree with [2, 3], where a different method of measurement was used.

The authors are grateful to Acad. V. N. Kondrat'ev for his interest and to N. M. Meleshin for assistance with the measurements.

LITERATURE CITED

[1] M. M. Khaletskii, Report of Inst. Chem. Phys., Acad. Sci. USSR, March 13, 1953.

[2] I. O. Elliot, Phys. Rev. 101, 684 (1956).

[3] G. Culler, S. Fernbach, and N. Sherman, Phys. Rev. 101, 1047 (1956).

Received November 2, 1956

Institute for Chemical Physics, USSR Academy of Sciences

Pd^{111m}

B. G. Dzantiev, V. N. Levkovskii, A. D. Malievskii, and M. V. Serdobov

(Presented by Academician V. N. Kondrat'ev November 23, 1956)

In an earlier article [1] it was established that when cadmium is irradiated with 14-Mev neutrons three palladium radioactivities are observed, with the half-lives 22 min, 5.5 hrs, and 14 hrs. A radiochemical investigation showed that T = 22 min and 14 hrs belong to the known isotopes Pd^{111} and Pd^{109} formed in the reactions $Cd^{114}(n,\alpha)Pd^{111}$ and $Cd^{112}(n,\alpha)Pd^{109}$. It was not shown to which palladium isotope or isomer the 5.5-hr half-life can be ascribed.

The literature contains only one brief report [2] to the effect this half-life was observed when palladium was irradiated with deuterons and was identified with the isomer Pd^{111m} which decays according to the scheme

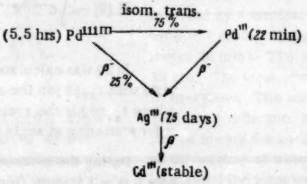

On this basis Pd^{111m} was included in Seaborg's 1953 tables of isotopes [3] with the degree of certainty "B". However it is not found in the 1954 tables of Nesmeianov [4].

TABLE 1

No. of experiment	Volume of saturated solution of $Pd(C_7H_6O_2N)_2$ in benzene, ml	Weight of $Pd(C_7H_6O_2N)_2$ separated from solution, mg	Solubility, mg/100 ml
1	10	7.3	73
2	10	7.0	70
3	10	7.9	79

We therefore considered it advisable to obtain clear evidence for assigning the 5.5-hr palladium radioactivity to a definite isotope or isomer. We have performed a chemical separation of isomers in the mixture of radioactive palladium isotopes formed in the reactions $Cd(n,\alpha)$ and $Pd(n,\gamma)$.

The chemical separation of nuclear isomers is based on the well-known Szilard-Chalmers effect. In an isomeric transition which has been completely or partly converted the atoms in the ground state are multiply ionized, that is, they change their valence and consequently, their chemical properties and can under certain conditions be separated from the atoms of the parent isomer by ordinary chemical methods. The most favorable conditions for successful separation are the following: the isomer in the higher excited state enters an organic compound which is soluble in organic solvents and is insoluble in water. The inorganic ions of the daughter isomer leave the organic molecules after the isomeric transition, are simply washed out with water, and are then precipitated with a carrier by a specific precipitant.

In developing a method of separating palladium isomers we tested several organic reagents which form water-insoluble compounds with palladium: dimethylglyoxime, acetoxime, salicylaldoxime, and α-nitrosoβ-naphthol. The most suitable was salicylaldoxime, which selectively precipitates palladium from strongly acid aqueous solutions in the form $Pd(C_7H_6O_2N)_2$. The precipitate after drying at 110° is of constant composition: 28.17% Pd.

Table 1 gives the data on the solubility of palladium salicylaldoximate in benzene obtained by weighing; Table 2 gives the data on the distribution coefficient of palladium salicylaldoximate between benzene and water, obtained by using radioactive Pd^{109}.

TABLE 2

No. of experiment	Radioactivity of Pd^{109} precipitated from 1 ml of a benzene solution, pulses/min	Radioactivity of Pd^{109} in H_2O (100 ml) after shaking together with 1000 ml of a benzene solution, pulses/min	water/benzene distribution coefficient
1	35100	430	$1.2 \cdot 10^{-4}$
2	32500	560	$1.7 \cdot 10^{-4}$
3.	36800	550	$1.5 \cdot 10^{-4}$

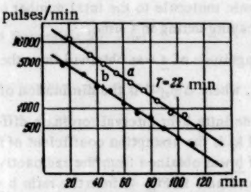

Fig. 1. Decay of radioactivity of Pd^{111} washed from a benzene solution of the salicylaldoximate of a mixture of palladium isotopes formed by the (n, γ) reaction. The radioactivity was measured: a) through 310 mg /cm² Al; b) through 440 mg/cm² Al.

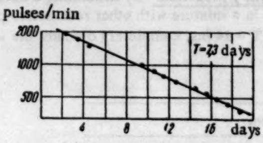

Fig. 2. Decay of radioactivity of Ag^{111} washed from a benzene solution of the salicylaldoximate of a mixture of radioactive palladium isotopes formed by the (n, γ) reaction.

It follows from Tables 1 and 2 that the salicylaldoximate is suitable for the separation of palladium isomers; it dissolves satisfactorily in benzene (70 mg/100 ml) and less by 4 orders of magnitude in water.

Separation of the isomers Pd^{111m} and Pd^{111} formed by $Cd^{114}(n, \alpha)Pd^{111}$. 400 g of cadmium nitrate were irradiated for 4 hrs in a 14-Mev neutron beam of ~ 10^7 neutrons /cm²-sec. The irradiated salt was dissolved in water and palladium salicylaldoximate was precipitated from the solution with a carrier (100 mg). The solution above the precipitate was poured off and the precipitate was washed several times with a 1% solution of nitric acid until the wash water showed no trace of unbound salicylaldoximate. The washed precipitate was dissolved in 200 ml of hot benzene, the solution was diluted with 2 liters of cold benzene and washed a few times with water and an acid (pH ~ 1) solution of $Pd(NO_3)_2$ (until we obtained a transparent lemon yellow solution which forms a layer quickly and cleanly in water).

Ten hours after the end of the irradiation the benzene solution was vigorously shaken in a separating funnel with 150 ml of an acid (pH ~ 1) aqueous solution of $Pd(NO_3)_2$ (50 mg). The water layer was removed and the palladium in it was precipitated by dimethylglyoxime. The precipitate was quickly dried and its radioactivity was measured by a Geiger counter. The radioactivity had a 21.5 min half-life, which is in good agreement with the half-life of Pd^{111} given in the literature.

It was thus proved that a mixture of radioactive palladium isotopes formed by Cd(n, α)Pd reactions contains Pd^{111m}, which is genetically related to Pd^{111} (T = = 22 min).

Identification of Pd^{111m} (T = 5.5 hrs) in a mixture of radioactive palladium isotopes formed in Pd(n, γ) reactions. 50 mg of metallic palladium was irradiated for 1 hr in a fission neutron flux of ~ $5 \cdot 10^{11}$ neutrons /cm²-sec. The irradiated metal was dissolved in aqua regia and the palladium was precipitated by salicylaldoxime. The precipitate was washed and dissolved in benzene as described above. The solution was divided into two equal parts. By means of shaking together with solutions of carriers every 2 hrs for one day Pd^{111} was separated from one part and Ag^{111} from the other. The palladium was then precipitated from an aqueous solution of dimethylglyoxime and the silver from hydrochloric acid.

Figure 1 shows typical decay curves of the radioactivity of palladium precipitates. The radioactivity of the precipitates was measured through aluminum filters of 310 mg/cm²(a) and 440 mg/cm² (b). In measurements without absorbers the 22-min half-life of Pd^{111} considerably distorts the 14-hour decay of Pd^{109} whose

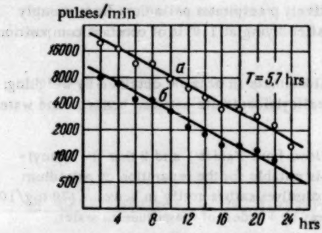

Fig. 3. Curves of Pd^{111m} decay obtained by repeated separation at equal time intervals of the daughter Pd^{111} (22 min) (a and b, see Fig. 1).

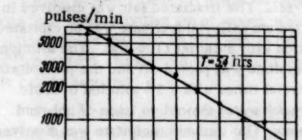

Fig. 4. Pd^{111m} decay curve obtained by repeated separation of the daughter Ag^{111} (7.3 days).

yield from the (n, γ) reaction is a few orders higher than that of Pd^{111m}. Figure 2 shows a typical decay curve of the radioactivity of silver precipitates. Figures 3 and 4 illustrate the kinetics of the variation of initial radioactivities of Pd^{111} and Ag^{111} as a function of the time of separation. Both radioactivities decay with $T \approx 5.5$ hrs, which is in good agreement with the half-life of Pd^{111m} given in the literature.

Thus it was established that Pd^{111m} with $T = 5.5$ hrs is formed in a $Pd(n, \gamma)$ reaction and its genetic relation was shown to Pd^{111} ($T = 22$ min) and Ag^{111} ($T = 7.5$ days).

The data of this experiment were used to evaluate the internal conversion coefficient of the isomeric transition $Pd^{111m} \rightarrow Pd^{111}$. Since separation of the isomers can be expected only in case of a converted transition the lower limit of the internal conversion coefficient can be defined as the ratio of the number of Pd^{111m} atoms (a) decaying during a definite time interval and escaping from the organic molecule to the total number of Pd^{111m} atoms (b) decaying during this time.

The magnitude of a was obtained from the ratio $a = \frac{\Delta I_{Pd^{111}}}{k_1}$, where $\Delta I_{Pd^{111}}$ is the diminution of Pd^{111} activity in a definite 2-hr interval (ordinate difference in Fig. 3) and k_1 is the absorption coefficient of Pd^{111} emission in the aluminum filter and counter wall. The magnitude of b was obtained from the radioactivity of Ag^{111} accumulated during the same time interval (the corresponding ordinate in Fig. 4) from the ratio $b = \frac{I_{Ag^{111}}}{k_2}$ (k_2 is the absorption coefficient of Ag^{111} radioactivity in the counter wall).

The internal conversion coefficient calculated in this way was $\alpha = \frac{a}{b} \geq 0.185$. Taking into account the given decay scheme of $Pd^{111m} \rightarrow Pd^{111}$, $\alpha \geq 0.185 : 0.75 = 0.25$.

Determination of the relative yields of Pd^{111} and Pd^{111m} in the (n, γ) reaction. By irradiating a natural mixture of palladium isomers with thermal neutrons Pd^{111m} is formed in a mixture with other radioactive palladium isotopes. The radioactivity of the latter, principally Pd^{109} with $T = 14$ hrs, completely obscures the weak radioactivity of Pd^{111m}. It is therefore impossible to determine the yield of Pd^{111m} from its radioactivity in this case. In the present work the relative yields of Pd^{111m} and Pd^{111} were determined by investigating the kinetics of accumulation of radioactive silver in samples of irradiated palladium.

TABLE 3

Time after termination of of irradiation, hrs	Radioactivity of precipitates			
	1	2	3	Average
5.5	$3.78 \cdot 10^6$	$3.82 \cdot 10^6$	$3.78 \cdot 10^6$	$(3.79 \pm 0.02) \cdot 10^6$
15	$5.95 \cdot 10^4$	$6.70 \cdot 10^4$	$5.75 \cdot 10^4$	$(6.13 \pm 0.38) \cdot 10^4$
27	$1.91 \cdot 10^4$	$1.89 \cdot 10^4$	$2.20 \cdot 10^4$	$(2.00 \pm 0.13) \cdot 10^4$
80	$7.00 \cdot 10^3$	$5.80 \cdot 10^3$	$5.70 \cdot 10^3$	$(6.10 \pm 0.53) \cdot 10^3$

0.5 g of metallic palladium was irradiated with fission neutrons for 15 minutes. The irradiated metal was dissolved in aqua regia and the solution was divided into three parts. In each part of the silver was precipitated (by repeated addition of a carrier) 5.5, 15, 27, and 80 hrs after termination of the irradiation. The AgCl precipitates were reprecipitated from ammonia and dried and their radioactivity was measured by a Geiger counter. The results are given in Table 3.

The relative Pd^{111} and Pd^{111m} yields were calculated from these data as follows: the radioactivity of silver precipitated in 5.5 hrs ($I_{5.5\,hrs}$) results from the decay of all of the Pd^{111} (22 min) and half of the Pd^{111m} (5.5 hrs); the sum of the radioactivities of Ag^{111} precipitated in 15, 27, and 80 hrs (ΣI) results from the decay of the remaining half of Pd^{111m} (according to Table 3 it is easily seen that the radioactivities precipitated at 15, 27, and 80 hrs are genetically related only to the 5.5-hr ancestor). Hence $\sigma_{Pd^{111}}/\sigma_{Pd^{111m}} = (I_{5.5\,hrs} - \Sigma I)/2\Sigma I = (3.79 \cdot 10^6 - 8.73 \cdot 10^4)/2 \cdot 8.73 = 22$.

LITERATURE CITED

[1] B. G. Dzantiev, V. N. Levkovskii, and A. D. Malievskii, Doklady Akad. Nauk SSSR 113, 3, 537 (1957).

[2] C. L. McGinnis, Phys. Rev. 87, 202 (1952).

[3] I. M. Hollander, I. Perlman, and G. T. Seaborg, Rev. Mod. Phys. 25, 2, 469 (1953).

[4] An. N. Nesmeianov, A. V. Lapitskii, and N. P. Rudenko, The Production of Radioactive Isotopes (Moscow, 1954).

Received November 20, 1956

Institute Chemical Physics, USSR Academy of Sciences

ON THE APPLICATION OF A VARIATIONAL PRINCIPLE TO BINARY ALLOYS IN THE ISING SYSTEM

I. A. Kvasnikov

(Presented by Academician N. N. Bogoliubov November 14, 1956)

As was shown in an earlier note [2], for the determination of the statistical sum of a binary alloy it is necessary to solve an auxiliary problem concerning an Ising antiferromagnetic. In the present note by using the variational principle of N. N. Bogoliubov [2] a different division of the antiferromagnetic Hamiltonian will be made ([2](1)), wherein some of the terms of $\mathscr{H}_1$ are transferred to $\mathscr{H}_0$ so that $Z_0 = \mathrm{Sp}\left\{\exp(-\mathscr{H}_0)\right\}$ can be calculated. Namely, $\mathscr{H}_0$ includes the interaction terms of groups of neighboring sites; the interaction between these groups and the interaction with distant neighbors remains in $\mathscr{H}_1$. These groups are most simply chosen to be pairs of sites. For simplicity we neglect the interaction with distant neighbors, which can be allowed for analogously [2]. An increase of the number of sites in each group included in $\mathscr{H}_0$ (for the next approximation it is natural to choose groups each of which consists of a central site and the "cloud" of all nearest neighbors) will evidently by increase of the calculated part lead to a better approximation.

We shall use the letter $\mathscr{H}$ to denote the Hamiltonian divided by the temperature θ; B is the magnetic field in Bohr magnetons divided by θ; N is the number of lattice sites; $E = e/\theta$ is the volume integral divided by the temperature. We shall assume that all lattice sites are equivalent and that opposite crystal boundaries are joined. Accordingly for an antiferromagnetic we have

$$\mathscr{H} = \mathscr{H}_0 + \mathscr{H}_1 = \frac{1}{2} E \sum_{\langle ij \rangle} \sigma_i \sigma_j - B \sum_{i=1}^{N} \sigma_i, \tag{1}$$

$$\mathscr{H}_0 = \sum_{l-1}^{N/2} \mathscr{H}_{2l}, \quad \mathscr{H}_k = -(B-\beta_0)\,\sigma_k - (B-\beta_1)\,\sigma_{k+1} + \varepsilon \sigma_k \sigma_{k+1}.$$

Here β_0 and β_1 are variational parameters referring to two sublattices; ϵ is a parameter which characterizes the effective interaction of a pair of neighboring sites. It is easily seen that for $\epsilon = 0$ this choice of $\mathscr{H}_0$ agrees with Eq. (6) of [2]. In accordance with the previously described method [1], (4) we obtain after some simple calculations: *

$$\begin{aligned}\frac{2}{N}\ln Z_{inf} &= 2\ln 2 + \ln\left[\operatorname{ch}\gamma_0 \operatorname{ch}\gamma_1 \operatorname{ch}\varepsilon - \operatorname{sh}\gamma_0 \operatorname{sh}\gamma_1 \operatorname{sh}\varepsilon\right] + \\ &+ \beta_0 \frac{\operatorname{th}\gamma_0 - \operatorname{th}\gamma_1 \operatorname{th}\varepsilon}{1-\operatorname{th}\gamma_0 \operatorname{th}\gamma_1 \operatorname{th}\varepsilon} + \beta_1 \frac{\operatorname{th}\gamma_1 - \operatorname{th}\gamma_0 \operatorname{th}\varepsilon}{1-\operatorname{th}\gamma_0 \operatorname{th}\gamma_1 \operatorname{th}\varepsilon} + (E-\varepsilon)\frac{\operatorname{th}\varepsilon - \operatorname{th}\gamma_0 \operatorname{th}\gamma_1}{1-\operatorname{th}\gamma_0 \operatorname{th}\gamma_1 \operatorname{th}\varepsilon} - \\ &- E(c-1)\frac{(\operatorname{th}\gamma_0 - \operatorname{th}\gamma_1 \operatorname{th}\varepsilon)(\operatorname{th}\gamma_1 - \operatorname{th}\gamma_0 \operatorname{th}\varepsilon)}{(1-\operatorname{th}\gamma_0 \operatorname{th}\gamma_1 \operatorname{th}\varepsilon)^2},\end{aligned} \tag{2}$$

where for convenience we have denoted $\gamma_0 = B - \beta_0$, $\gamma_1 = B - \beta_1$.

The variational parameters β_0, β_1, and ϵ are determined from the transcendental equations

$$\frac{\partial \ln Z_{inf}}{\partial \beta_0} = \frac{\partial \ln Z_{inf}}{\partial \beta_1} = \frac{\partial \ln Z_{inf}}{\partial \varepsilon} = 0. \tag{3}$$

---

* [In this paper 'sh' ≡ 'sinh', 'ch' ≡ 'cosh', 'th' ≡ 'tanh' – editor's note.]

As in [1, 2] we shall consider Z_{inf} to be an approximate expression for the statistical sum of the antiferromagnetic.

The magnetization per particle from (2) and (3) is given by

$$M = \frac{1}{2}\,\frac{(\text{th}\,\gamma_0 + \text{th}\,\gamma_1)(1 - \text{th}\,\varepsilon)}{1 - \text{th}\,\gamma_0\,\text{th}\,\gamma_1\,\text{th}\,\varepsilon}. \tag{4}$$

In order to avoid laborious calculation we shall consider the application of these results to a 50% binary alloy, using (2) and (4) of [2]. Assuming M = 0 we obtain from Eqs. (3) and (4):

$$B = 0;\quad \gamma_0 = -\gamma_1 = \gamma;\quad \varepsilon = E = \frac{e}{\theta}. \tag{5}$$

The average thermodynamical energy per alloy particle as determined by Eq. (20) of [2], will be

$$\overline{E} = \frac{\varepsilon_0}{8} - \frac{e}{2}\,\frac{c\,\text{th}^2\gamma\,(1 + \text{th}\,E)^2 + \text{th}\,E\,(1 - \text{th}^2\gamma)^2}{(1 + \text{th}^2\gamma\,\text{th}\,E)^2}, \tag{6}$$

where c is the number of nearest neighbors for the given lattice and ϵ_0 is a constant. The magnitude of γ is determined from

$$\gamma = E\,(c - 1)\,\frac{\text{th}\,\gamma\,(1 + \text{th}\,E)}{1 + \text{th}^2\gamma\,\text{th}\,E}. \tag{7}$$

From this equation it follows in particular that for $\theta > \theta_0$ we have $\gamma = 0$, with the critical temperature θ_0 determined by

$$1 = E_0\,(c - 1)\,(1 + \text{th}\,E_0), \tag{8}$$

where $E_0 = e/\theta_0$.

Thus, unlike [2], we find that for $\theta > \theta_0$ the average energy and specific heat of the alloy, calculated in units of the Boltzmann constant, are functions of the temperature:

$$\overline{E} = \frac{\varepsilon_0}{8} - \frac{e}{2}\,\text{th}\,\frac{e}{\theta}, \tag{9}$$

$$C = \frac{\partial \overline{E}}{\partial \theta} = \frac{e^2}{2\theta^2}\left(1 - \text{th}^2\,\frac{e}{\theta}\right). \tag{10}$$

The specific heat to the left of θ_0 can be obtained from (6) and (3):

$$C = \frac{[2\,(c-1)\,E_0 - 1]\,(6 + 4E_0) + 3\,(c - 1)}{2\,(c - 1)\,[3 - 2\,(c - 1)\,E_0]}. \tag{11}$$

In the simple case of a cubic lattice the numerical solution of (8) leads to $E_0 \cong 0.171$; then the specific heat on the left of the Curie point is $C \cong 1.535$ and on the right by Eq. (10) $C \cong 0.0142$, so that the discontinuity of the specific heat only slightly exceeds the amount of discontinuity which follows from the Bragg-Williams theory (see also [2]). It must also be noted that the values of E_0 obtained from (8) and (11) of [2] are of the same order of magnitude; for example, for c = 6 according to (11) of [2] we have $E_0 = 1.166$.

Applying the scheme described here to the Ising ferromagnetic system we obtain for the mean magnetic moment of a particle a formula which from the point of view of the variational principle of [1] is an improvement on the Weiss formula:

$$M = \frac{1}{N}\,\frac{\partial \ln Z}{\partial B} = \text{th}\,(B + J\,(c - 1)\,M)\,\frac{1 + \text{th}\,J}{1 + \text{th}^2\,(B + J\,(c - 1)\,M)\cdot\text{th}\,J}, \tag{12}$$

where J is the volume integral divided by the temperature θ. The equation for the critical temperature θ_0 analogous with (8) is

$$1 = J_0(c-1)(1+\operatorname{th} J_0). \tag{13}$$

In the practical case $B \ll 1$ for $\theta > \theta_0$ we obtain for the intensity of magnetic susceptibility

$$\chi \cong \frac{1+\operatorname{th} J}{\theta - \theta_0 J_0 (c-1)(1+\operatorname{th} J)}, \tag{14}$$

which differs from the Curie-Weiss law (see also [1]):

$$\chi \cong \frac{1}{\theta - \theta_0}.$$

Assuming in (12) $B = 0$ we obtain an equation for the spontaneous magnetization as a function of temperature. A direct calculation for the temperatures $\theta/\theta_0 = 1, 0.9, 0.8, 0.7, 0.6$ leads, respectively, to the values $M = 0.0, 0.533, 0.718, 0.838, 0.912$, which are somewhat higher than the values obtained through the Weiss theory: $M = 0.0, 0.525, 0.710, 0.828, 0.907$.

The relations for the energy and specific heat of an Ising ferromagnetic are analogous to (9)-(11).

From a similar examination of the Heisenberg model instead of (12) for the susceptibility we obtain the more complicated expression

$$M = \operatorname{th}\gamma \frac{1+\operatorname{th}J}{1+\operatorname{th}J\cdot\operatorname{th}^2\gamma + e^{-J}\operatorname{th}J\cdot\operatorname{sh}J\cdot(1-\operatorname{th}^2\gamma)},$$

where $\gamma = B + J(c-1)M$.

I am deeply grateful to Academician N. N. Bogoliubov who directed this work.

LITERATURE CITED

[1] I. A. Kvasnikov, Doklady Akad. Nauk SSSR 110, 5 (1956)

[2] I. A. Kvasnikov, Doklady Akad. Nauk SSSR 113, 3, 544 (1956)

[3] F. C. Nix and W. Shockley, Progr. Phys. Sci. USSR 20, 344 (1938) (Russian translation); G. F. Newell and E. W. Montroll, Rev. Mod. Phys. 25, 353 (1953).

Received November 12, 1956

M. V. Lomonosov Moscow State University

OPTICAL SYSTEMS WITH PHASE LAYERS

G. G. Sliusarev

(Presented by Academician V. P. Linnik July 16, 1956)

At the present time we know two types of optical systems for forming images of objects. The characteristic which distinguishes the two types is the variation of the length of the optical path with the aperture angle. In the ordinary well-known optical systems which consist of lenses and mirrors the length of the optical path from an object point to its image is constant or almost constant along all rays intersecting any point of the entrance pupil. For the second group of less familiar and less widely used optical systems, an example of which is a Soret plate or its modification (the zone plate of Wood [1] et al.) the length of the path is nonconstant and can be changed by any number of wavelengths, but steps are taken so that the length of the optical path for all points of the functioning part of the pupil can be represented by $a + k\lambda$, where a is the smallest possible part of a wavelength; k is any integer and λ is the wavelength.

It can be seen that "ordinary" optical systems are a special case ($k = 0$) of the second type. But under certain conditions the properties of the first type differ so much from those of the second type that the merging of these two types into one would be inadvisable from a practical point of view.

Systems of the second type have not been used in practice for three reasons: 1) all systems known at the present time collect not more than 40 % of the incident energy at a point; 2) they possess very appreciable and in principle uncorrectable chromatic aberration; 3) because of the huge number (of the order of thousands) of zones required to attain sufficient optical power there are great technological difficulties involved in the manufacture of such plates.

The only rational attempt to use a zone plate made by photographing Newton rings was that of O. E. Myers [2], who used it as the objective of a spectrograph; large chromatic aberration is here no longer an obstacle. However, the images were of poor quality and the required exposure time was 16 times greater than for a simple lens with the same relative aperture.

Raiskii's experiments [3] using dark rings deposited on spherical reflecting surfaces proved the existence of diffraction foci.

It is the purpose of the present article to direct attention to several possibilities for systems consisting of lenses and modified zone plates. As will be shown below all of the enumerated shortcomings of zone plates can either be completely eliminated or used for compensation of the residual chromatic aberration (of the secondary spectrum) of ordinary optical systems.

As a result we can obtain a very good correction of the secondary spectrum of astronomical and other long-focus systems for which this aberration reaches very high values. It is found that the number of interfering beams is relatively small, of the order 30-40 for a focal length of 1000-2000 mm and 1 : 10 relative aperture.

The first and principal defect of Soret or Wood zone plates is the dispersing of the light energy in images of different orders; this results from the fact that the optical length of the path which connects an object point and its image is not constant. But it can become constant if the zone plate has a special form determined by the condition that throughout an entire zone the optical path length is constant but that there is a phase discontinuity of 2π at the transitions between zones. Among the innumerable possible plate profiles we indicate some schematically in Fig. 1. The maximum thickness is d_0, which is equal to $\lambda_0/(n_0 - 1)$, where n_0 and λ_0 are, respectively, the refractive index and wavelength for which the plate is calculated; this will hereinafter be

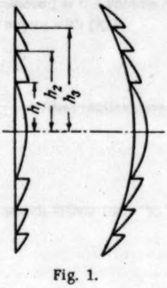

Fig. 1.

called a phase plate. The thickness of the phase layers varies according to the law $d = d_0 - a(h^2 - h_k^2)$, where $\underline{a}$ is a constant which depends only on the position of the object and of the image and on the wavelength; $\underline{h}$ is the height of the beam cross section; h_k is the height of the edge of the k-th zone. Here $h_k < h < h_{k+1}$.

The described phase plates can be produced by depositing on one lens surface thin layers whose thickness varies according to the rule indicated or by indenting through a special method of polishing (V. A. Savin).

The focal length f_0' of a phase plate, i.e., the quantity defined by the equation $\frac{1}{s'} - \frac{1}{s} = \frac{1}{f_0'}$, where $\underline{s}$ and s' are the distances from the plate to the object and to its image for the fundamental wavelength λ_0 is calculated by the formula

$$f_0' = h_1^2/2\lambda_0. \tag{1}$$

For wavelengths different from λ_0 it is impossible to find an abscissa s' for which 100% of the radiant energy from the object would be collected. The abscissa of the point S', where the maximum of radiant energy is collected is determined from

$$\frac{1}{s_\lambda'} - \frac{1}{s_0'} = \frac{1}{f_\lambda'}, \text{where } f_\lambda' = \frac{h_1^2}{2\lambda}, \tag{2}$$

which is known from the theory of zone plates.

This equation gives a huge value for the chromatic aberration $\Delta s'$ of both zone and phase plates, namelv

$$\Delta s' = -2s'^2 \frac{\Delta\lambda}{h_1^2} = -\frac{s_1^2}{f_0'} \frac{\Delta\lambda}{\lambda}. \tag{3}$$

The chromatic aberration in the usually considered spectral region C-F (656-486 mμ) is $^1/_3$ of s'^2/f', whereas for lenses it is $^1/_{60}$ to $^1/_{64}$ for ordinary crown glass, which is 20 times less.

Calculations show that at a focus corresponding to a wavelength $\lambda \neq \lambda_0$ the energy can be determined by the formula

$$E(\lambda) = \left(\frac{\lambda_0}{\lambda}\right)^2 \frac{\sin^2 B/2}{(B/2)^2}, \text{ where } B = 2\pi\left[1 - \frac{\lambda_0}{\lambda}\frac{n-1}{n_0-1}\right], \tag{4}$$

if the energy of λ_0 rays at the focus is taken as unity. When, for example, we have λ_0 = 510 mμ, then for λ = = 380 mμ, E = 0.886; for λ = 600mμ, E = 0.671, and for λ = 700mμ, E = 0.413. Thus a phase plate presents a certain analogy with a light filter; it absorbs the outer regions of the spectrum more than the middle; but if we keep in mind the spectral sensitivity of the receiver (eyes, photographic plates, etc.) the losses which thus result are very small; for eyes they do not exceed 2-3%.

The question naturally arises: does not this phenomenon cause scattering of light and reduce the resolving power of the system ? Before answering this question it is necessary to calculate the energy distribution in the plane which contains the image of a point and which is located in accordance with Eq. (2).

Rather complicated calculations based on the Huygens-Fresnel-Kirchhoff principle and using the properties of Bessel functions yield the following formula:

$$E = \frac{4J_1^2(n)}{n^2}\frac{\sin^2 B/2}{(B/2)^2} + \frac{1}{q^2}\left\{\frac{J_1(n)}{6}\left[\frac{n}{2} - J_1(n)\right]\left[\left[\frac{12\sin B}{B^3} + \left(1 - \frac{12}{B^2}\right)\frac{\sin^2 B/2}{(B/2)^2}\right]\right] + \right.$$
$$\left. + [J_0(n) - 1]^2\left[\left[\cos B/2 - \frac{\sin B/2}{B/2}\right]\right]\frac{1}{B^3} + \ldots\right\}, \tag{5}$$

where q is the number of interfering zones of the phase plate; $n = \frac{2\pi}{\lambda} z \sin\omega'$; z is the distance from the axis to the point for which the energy is determined; ω' is the aperture angle of the beam. Since q in the cases of interest is not less than 30 to 40 and the expressions in double brackets have small numerical values for all values of B we can assume with entirely sufficient accuracy that

$$E = \frac{4J_1^2(n)}{n^2} \frac{\sin^2 B/2}{(B/2)^2}. \tag{6}$$

Thus the distribution is the same as for an ideal optical system with the same aperture angle, but in our case the factor $\left(\frac{\sin B/2}{B/2}\right)^2$ appears, which depends on the wavelength. This formula confirms the "filtering" effect of a phase plate although it must be noted that unlike ordinary light filters the action of a phase plate varies as a function of several quantities (such as the position of the plane of the instrument).

The quality of the images of points outside the optical axis of the system can be determined on the basis of the third order aberrations of a system of lenses and phase plate. These aberrations are easily determined by calculating the dependence of the optical path length on the coordinates in the phase plate. From the expressions for the aberrations (which are not given here for lack of space) there result certain curious properties of phase plates:

1) The spherical aberration is determined by the coefficient c of the series expansion of the phase plate thickness as a function of h:

$$d(h) = \frac{\lambda_0}{n_0 - 1} - \frac{h^2}{2f'_0(n_0 - 1)} + \frac{h^4}{c^3} + \dots$$

2) The curvature of the surface of the image is zero for any optical power of the phase plate.

3) The radius of the surface which bears the phase layers does not affect third-order aberration.

4) It is almost impossible to alter the remaining forms of aberration of a phase plate. However for the above-considered case of an apochromatic system consisting of two lenses and a phase plate these aberrations are vanishingly small. In this latter case it is possible not only to correct the secondary spectrum but also spherico-chromatic aberration, which is impossible in the case of ordinary two-lens objectives.

Appendix. In addition to the described possibility of forming a two-lens objective with a phase surface characterized by a very high degree of correction of chromatic aberration, which is especially useful for astronomical purposes, it is possible to use existing objectives of refractors and by adding a specifically calculated lens with a phase surface and shortening its focal length by about $^1/_7$ to thus obtain an apochromat with high quality of the central image.

There are other possible applications which have not yet been fully worked out.

LITERATURE CITED

[1] R. Wood, Physical Optics (1936) (Russian translation).

[2] O. E Myers, Am. J. Phys. 19, 359 (1951).

[3] S. M. Raiskii, Progr. Phys. Sci. USSR 17, 4 (1954).

[4] C. V. Fragstein and K. Weber, Optik 1954, No. 6, 270.

Received July 12, 1956

THE SPECIFIC HEAT OF CHAIN STRUCTURES AT LOW TEMPERATURES

I. V. Sochava and O. N. Trapeznikova

(Presented by Academician A. F. Ioffe November 9, 1956)

At the present time there is no unity of opinion regarding the character of the temperature dependence of the specific heat of chain and laminar structures at low temperatures. All of the theoretical articles on this question [1-8] can be divided into two groups depending on whether the rigidity of the chains and layers is taken into account or not. The most fundamental difference of opinion concerns the temperature region where the interactions of chains and layers can be neglected.

Tarasov [1, 2], Gurney [4], Rosenstock [5], and Krumhansl and Brooks [6] neglect rigidity and for noninteracting chains obtain a linear temperature dependence of the specific heat, while for noninteracting layers they obtain a parabolic law regardless of whether a chain or layer is regarded as a continuum or its atomic structure is taken into account.

Lifshits [3], Komatsu [7], and Newell [8] took the rigidity into account; for a layer they obtain a linear law and for chains a $T^{1/2}$ law (Lifshits), likewise for the absence of interaction.

Existing experimental information does not enable us to make a unique choice between these two directions although most of the data shows poor agreement with the theories of Tarasov and others.

For further determination of the character of the temperature dependence of the specific heat of chain structures at low temperatures we have measured the specific heats of polyethylene from 58 to 273°K and of polyvinyl alcohol from 58 to 245°K. The experimental findings for the specific heat of teflon [9] and their interpretation by Tarasov [2] led us to expect a linear or $T^{1/2}$ dependence of the specific heat in this range.

Both polyethylene and polyvinyl alcohol are linear organic polymers with strong valence bonds of atoms along the chains and weaker intermolecular interactions between chains. Special interest attaches to the specific heat of polyethylene, which is the simplest of all existing organic polymers because at low temperatures it results entirely from the transverse and longitudinal vibrations of the chains. (CH vibrations cannot yet be excited at these temperatures.)

The adiabatic vacuum calorimeter used in this work does not differ essentially from those described many times in the literature.

The samples were placed in a glass cylinder filled with helium which contained a silver cross to speed up heat exchange. The temperature was measured by a platinum thermometer calibrated in the Low Temperature Laboratory of the VNIIM (All-Union Research Institute of Meteorology). Temperature adjustment required about 20-25 minutes per degree. The samples were in the form of small pieces which did not exceed 1 mm^3 in volume. The available factory-produced samples of polyethylene and polyvinyl alcohol were of commercial purity. We did not perform a special chemical analysis of the samples. The weight of the polyethylene was 19.2 g; that of the polyvinyl alcohol was 18.6 g. The specific heat of the empty calorimeter was measured over the entire range in advance at intervals of 5-8°. The literature contains indications that glass which contains Na_2SiO_3, such as the No. 23 glass which we used, has a chain structure with weakly interacting chains. This fact enables us to regard the specific heat of the glass as not merely an auxiliary quantity in calculating the specific heat of the polymers, and all the more so because we found no information in the literature regarding the specific heat of No. 23 glass at low temperatures. Specific heats were measured below 200°K at intervals of 2.5 to 3°. The spread of the experimental values did not exceed 1.5%.

TABLE 1

T, °K	Poly-ethylene	Polyvinyl alcohol	No. 23 glass	T, °K	Poly-ethylene	Polyvinyl alcohol	No. 23 glass
	c_p, cal/g-deg				c_p, cal/g-deg		
58	0.095_7	0.056_9	0.045_0	165	0.237_6	0.175_8	0.130_2
60	0.099_9	0.061_8	0.046_6	170	0.243_8	0.180_5	0.133_6
65	0.110_2	0.071_4	0.050_6	175	0.249_5	0.186_4	0.136_5
70	0.118_5	0.078_4	0.055_7	180	0.255_2	0.190_7	0.139_9
75	0.126_3	0.086_0	0.060_1	185	0.260_3	0.195_0	0.143_2
80	0.134_0	0.092_9	0.064_7	190	0.266_0	0.200_4	0.146_8
85	0.140_8	0.098_8	0.068_7	195	0.272_2	0.204_7	0.149_6
90	0.148_0	0.103_7	0.073_4	200	0.279_0	0.209_5	0.152_6
95	0.155_3	0.110_1	0.077_5	205	0.285_2	0.215_4	0.155_3
100	0.161_5	0.113_3	0.081_8	210	0.291_9	0.219_2	0.158_3
105	0.168_2	0.118_7	0.086_2	215	0.298_7	0.224_0	0.161_4
110	0.173_9	0.121_9	0.090_8	220	0.306_9	0.229_4	0.164_0
115	0.180_1	0.125_7	0.095_3	225	0.315_2	0.236_3	0.166_1
120	0.185_8	0.130_5	0.098_6	230	0.323_5	0.240_6	0.169_4
125	0.192_0	0.134_8	0.102_7	235	0.332_8	0.245_5	0.172_1
130	0.197_2	0.139_7	0.106_7	240	0.342_6	0.249_2	0.175_5
135	0.202_4	0.144_0	0.110_4	245	0.354_0	0.256_2	0.177_1
140	0.208_1	0.148_8	0.114_1	250	0.364_4		0.179_8
145	0.214_3	0.155_2	0.117_1	255	0.376_3		0.182_2
150	0.221_0	0.160_1	0.120_4	260	0.388_7		0.184_5
155	0.225_7	0.164_9	0.124_1	265	0.401_6		0.186_5
160	0.231_9	0.170_8	0.127_1	270	0.415_1		0.188_5

Table 1 contains the experimental values of the specific heat and the values calculated from the smoothed experimental curve.

The character of the temperature dependence can easily be judged from the slope of the curve of log C with respect to log T. In accordance with what was stated above, at temperatures where the interaction between chains can be neglected the specific heat can be represented by $C = AT^m$, where m = 1 or $^1/_2$ and A = const. On a logarithmic scale these functions are straight lines with slope 1 and $^1/_2$, respectively. The slope of the experimental curves gives the experimental value of m.

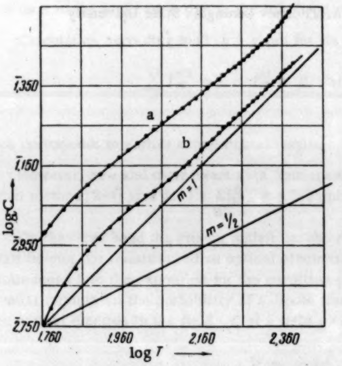

Fig. 1. log C as a function of log T for polyethylene (a) and polyvinyl alcohol (b) at low temperatures. For comparison the straight lines with m = 1 and $^1/_2$ are given.

Figure 1 shows that for polyethylene from 58 to 95°K m varies continuously from a value above unity to 0.89. From 95 to 185°K m remains constant and equal to 0.89, but above 185°K m increases continuously—this is associated with the beginning of devitrification of the polymer in this region. For polyvinyl alcohol from 58 to 120°K the specific heat curve shows an additional specific heat which may result from the excitement of OH group rotations. This quantity comprises about 15% of the total specific heat at T = 80°K which was obtained by smooth extrapolation of the curve. From 120 to 245°K, m is constant at 0.96. In the investigated temperature range no region of vitrification was observed for polyvinyl alcohol. The experimental value of m for glass is also very close to unity, but deviates therefrom toward lower values. Since the glass contains other components besides Na_2SiO_3 chains we cannot include it in the over-all investigation.

Our experimental data as well as the data of other authors on the specific heat of rubber [10] and of teflon [9] in logarithmic plots give m smaller than but very close to unity. For different polymers the difference from unity varies. Hence the following conclusion intrudes itself: the specific heat formula of Tarasov et al. is in better agreement with experiment than that of Lifshits, although the deviation of the experimental values of m from unity shows that it is necessary to take the rigidity of real chains into account. We believe that a more exact theory of the temperature dependence of specific heat can be obtained by an intelligent combination of the two existing forms. Stockmayer [11] has attempted to construct such a theory.

LITERATURE CITED

[1] V. V. Tarasov, J. Phys. Chem. (USSR) 24, 111 (1950).

[2] V. V. Tarasov, Doklady Akad. Nauk SSSR 100, 2, 307 (1955).

[3] I. M. Lifshits, J. Exptl.-Theoret. Phys. (USSR) 22, 471, 475 (1952).

[4] R. W. Gurney, Phys. Rev. 88, 415 (1952).

[5] H. Rosenstock, J. Chem. Phys. 21, 2064 (1953).

[6] J. Krumhansl and H. Brooks, J. Chem. Phys. 21, 1663 (1953).

[7] K. Komatsu and Nagimiya, J. Phys. Soc. Japan 6, 438 (1951).

[8] G. F. Newell, J. Chem. Phys. 23, 2431 (1955).

[9] G. T. Furucawa, R. E. McCoskey, and G. J. King, J. Res. Nat. Bur. Stand. 49, 4 (1952).

[10] N. Bekkedahl and H. Matheson, J. Res. Nat. Bur. Stand. 15, 503 (1935).

[11] W. H. Stockmayer and C. E. Hecht, J. Chem. Phys. 21, 1984 (1953).

Received November 1, 1956

A. A. Zhdanov Leningrad State University

ON THE TOTAL SUMMATION RULE FOR OSCILLATOR STRENGTHS OF ALKALI METALS

I. B. Bersuker

(Presented by Academician V. A. Fok December 12, 1956)

V. A. Fok has shown [1] that for a system consisting of a single optical electron outside a closed shell (such as an alkali metal) the sum of the oscillator strengths for the experimentally observed electronic transitions must be greater than unity since it includes actually unrealizable (but included in the summation rule) negative oscillator strengths for transitions into internal occupied states of the atomic core. In addition a small correction g results from consideration of the exchange operator in the equation of the valence electron. Thus the sum of the experimentally measured oscillator strengths is given by

$$\sum_{n',l'} f_{nl}^{n'l'} = 1 - \sum_{n_l\, l'} f_{nl}^{n_l\, l'} + g, \tag{1}$$

where $f^{n_l l'}$ are the oscillator strengths for purely theoretical transitions into internal states of the core, and the prime next to the summation sign in the left-hand side of the equation denotes that these transitions are excluded.

Calculation according to (1) has given for Na

$$\sum_{n'}{}' f_{30}^{n'2} = 1 - f_{30}^{21} + g \quad (f_{30}^{21} = -0.037, \quad g = -0.006),$$

which corresponds to earlier experimental results.

However, new and more exact data from measurements of oscillator strengths in alkali metals by the dispersion method [2-4] give for Na $\sum_{n'} f_{30}^{n'1} = 1.26$, which is not in agreement with the value calculated from (1).

On the other hand the present author has shown [5] that in systems of a certain form, to which the alkali metals belong, for transitions of an optical electron perturbed by an electromagnetic wave a correction must be introduced into the expression for the transition probability and consequently for the oscillator strength. Indeed the usual formula for the probability of a dipole transition was derived on the assumption that the perturbation of an optical electron in the field $\vec{\mathscr{E}}$ of a light wave is

$$W = -(\vec{\mathscr{E}}, \mathbf{D}) = e\,(\vec{\mathscr{E}}, \mathbf{r}). \tag{2}$$

But the equation of the valence electron of an alkali atom

$$[\hat{H}(\mathbf{r}) + V(\mathbf{r})]\,\psi - \hat{A}\psi = E\psi \tag{3}$$

in the field of a light wave contains besides the perturbation W the screening potential $V(\vec{r})$ and the exchange operator $\hat{A}$ resulting from the distortion of the "ψ-cloud" of the internal electrons. I believe there is no justification for neglecting the effect of these changes on the transition of an optical electron. We can take account of the influence of the core on optical electron transitions when perturbed by an electromagnetic wave by the method shown here of introducing an additional periodic perturbation W' in the form of the potential energy of an optical electron in the field of the core wave which has been polarized noninertially by the outside wave field.

For alkali and similar atoms the additional perturbation can conveniently be represented as follows:

$$W' = \begin{cases} \dfrac{e\,(\mathbf{P},\ \mathbf{r})}{r_0^3}, & r \leqslant r_0, \\ \dfrac{e\,(\mathbf{P},\ \mathbf{r})}{r^3}, & r \geqslant r_0, \end{cases} \tag{4}$$

where r_0 is the radius of the core: $\vec{\mathbf{P}} = 2\,\vec{\mathcal{E}}$ is the dipole moment of the core; α is its polarizability. (4) corresponds to the field of a uniformally polarized dielectric sphere (it is assumed that the wavelength is much greater than the dimensions of the system).

The total perturbation of an optical electron in the field of a light wave is

$$W + W' = e\,(\vec{\mathcal{E}},\ \mathbf{r} + \vec{\chi}), \tag{5}$$

where

$$\chi = \begin{cases} \dfrac{\alpha}{r_0^3}\,\mathbf{r}, & r \leqslant r_0; \\ \alpha\,\dfrac{\mathbf{r}}{r^3}, & r \geqslant r_0. \end{cases} \tag{6}$$

In accordance with (5) the expression for the transition probability must have the matrix not simply of the radius vector but of the sum $\vec{\mathbf{r}} + \vec{\chi}$ and the expression for the oscillator strength becomes

$$f_{nl}^{n'l'} = \frac{1}{3g_{nl}}\,\frac{Q_{nln'l'}}{4l^2_{\max} - 1}\,(E_{n'l'} - E_{nl})\left[\int_0^\infty (r + \chi)\, f_{nl}(r)\, f_{n'l'}(r)\, dr\right]^2. \tag{7}$$

Here g_{nl} is the statistical weight of the initial state; $l_{\max}$ is the larger of l, l'; $Q_{nln'l'}$ is a constant summed over different states of the initial and final levels.

Summing (7) with the aid of the Schroedinger equation for the radial part of the valence electron wave function and using the expansion $(r + \chi)\, f_{nl} = \sum_{n'} c_{n'} f_{n'l'}$ and all other transformations usually employed in deducing the total summation theorem of oscillator strengths, we arrive at the expression

$$\sum_{n'} f_{nl}^{n'l+1} = \frac{(2l+3)(l+1)}{3(2l+1)}\Big[1 + \Big(2\frac{\alpha}{r_0^3} + \frac{\alpha^2}{{}_0^6}\Big)\int_0^{r_0} [f_{nl}(r)]^2\, dr - {} - \frac{4\alpha l}{2l+3}\int_{r_0}^\infty [f_{nl}(r)]^2 \frac{dr}{r^3} + 2\alpha^2\,\frac{l+3}{2l+3}\int_{r_0}^\infty [f_{nl}(r)]^2 \frac{dr}{r^6}\Big] + g'_{l,\,l+1}, \tag{8}$$

$$\sum_{n'} f_{nl}^{n'l-1} = \frac{(1-2l)\,l}{3(2l+1)}\Big[1 + \Big(2\frac{\alpha}{r_0^3} + \frac{\alpha^2}{r_0^6}\Big)\int_0^{r_0} [f_{nl}(r)]^2\, dr + {} + 4\alpha\,\frac{l+1}{2l-1}\int_{r_0}^\infty [f_{nl}(r)]\,\frac{dr}{r^3} - 2\alpha^2\,\frac{2-l}{2l-1}\int_{r_0}^\infty [f_{nl}(r)]^2 \frac{dr}{r^6}\Big] + g'_{l,\,l-1},$$

where g' denotes the exchange correction taking account of the additional perturbation.

For the principal series of alkali metals and similar atoms $l = 0$ and

$$\sum_{n'} f_{n0}^{n'1} = 1 + \Big(2\frac{\alpha}{r_0^3} + \frac{\alpha^2}{r_0^6}\Big)\int_0^{r_0} [f_{nl}(r)]^2 dr + 2\alpha^2\int_{r_0}^\infty [f_{nl}(r)]^2\,\frac{dr}{r^6} + g', \tag{9}$$

whence for the sum of oscillator strengths only of experimentally observed transitions we obtain

$$\sum_{n'}{}' f_{n0}^{n'1} = 1 + \left(2\frac{\alpha}{r_0^3} + \frac{\alpha^2}{r_0^6}\right)\int_0^{r_0} [f_{nl}(r)]^2 dr + 2\alpha^2 \int_{r_0}^{\infty} [f_{nl}(r)]^2 \frac{dr}{r^6} - \\ - \sum_{n_i < n} f_{n0}^{n_i 1} + g'. \tag{10}$$

TABLE 1

Atom	$\Sigma_{n'} f_{n'}^{n'1}$		
	By Eq. (1)	By Eq. (10)	Experimental
Na	1.031	1.248	1.26
K	1.135	1.269	—
Ca^+	1.187	1.453	—
Cs	—	—	1.21

The calculations according to (10) for Na, K, Ca^+ using the tables of wave functions for the optical and internal electrons in [6-9] are given in Table 1. For comparison we also give the results of calculations according to Eq. (1) and the experimental values that are available. α was taken as the polarizability of the corresponding ion. The radius of the core r_0 was taken to be the average radius of the outermost internal orbit. The exchange correction, which is very small for systems of the type under consideration [1], was neglected for K and Ca^+, but was included for Na without taking account of the additional perturbation (according to the data in [1]).

It can be seen from Table 1 that the difference between our results and experiment for Na is less than 1%. This can serve as a confirmation of our hypothesis that for induced transitions in alkali metals and similar atoms the atomic characteristic of the "oscillator strength" is Eq. (7).

In conclusion I take this opportunity to express my deep appreciation to Iu. E. Perlin for his continued interest and for valuable discussions.

LITERATURE CITED

[1] V. Fock, Z. Phys. 89, 744 (1934).

[2] G. S. Kvater, Bull. Acad. Sci. USSR,Phys. Ser. 9, 236 (1945).

[3] G. S. Kvater, Bull. Leningrad State Univ. 1947, No. 2, 135.

[4] G. S. Kvater and T. G. Meister, Leningrad State Univ. 1952, No. 9, 137.

[5] I. V. Bersuker, Sci. Records Kishinev Univ. 17, 119 (1955).

[6] V. Fock and M. Petrashen, Sow. Phys. 6, 368 (1934).

[7] D. R. Hartree and W. Hartree, Proc. Roy. Soc. 166, 450 (1938).

[8] D. R. Hartree and W. Hartree, Proc. Cambr. Phil. Soc. 34, 550 (1938).

[9] D. R. Hartree and W. Hartree, Proc. Roy. Soc. 164, 167 (1938).

Received December 20, 1955 Beltskii State Pedagogical Institute

PHOTOCONDUCTIVITY OF VIOLANTHRONE AND PYRANTHRONE

A. T. Vartanian and I. A. Karpovich

(Presented by Academician A. N. Terenin September 18, 1956)

Akamatu and Inockuchi have found [1] that films of indanthrone dyes – violanthrone, isoviolanthrone, and pyranthrone – produced by sublimation are photoconducting. By extrapolating a certain "linear" part of the long-wave tail of the photoconduction curve until it intersects with the wave number axis the authors have determined the long-wave photoconduction limits of these dyes and the corresponding optical activation energies E. For violanthrone and pyranthrone E was 0.84 and 1.14 ev, respectively, which is in satisfactory agreement with values which they had previously [2] obtained for the thermal activation energy (0.78 and 1.08 ev) and also with the long-wave absorption limits of sublimed layers [1]. But it should be noted that the long-wave absorption band of sublimed films of violanthrone, isoviolanthrone, and pyranthrone are unusually wide even for the solid state of the dyes and have an extremely weak structure. Thus it is impossible to establish a direct relation between the absorption of sublimed films and solutions of these dyes. Yet the absorption by films produced through rubbing of violanthrone and pyranthrone powder on a quartz surface is distinguished by considerable selectivity [3]. The absorption band of such films has maxima (Fig. 1,1 and 2) which correspond to the absorption maxima of solutions of the dyes in xylene with the usual solid-state shift [4] of 40-45 mμ in the long-wave direction. It was also observed that the absorption spectrum of a singly sublimed film possesses a wider band and a clearer structure than a film produced by rubbing; yet the similarity between these spectra is greater than between the spectra of films produced by rubbing and by multiple sublimation. Since the dyes, which do not change in sublimation, have absorption spectra which are very similar independently of whether the films were produced by precipitation from a solution, by rubbing or by sublimation [3] we can assume that the multiple sublimation employed by Akamatu and Inockuchi for purification of the dyes resulted in some irreversible structural changes.

The present article presents the results of an investigation of photoconduction in films produced by rubbing powders of violanthrone (indanthrone dark blue BO) and pyranthrone (indanthrone golden orange G).

The apparatus used was similar to that which was described in detail in [5]. Films varying in thickness from 0.1 to a few microns were deposited on a quartz "finger" with platinum electrodes separated by 1 mm. The photoconduction was investigated in a vacuum although the experiments showed that the presence of air has no essential effect on the results. The light source was a 100-watt incandescent tungsten lamp. For decomposition of the light we used an ISP-17A mirror monochromator with a glass optical system. The spectral energy distribution was determined by using a thermopile. Currents of the order of 10^{-13} amperes were measured by a dc amplifier.

Layers of violanthrone and pyranthrone produced by rubbing show considerable dark conduction which increases with temperature according to the law $\sigma = a \exp -\left(\frac{\epsilon}{2kT}\right)$, where ϵ is 1.0 ± 0.05 and 1.15 ± 0.05, respectively, for violanthrone and pyranthrone.

When the films are illuminated a stationary photocurrent is established in a few seconds and decays almost as rapidly when the illumination is terminated. Under prolonged irradiation a further increase of the photocurrent during illumination is often observed. After termination of such protracted illumination the photocurrent decays rapidly at first but a residual photocurrent is always observed, which decays slowly. The results given below refer to the photocurrent which is established and decays in 3-5 seconds. Under monochromatic illumination the

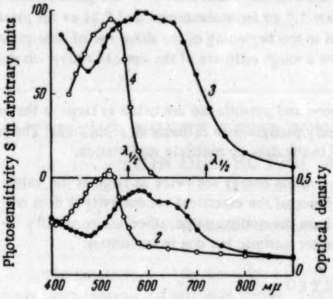

Fig. 1. 1) Spectral absorption curve of a solid film of violanthrone; 2) the same for pyranthrone; 3) spectral photosensitivity curve of a thin film of violanthrone, n = 0.9; 4) the same for pyranthrone, n = 0.7.

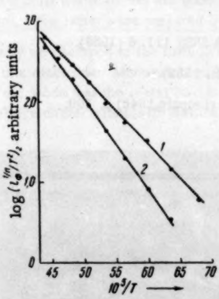

Fig. 2. Photoelectric straight lines: 1) violanthrone, n = 0.72; 2) pyranthrone, n = 0.7.

measured photocurrent was of the same order of magnitude as the dark current.

The photocurrent obeys Ohm's law, at least in fields up to 4000v/cm. The dependence of the photocurrent i_{ph} on the illumination intensity L is expressed by $i_{ph} = aL^n$, where a and n are constants. For the films which we investigated the values of n were smaller than unity and, depending on the thickness of the film and the level of illumination, lay between 0.7 and 0.9. At temperatures from −40 to +50° the temperature dependence of the photocurrent also follows the law $i_{ph} = b\exp -\left(\frac{\epsilon_{ph}}{2kT}\right)$, where $\epsilon_{ph} = 0.4$ ev.

Figure 1 (3 and 4) shows the spectral curves of the photosensitivity S of thin films of violanthrone and pyranthrone. As a measure of the photosensitivity we took the expression $i_{ph}^{1/n}/L$ which gives the nonlinear dependence of the photocurrent on the intensity of illumination [6]. As can be seen from Fig. 1 these curves are in good agreement with the absorption curves of solid layers. The long-wave decay region of the photosensitivity shows a linear relation between $\log S$ and λ.

The photosensitivity curves in Fig. 1 cannot be compared with the curves obtained by Akamatu and Inockuchi [1] because the absorption spectra of these authors are extremely different from ours. Moreover, their photosensitivity curves do not cover the entire absorption band but only the long-wave portion from about 640 to 1800 mμ. For some part of this region they find a linear relation between S and $1/\lambda$ and employ this in determining the photoconduction limit. This is aside from the fact that the extrapolation method which they used to determine the photoconduction limit is lacking in justification and that the reality of the linear parts of the photosensitivity curves of isoviolanthrone and pyranthrone is doubtful.

In order to determine the optical activation energy we used two different methods which had already been employed in investigations of inorganic photoconductors.

1. According to Moss [7] as the "long-wave limit" of the photoconductivity we can take the wavelength for which the sensitivity is one-half of its maximum value immediately preceding its exponential decline ($\lambda_{1/2}$). From Curves 3 and 4 of Fig. 1 it follows that $\lambda_{1/2}$ for violanthrone is 720 mμ and for pyranthrone 560 mμ. Corresponding to these values of $\lambda_{1/2}$ the optical activation energy $E_{\lambda_{1/2}}$ is 1.71 and 2.2 ev, respectively.

2. The optical activation energy can also be determined by the method of "photoelectric straight lines." Lange and Schmidt [8] have shown that for a photocurrent which is excited through irradiation of a photoconductor by all of the light from a black body at temperature T the relation $i_{ph} = AT^2 \exp(-E_{ph}/kT)$ is fulfilled, from which it follows that there is a linear relation between $\log(i_{ph}/T^2)$ and $1/T$. The slope of the straight line determines the optical activation energy E_{ph}. It was shown earlier [6] that for films of the same dye with different values of n the slope of the "photoelectric straight lines" depends on n and that therefore the values of E_{ph} obtained from these lines does not have a definite physical meaning. The slope of the lines is independent of n and is determined only by the nature of the dye if instead of $\log(i_{ph}/T^2)$ we plot $\log(i_{ph}^{1/n}/T^2)$ on the ordinate

axis. The "photoelectric straight lines" plotted with account taken of the "nonlinearity" of the photocurrent are shown in Fig. 2. The values of E_{ph} obtained from these lines are 1.7 ev for violanthrone and 2.24 ev for pyranthrone; these are in good agreement with $E_{\lambda_{1/2}}$ and correspond to the beginning of the sharp rise of absorption by the dyes in the solid state. The last fact can be used to give a rough estimate of the optical activation energy from the absorption curves.

Our values for the optical activation energy of violanthrone and pyranthrone are twice as large as the values obtained by Akamatu and Inockuchi [1]. This discrepancy is only partly due to differences of method. The principal cause of the difference is evidently the change produced in the dyes by multiple sublimation.

From the fact that the values obtained for the optical activation energy are twice as large as the values of the activation energy obtained from the temperature dependence of the electrical conductivity it does not follow that the thermal activation energy differs considerably from the optical value, since the possibility remains that the conductivity of the films investigated by us was not intrinsic but due to impurities.

LITERATURE CITED

[1] H. Akamatu and H. Inockuchi, J. Chem. Phys. 20, 1481 (1952).

[2] H. Akamatu and H. Inockuchi, J. Chem. Phys. 18, 810 (1950).

[3] A. T. Vartanian, J. Chem. Phys. (USSR) 30, 1028 (1956).

[4] A. T. Vartanian, J. Tech. Phys. (USSR) 20, 847 (1950).

[5] A. T. Vartanian, J. Phys. Chem. (USSR) 20, 1065 (1946).

[6] A. T. Vartanian and I. A. Karpovich, Doklady Akad. Nauk SSSR 111, 6 (1956).

[7] T. S. Moss, Photoconductivity in the Elements (Butterworth, 1952).

[8] B. Lange, Die Photoelemente und ihre Anwendung, 1 Teil (Leipzig,1940) p. 109.

Received September 14, 1956

THE INFLUENCE OF ELECTRIC FIELDS ON THE PROPERTIES OF THIN DIELECTRIC AND SEMICONDUCTING FILMS

Iu. M. Volokobinskii

(Presented by Academician A. F. Ioffe December 19, 1956)

The dependence of the breakdown potential of thin insulating films on their thickness has been studied by many investigators. An extensive review of articles on this question has appeared [1]. There has been less thorough study of the dependence of thin film conduction on field strength. No complete explanation has been given of the relation between the electrical conductivity of a thin film and its electric strength. Experiments devoted to this problem are described below.

We have investigated the electrical conductivity and electric strength of thin films of several oxides, sulfides, and other compounds. The metals were usually coated with oxide films electrolytically or by heating. In the case of metals whose oxides are good conductors but whose sulfides are poor conductors we studied the sulfide films. The latter were prepared by sulfonating the surfaces of the metals in sulfur vapor.

Usually we clamped to the surface of an oxide film a small plate of Cu_2S 3 mm in thickness and 0.5 cm^2 in area as one electrode. Monovalent copper sulfide Cu_2S possesses conductivity amounting to 40 $ohm^{-1} \cdot cm^{-1}$. The other electrode was the metal backing of the oxides. The test circuit resembles that used to obtain the current-voltage characteristics of semiconductor rectifiers.

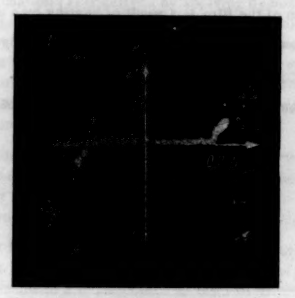

Fig. 1.

In the investigation of films of MgO, Al_2O_3, ZnO, CdS, NiO, Ta_2O_5, Nb_2O_5, varying in thickness from 30 to 1000 Å we observed the transfer of metallic ions from the backing to the Cu_2S which is a p-type conductor. The presence of the transferred ions in the copper sulfide is detected in some instances, in aluminum for example, by spectral analysis and is revealed by rectifying properties of the investigated arrangement. The ion current induces heating of the film on some parts of its boundary. The above compounds have been placed in the approximate order of decrease of the relative fraction of the ion component of conductivity.

In the case of Nb_2O_5 ion transfer is small and sometimes absent. Then the current-voltage characteristic is of the form given in Fig. 1. The resistance of the film for an effective voltage below 0.2 v is large, after which it is reduced and the current rises sharply. The current rise is associated with quantum mechanical effects and the voltage dependence of the current is complicated, although this is not shown in the photograph. Further, more intensive study of the current-voltage characteristic is possible and would be useful to determine the nature of the processes which occur in thin films. With reduced potential the film resistance again increases and resumes its former value. The current-voltage characteristic is reproduced as photographed from the screen of a cathode ray oscilloscope when a 50-cycle voltage is applied. If the voltage is raised a little above 0.2 v there is an appreciable transfer of Nb into Cu_2S and rectification occurs. With increases up to 0.4-1.0 v the film is punctured.

Higher voltages can be applied as follows. When on the oxide film which covers the aluminum we place a plate of chemically pure tellurium and apply the potential, the puncturing of the oxide film results in fusing

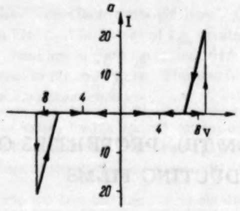

Fig. 2.

of the plate with the electrode and the formation of a transition region. This layer has high resistance at low voltages. With increased voltage to about 8.4 v the resistance of the film drops sharply and the current rises abruptly. The voltage at which the jump occurs varies little from instance to instance. When the voltage is lowered to 6.3 v the resistance of the film resumes its former value. The dynamic current-voltage characteristic at 50 cycles is shown in Fig. 2.

The investigation of other films such as an oxide film on tantalum shows smooth dependence of the current on voltage. In the voltage range from (0.3-0.4) V_{bp} to V_{bp} (breakdown potential) the current rises exponentially. Only very close to the breakdown potential does the current-voltage characteristic become parallel to the current axis. The permissible current without breakdown is 0.2 amperes.

For some systems such as an aluminum oxide film the voltage dependence of the current with increased temperature is smoother.

In some instances experiment shows a sharp and sometimes abrupt current rise at a definite potential applied to the film without breakdown. This increased conductivity does not always result in breakdown. In some cases the breakdown potential of the dielectric film is several times larger than the potential at which the conductivity rises considerably.

The experimental results can be explained by the following hypotheses. The breakdown requires a certain amount of energy W_d for disruption of the film. This energy is obtained through heating of the film by the current. The thin film reduces its resistance at a small potential; the quantity of heat liberated per unit time is small and the rate of heat removal is such that the film is not heated nor disrupted. The passage of a large current without heating of the film does not result in its disruption and after removal of the potential the resistance of the film is restored. Breakdown is associated with disruption of the film as a result of heating by a current passing through it and is a secondary phenomenon.

LITERATURE CITED

[1] A. A. Vorob'ev and E. K. Zavadovskaia, Electric Strength of Solid Dielectrics(Moscow, 1956) p. 131.

Received November 1, 1956

ON THE DETERMINATION OF MOLECULAR VOLUMES IN SOLUTIONS BY THE USE OF POLARIZED LUMINESCENCE

N. D. Zhevandrov and V. P. Nikolaev

(Presented by Academician A. N. Terenin November 28, 1956)

S. I. Vavilov [1] has shown that it is possible to study problems associated with the nature of the liquid state by using the luminescence of solutions. One of these methods is the study of the fluorescence polarization limit. The fluorescence of solutions is polarized only in anisotropic excitation. The degree of polarization p is determined by the lifetime τ of the excited molecular state and the angle of rotation of the molecule during this time as a result of Brownian rotation, which, in turn, depends on the temperature T and viscosity η of the medium and the effective molecular volume V. This quantity is expressed quantitatively by the Levshin-Perrin formula

$$\frac{1}{p}=\frac{1}{p_0}+\left(\frac{1}{p_0}-\frac{1}{3}\right)\frac{RT}{V\eta}\tau. \tag{1}$$

Here p_0 is the fluorescence polarization limit which corresponds to $T/\eta \to 0$ (i. e., to the absence of Brownian rotation). This quantity is obtained by extrapolation of the linear dependence of $1/p$ on T/η.

Equation (1) is derived by applying hydrodynamics and the theory of Brownian rotation to a single molecule regarded as a solid sphere; η is the macroscopic viscosity of the medium. In connection with the motion of a single molecule it is necessary to use molecular viscosity or microviscosity. It is impossible to state in advance the relation between the macroscopic and molecular viscosity. An important result of polarization measurements by several authors was the establishment of the fact that these quantities are both of the same order. Also, as stated by Vavilov, the deviations from hydrodynamical formulas can provide valuable information concerning the microstructure of liquids.

Equation (1) contains the effective volume V of a molecule. If on the basis of the experimental findings which have been mentioned we take η to be the macroviscosity and use the results of viscosimetric measurements it is possible to determine such volumes. On the other hand molecular volumes can be evaluated from their structural formulas and the known bond lengths and then compared with experimental values.

It is also possible to measure the fluorescence polarization of the same fluorescing substance in different solvents. This enables us to draw conclusions regarding the presence and character of the solvate envelopes, by which we mean a monomolecular layer of solvent surrounding a molecule of the dissolved substance and more or less strongly bound to it. An investigation of solvate envelopes is of interest for physical chemistry. In particular, as has been mentioned by Levshin [2], they can also play an important part in the luminescence of solutions together with molecular association and other physicochemical factors.

In the present work fluorescence polarization was measured by Kavraiskii's polariscope [3] with a compensating pile. This polariscope possesses a number of advantages compared with the Savart polariscope and has already been used to investigate luminescence polarization [4].

Measurements were carried out over a relatively small temperature range from 20-60° (at higher temperatures the results are sometimes complicated by temperature quenching). In this range the linearity of $1/p\ (T/\eta)$ was well observed. The viscosity of the solvents at different temperatures was measured by the usual viscosimetric method by the rate of flow through a capillary. Temperature constancy was maintained by an ultrathermostat. Fluorescence duration τ was measured by a phase fluorometer.*

As solvents of sufficient viscosity in the given temperature range we were able to use only glycerin, castor oil, and vaseline oil. The intrinsic emission of doubly distilled glycerin is negligible and the blue emission of the oils could be eliminated with sufficient reliability by filters from the yellow-green emission of the investigated materials. The concentrations of the solutions varied from 10^{-4} to 10^{-5} g/cm^3. Three groups of fluorescing organic substances were investigated: phthalimides, acridine derivatives and arylamine derivatives of anthracene — 9 substances altogether.

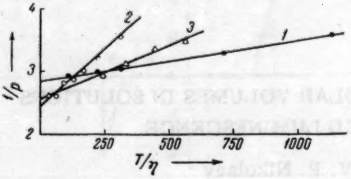

Fig. 1. Fluorescence polarization limit of 9, 10-diphenyldiaminoanthracene: 1) in glycerin, 2) in castor oil, 3) in vaseline oil.

Curves showing the dependence of $1/p$ on T/η for one of the substances as an example are given in Figs. 1 and 2. The data are collected in Table 1. The effective volumes V were calculated by Eq. (1) and the molecular radii r were then obtained (using a spherical molecular model).

When the mean molecular radii r' are computed from known bond lengths and structural formulas we obtain the following approximate estimates:

Substance	Phthalimides	Acridines	Anthracenes
r', A	2	3	5

In the same way we can estimate the sizes of the molecules of the solvents. The glycerin molecule can also be considered roughly spherical with diameter d ≈ 3 A. The molecule of the triglyceride of ricininic acid, which comprises 86 % of castor oil, is very much extended in one direction and can more accurately be regarded as an ellipsoid of rotation with its minor axis equal to the diameter of the glycerine molecule and its major axis 8 times longer.

The results given in Table 1 reveal an increase of effective molecular volume of the different classes with complication of the structure, which can be seen in the glycerin solutions (80-190 Å^3 for phthalimides, 280-570 Å^3 for acridines and 2040-3700 Å^3 for anthracenes).

When we compare the experimental values of r with the calculated values of r' and d using the model of a monomolecular solvate shell ($r = r' + d$), in the case of the glycerin solutions we find agreement in order of magnitude for the acridines and anthracenes, while for the phthalimides experiment gives a lower value than the calculation. For castor oil this model is entirely different from reality, as r in this instance is of the same order and in some cases even considerably smaller than in glycerin, whereas according to the model it should be considerably larger. Vaseline oil, in which only anthracenes are dissolved, possesses a small solvate effect judging from our results.

Thus the experimental results cannot be interpreted unambiguously using the concept of solvate shells. However there is another possibility of interpreting the results — from the point of view of different macroscopic and molecular viscosities. Previous experiments with one solvent only showed agreement in order of magnitude. A comparison of different solvents can possibly show inconsistency in the use of values of the macroscopic viscosity of Eq. (1). The physical nature of the phenomenon (which can be described formally both as a change of effective volume and as a difference of macroscopic and molecular viscosities) lies in the interaction of the molecular fields of the solvent and solute.

In this connection it is interesting to compare the effective volumes with the values of the dipole moments of solute and solvent molecules. An analysis of experimental findings shows that there is no parallelism between

---

* The authors are deeply grateful to M. D. Galanin for making the fluorometer available.

TABLE 1

Summary

Fluorescent materials	Solvents	p, %	$\tau \cdot 10^9$, sec	V, Å^3	r, Å
3-Aminophthalimide 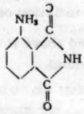	glycerin	40	11.5	190	3.6
	castor oil	41	10.5	350	4.4
3-Dimethylamino-6-aminophthalimide 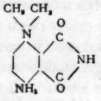	glycerin	40	1.1	80	2.6
	castor oil	33	3.2	170	3.5
Acridine orange	glycerin	38	2.5	550	5.1
	castor oil	36.5	3.9	990	6.2
2-Aminoacridine 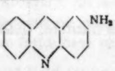	glycerin	37	5.7	570	5.2
	castor oil	38	4.6	230	3.8
3-Aminoacridine 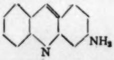	glycerin	38	6.6	310	4.2
	castor oil	37	5	200	3.6
3-6-Diaminoacridine	glycerin	43.5	3.9	280	4.1
	castor oil	40	6	765	5.7
9-10-Diphenyldiaminoanthracene 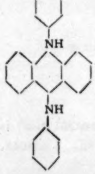	glycerin	35	6.7	3700	9.6
	castor oil	41	2.7	165	3.4
	vaseline oil	39	4.4	790	5.8
9-10-Dimetachlorophenyldiamino-anthracene	glycerin	38	8.3	2040	7.9
	castor oil	42	4.2	420	4.6
	vaseline oil	32	4.6	1000	6.2
9-10-Diorthomotoxyphenyldiamino-anthracene	castor oil	33	7.6	1080	6.3
	vaseline oil	39	5.5	960	6.1

these quantities. For example, the dipole moment of the triglyceride of ricininic acid is evidently larger than that of glycerin on the basis of the additivity of bonds in these molecules and the known dipole moments of the individual bonds [5, 6], but the solvate effect of castor oil is considerably smaller than that of glycerine.

Among the acridines 2-aminoacridine and 3-aminoacridine possess larger moments than 3-6-diaminoacridine and acridine orange, but the first corresponds to a smaller solvate effect of castor oil than the second. At the same time among the phthalimides the smallest solvate effect of this solvent corresponds to 3-dimethylamino-6-aminophthalimide, whose dipole moment is smaller than that of 3-aminophthalimide.

It must also be noted that the limiting degree of fluorescence polarization of the same substance in different solvents varies, although the differences are small. This can be explained only by the effect of the solvent on the electron shell of the molecule, which results in some change of the radiation oscillator.

For a more detailed study of the indicated effects by the method described above it would be desirable to use a homologous series of solvents such as different alcohols at low temperatures.

LITERATURE CITED

[1] S. I. Vavilov, Collected Works 2, p. 9 (1952).

[2] V. L. Levshin, Bull. Acad. Sci. USSR, Phys. Ser. 20, 397 (1956).

[3] V. V. Kavraiskii, J. Exptl.-Theoret. Phys. (USSR) 20, 619 (1950).

[4] N. D. Zhevandrov, Bull. Acad. Sci. USSR, Phys. Ser. 20, 570 (1956).

[5] M. V. Vol'kenshtein, Structure and Physical Properties of Molecules (Moscow-Leningrad, 1955), Ch. 6.

[6] P. Debye, Polar Molecules (Moscow-Leningrad, 1931), Sect. 13 (Russian translation).

Received November 23, 1956

P. N. Lebedev Physics Institute, USSR Academy of Sciences

ON DIFFERENTIAL ELECTROSTATIC FIELDS IN THE SPECTROSCOPY OF CHARGED PARTICLE BEAMS

M. I. Korsunskii and V. A. Bazakutsa

(Presented by Academician L. A. Artsimovich December 14, 1956)

The most important task in the spectroscopy of charged particle beams is the devising of ion-optical systems which will permit the construction of efficient spectral instruments of high resolving power. Ion-optical systems for this purpose must be highly dispersive and also exhibit highly perfected focusing.

The currently popular cylindrical condenser field permits good focusing of a weakly diverging charged particle beam but shows relatively small dispersion. The dispersion in such fields can be increased by enlarging the radius of the equilibrium trajectory, but this is not advantageous in practice. Therefore for the purpose of increasing dispersion without changing the equilibrium trajectory radius fields have been used which decrease radially more rapidly than the cylindrical condenser field. In particular, a spherical condenser field [1-4] in electrostatic analyzers and mass spectrographs results in a doubling of the dispersion with unaltered equilibrium trajectory radius, thus permitting higher resolution and efficiency of the instruments without increasing their dimensions. A spherical condenser in electrostatic analyzers and a double-focusing mass spectrograph [5] was found to be very efficient. In recent years calculations have been made of the ion-optical properties of other types of inhomogeneous electrostatic fields [6, 7] for the purpose of increasing the dispersion and improving the focusing, but these fields have not been used in practice.

A differential field possesses interesting properties [8]. One of the special cases of a differential field is defined by radial and axial components of the form

$$E_r = \frac{E_1}{r} - E_2 r, \tag{1}$$

$$E_z = 2 E_2 z, \tag{2}$$

where E_1 and E_2 are constants associated with the inhomogeneity factor η and the radius of the equilibrium trajectory as follows:

$$\eta = 2 - \frac{2 \frac{E_2}{E_1} r_0^2}{1 - \frac{E_2}{E_1} r_0^2}, \quad \eta = 3 + \frac{\partial E}{\partial r} \cdot \frac{r}{E}\bigg|_{r=r_0}. \tag{3}$$

A differential field focuses in the radial and axial directions in accordance with a generalization of Barber's rule [9]: the source S, the vertex of the effective sector angle $\Phi\sqrt{\eta}$ and the image P lie on the same straight line (Fig. 1).

A displacement of the image by the amount $\underline{b}$ from the equilibrium trajectory at the point of first order focusing is expressed by

$$b = \delta \frac{r_0}{\eta}\left(1 + \frac{q}{p}\right) - \Delta r_0\left(\frac{q}{p}\right), \tag{4}$$

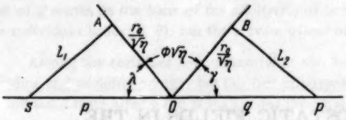

Fig. 1. L_1 is the distance from the source to the front edge of the field; L_2 is the distance from the image to the back edge of the field; Φ is the sector angle.

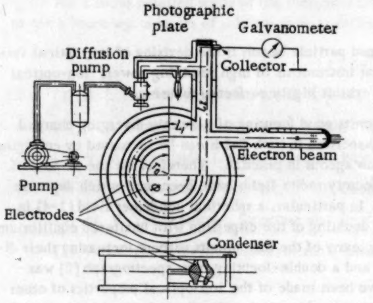

Fig. 2. Analyzer diagram.

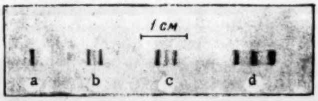

Fig. 3. Photograph of images of entrance slits: a) $\delta = 1.5 \cdot 10^{-3}$; b) $\delta = 3 \cdot 10^{-3}$; c) $\delta = 4.5 \cdot 10^{-3}$; d) $\delta = 6 \cdot 10^{-3}$.

where δ is a quantity which characterizes the energy spread of the particles and Δr_0 is the width of the entrance slit.

The energy dispersion

$$D_e = \frac{db}{d\delta} = \frac{r_0}{\eta}\left[1 + \frac{q}{p}\right] \tag{5}$$

depends essentially on η. For $\eta \to 0$, $D_e \to \infty$.

A more exact expression for the displacement is obtained by taking account of the second-order aberration terms [10] as follows:

$$\begin{aligned} b = r_0 \Big[& \frac{\delta}{\eta}\left(1 + \frac{q}{p}\right) - \frac{\Delta r_0}{r_0}\left(\frac{q}{p}\right) + \delta^2\alpha_1 + \psi_r^2\alpha_2 + \\ & + \left(\frac{\Delta r_0}{r_0}\right)^2 \alpha_3 + \delta\psi_r\alpha_4 + \delta\frac{\Delta r_0}{r_0}\alpha_5 + \psi_r\frac{\Delta r_0}{r_0}\alpha_6 \Big], \end{aligned} \tag{6}$$

where ψ_r is the angle of departure of a particle from the equilibrium trajectory upon entering the field; α_1, α_2, α_3, α_4, α_5, and α_6 are the aberration factors, which are complicated functions of q and p.

In the special cases where the condition

$$\frac{\partial b}{\partial \Delta r_0} = 0 \tag{7}$$

is satisfied, for a certain value $\delta \neq 0$ a number of aberration terms can be eliminated thus improving the focusing. In this case the width of the image will be independent of the width of the entrance slit and will be determined by the angle of divergence of the particles at each point of the entrance slit. This property of differential fields can be used to concentrate broad beams of monoenergetic charged particles.

For the experimental investigation of the properties of a differential field we constructed an analyzer in which the charged particle beam was rotated through the angle Φ = 27°. The field expressed by Eqs. (1) and (2) was created by two condenser plates in the form of equipotential surfaces defined by these equations.

The analyzer (Fig. 2) has an equlbrium radius r_0 = 200 mm, a field inhomogeneity factor $\eta = {}^1/_6$, and the distances L_1 and L_2 can be varied in accordance with the generalized Barber rule. The charged particle beam consisted of electrons from the electron gun of an 8L029 electron-beam tube with stabilized voltage.

With this instrument we obtained experimental results which are in good agreement with calculations. Thus, for example, with L_1 = 120 mm and L_2 = 700 mm the energy dispersion is 33 mm for 1% change of energy (calculated value 31.6 mm). When the source and image are equally distant from the edges of the field L_1 = = L_2 = 330 mm and the dispersion is 25.3 mm for 1% energy change (calculated value 24 mm). The difference between the experimental and calculated values of the dispersion results from the fact that the real field possesses an η which differs somewhat from the theoretical value.

Thus the energy dispersion of an electrostatic analyzer with a differential field exceeds the dispersion of a similar analyzer with cylindrical field by a factor of 12. In order to obtain such dispersion with a cylindrical analyzer the equilibrium radius would have to be increased to 2.4 m.

This experimental check of Condition (7) confirmed the possibility of improving the focusing and concentration into a narrow line of a wide beam of monoenergetic charged particles. Figure 3 contains photographs of images of three slits of 0.5 mm width 1 mm apart with the middle slit on the equilibrium trajectory. The distance of the entrance slit from the edge of the field was L_1 = 140 mm, the distance of the image from the other edge of the field was L_2 = 640 mm. The photographs were made with different values of δ. It can be seen from Fig. 3 that with $\delta = 1.5 \cdot 10^{-3}$ all three images merge into one clear thin line. From these photographs it is also seen that the aberration distortions even for beams which do not go along the equilibrium trajectory does not exceed 0.25 mm.

Consequently, a differential field enables us to devise a compact efficient electrostatic analyzer of high resolving power and large dispersion. By producing a field with η as small as possible (while focusing still takes place) the dispersion can be considerably increased. It should be noted that there is a possibility of producing differential fields for which η can be varied at the will of the experimenter. For example, this possibility involves the establishment of the required potential distribution near the equilibrium trajectory by the use of electrodes in the form of circular plates bearing a definite potential distribution.

The use of differential electrostatic fields in conjunction with an inhomogeneous differential magnetic field opens the possibility of constructing a compact efficient double-focusing mass spectrograph of high resolving power.

LITERATURE CITED

[1] F. W. Aston, Phil. Mag. 38, 710 (1919).

[2] E. M. Purcell, Phys. Rev. 54, 818 (1938).

[3] F. T.Rogers, Rev. Sci. Instr. 22, 10, 732 (1951).

[4] C. P. Browne, D. S. Craig, and R. M. Williamson, Rev. Sci. Instr. 22, 12, 952 (1951).

[5] R. Herzog, Z. Naturforsch. 8a, 2, 3 (1953).

[6] M. I. Korsunskii, J. Exptl.-Theoret. Phys. (USSR) 16, 1, 81 (1946).

[7] Iu. V. Vandakurov, J. Tech. Phys. (USSR) 25, 8, 1412 (1955).

[8] M. I. Korsunskii, Trans. Kharkov Polytekh. Inst., Ser. Engr.-Phys. 1956, No. 2.

[9] N. F. Barber, Proc. Leeds Phil. Soc. 2, 427 (1933).

[10] M. I. Korsunskii and V. A. Bazakutsa, Trans. Kharkov Polytekh. Inst., Ser. Engr.-Phys. 1956, No. 2.

Received October 26, 1956

V. I. Lenin Kharkov Polytechnic Institute

Cd (n, p) Ag CROSS SECTIONS WITH 14-MEV NEUTRONS

V. N. Levkovskii

(Presented by Academician V. N. Kondrat'ev November 23, 1956)

The cross sections of Cd(n, p) Ag reactions have been calculated by comparing the beta yields of these reactions with the yields of Cd^{112} (n, α)Pd^{109}, whose cross section was previously found to be $(1.35 \pm 0.27) \cdot 10^{-27}$ cm^2 [1].

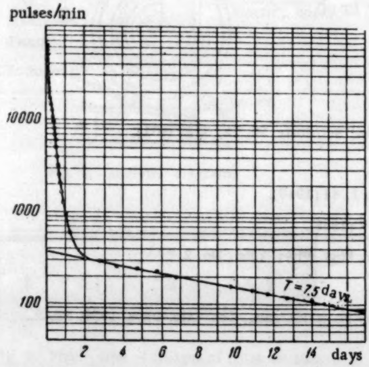

Fig. 1. Decay of radioactive silver separated from a cadmium target which had been irradiated with 14-Mev neutrons.

TABLE 1

Radiation	Half thickness $d_{1/2}$, mg/cm²	E_{max}, Mev		Correction for absorption in counter wall
		Calc.	Lit.	
Ag^{106}	96	2.21	1.96	0.70
Ag^{111}	40	1.02	1.04	0.44
Ag^{112}	195	4.30	4.20	0.84
Ag^{113}	97	2.23	2.20	0.70
Pd^{109}	42	1.06	0.96	0.45

Samples of cadmium nitrate were irradiated for 0.5-1 hr with 14-Mev neutrons; the samples were then dissolved and a carrier was used to separate palladium from the solution through precipitation by dimethylglyoxime. In the filtrate silver and the carrier were precipitated as AgCl. The precipitate was reprecipitated from ammonia and its radioactivity was measured by a standard cylindrical Geiger counter (44.5 mg/cm²). The radioactivity of the palladium precipitates was measured with identical geometry.

Figure 1 shows a typical radioactivity decay curve of a silver precipitate; Fig. 2 shows the results of a graphical analysis of the curve of Fig. 1. The half-lives were found to be 24 minutes, 3.2 hrs, 5.3 hrs, and 7.5 days, which are in good agreement with the half-lives given in the literature for Ag^{106}, Ag^{112}, Ag^{113}, and Ag^{111}.

Table 1 gives absorption data for the beta emission of Ag^{106}, Ag^{111}, Ag^{112}, and Ag^{113} obtained by measuring the radioactivity of silver precipitated from a cadmium target, through aluminum filters of different thicknesses, followed by graphical analysis of the total decay curves. The table also contains absorption measurements for Pd^{109} emission which are used in calculating the reaction cross sections. The third and fourth columns of the table show the maximum energies of the investigated beta emissions given in the literature and those calculated from our absorption measurements by the empirical relation $E = 2.12 \cdot 10^{-2} d_{1/2} + 0.17$ [2].

The table shows that our measurements of the maximum energies for the 24-minute, 3.2-hr, 5.3-hr, and 7.3-day radiation are in good agreement with the published values for beta emission from Ag^{106}, Ag^{112}, Ag^{113}, and Ag^{111}.

TABLE 2

Initial radioactivities allowing for decay during irradiation				Relative radioactivities			
Ag^{106}	Ag^{111}	Ag^{112}	Ag^{113}	Ag^{106}	Ag^{111}	Ag^{112}	Ag^{113}
37600	150	19500	3680	251,0	1.0	130 0	24.6
85000	376	49800	9350	226,0	1.0	133.0	24.9

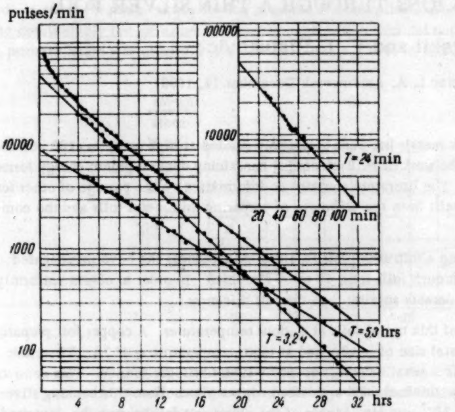

Fig. 2. Graphical analysis of Fig. 1.

TABLE 3

Initial radioactivities allowing for decay during irradiation		Ratio of initial radioactivities
Pd^{109}	Ag^{111}	$\alpha = \frac{I_{Ag^{111}}}{I_{Pd^{109}}}$
368	150	0.407
450	221	0.490
420	180	0.428

TABLE 4

Reaction	Cross section, mbarns
Cd^{106} (n, p) Ag^{106} (24mm)	(76 ±24)
Cd^{111} (n,p) Ag^{111}	(15.0±3.8)
Cd^{112} (n,p) Ag^{112}	(9.8 ±2.9)
Cd^{113} (n,p) Ag^{113}	(7.2 ±2.2)

Table 2 compares the initial activities of Ag^{106}, Ag^{111}, Ag^{112}, and Ag^{113} obtained from two independent experiments, and Table 3 gives the activities of Ag^{111} and Pd^{109} produced in three parallel irradiations.

The cross sections of the reactions were calculated from the data in Tables 1, 2, and 3 according to the known half-lives of Ag^{106}, Ag^{111}, Ag^{112}, Ag^{113} and the relative content of Cd^{106}, Cd^{111}, Cd^{112}, Cd^{113} in a natural cadmium isotope mixture.

According to published data [3] Ag^{106} has two isomers with T = 24 minutes and 8.2 days. The 8.2-day isomer decays only by electron capture; the 24-min isomer according to the literature [4] decays 69% through positron emission and 31% through electron capture. Our findings enable us to calculate the cross section for only the 24-min isomer.

The results of the cross section calculations are given in Table 4.

The author is indebted to Iu. Lapitskii for a great deal of assistance.

LITERATURE CITED

[1] B. G.Dzantiev, V. N. Levkovskii, and A. D. Malievskii, Doklady Akad. Nauk SSSR 113, 3, 537 (1957)

[2] E. Broda, Modern Radiochemistry (1953) p. 22.

[3] I. M. Hollander, I. Perlman, and G. T. Seaborg, Rev. Mod. Phys. 25, 2, 469 (1953).

[4] W. L. Bendel, F. I. Shore, H. N. Brown, and R. A. Becker, Phys. Rev. 90, 888 (1953).

Received November 20, 1956

Institute for Chemical Physics, USSR Academy of Science

PASSAGE OF VARIOUS GAS IONS THROUGH A THIN SILVER FOIL

V. G. Tel'kovskii and V. I. Pistunovich

(Presented by Academician L. A. Artsimovich December 14, 1956)

The passage of charged particles through metals has been thoroughly studied at high energies (100 kev and higher). At moderate energies we have only the work of H. Baetzner [1] containing data on proton energy losses in the 4-60 kev range for various metal foils. The literature contains no information on the passage of other ions with moderate energies through foils. This results from the difficulty of preparing thin metal foils and the complication of such experiments.

We have developed a method of preparing a thin silver foil to 40mμ of thickness and have investigated the passage of H^+, He^+, C^+, N^+, and O^+ ions through foils from 40 to 60 mμ thick. In order to obtain uniformly thin foils the size of the crystals must be considerably smaller than the foil thickness.

In [2, 3] a study was made of the aging of thin metal foils at various temperatures. A copper foil prepared at the temperature of liquid nitrogen has a crystal size of ~ 40Å and at room temperature ~ 400Å. Therefore in order to produce a fine-crystalline silver foil a metal backing cooled by liquid nitrogen is used. This consists of a degassed hammered aluminum foil of 1-2μ thickness and a polished copper plate. Onto this backing silver is evaporated at a residual gas pressure of $1\text{-}3 \cdot 10^{-7}$ mm Hg. Pieces of the aluminum foil bearing the deposited silver film are placed in a solution of NaOH. The aluminum dissolves leaving a thin silver foil on the surface. This is removed from the solution, dried, and placed in the receiving vessel for the studies. This is a quite simple and quick method of preparing silver foils of good quality and thickness from 50 to 80 mμ. Bombardment by helium ions of 20-40 kev reduces the foil thickness to 40 mμ. The foil thickness was determined with ± 4 % accuracy first by weighing and during the experiment by the proton energy losses in the foils, on the assumption that the energy losses are directly proportional to the foil thickness (see [1]). Foil uniformity was determined with a microphotometer. The measurements showed that the thickness varied not more than 2%.

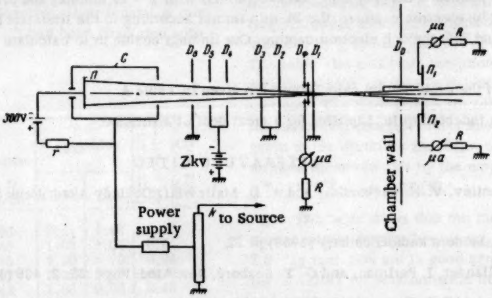

Fig. 1.

In these experiments we used a large magnetic mass spectrometer of about 5 m length and 25° beam deflection. Differential evacuation was accomplished by three diffusion pumps and traps cooled by liquid nitrogen. The ion source included an arc discharge and longitudinal magnetic field. The ion current density at the slit of the gas-discharge chamber reached 100 ma/cm² and could be regulated smoothly during the experimental work.

The receiving vessel was surrounded by a copper jacket at the temperature of liquid nitrogen. The inside pressure during work with helium and hydrogen was $6\text{-}8 \cdot 10^{-7}$ mm Hg and with the heavy gases $\sim 1 \cdot 10^{-7}$ mm Hg, thus enabling us to maintain a clean foil surface during the experiment.

In order to determine ion energy losses upon passage through the foil we used the retarding potential method. A common power supply for ion acceleration from the source and slowing down in the receiver enabled us to considerably reduce errors of measurement, which thus did not exceed 1%. The ion energy distribution in the primary beam was determined with an accuracy of 0.04-0.12% of the energy.

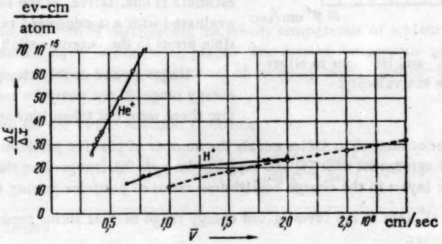

Fig. 2. Energy loss cross section of H^+ and He^+ ions in silver foil as a function of mean ion velocity. The broken line represents Baetzner's data.

A block diagram of the receiving chamber and of the measuring circuit is shown in Fig. 1. The diaphragm D_0 separated the receiving vessel from the remainder of the vacuum and defined the beam. The plates Π_1 and Π_2 served to regulate the intensity and position of the primary beam. The foil was fastened to the diaphragm D_ϕ. Diaphragms D_2 and D_3 passed ions at a ± 4° angle. Diaphragms D_4, D_5, and D_6 served as a shield from secondary negative particles. The receiver consisted of plate Π and cylinder C.

TABLE 1

Ion	E_{in} (kev)	Ipitial ion velocity v in 10^8 cm/sec	Mean velocity loss $-\frac{\Delta v}{\Delta x}$ (10^6 cm/sec mμ)
He^+	7.2	0.6	0.95
C^+	21.5	0.6	1.03
N^+	24.5	0.59	1.02
O^+	28	0.59	1.02

The measurements of energy losses and H^+ and He^+ ion velocities as a function of mean ion velocities are shown in Figs. 2 and 3. Table 1 gives the energy and velocity thresholds at which passage of the different ions is observed through a 55 mμ silver foil.

For comparison Fig. 2 contains the data of [1] which differ from our results at low velocities. This probably results from large errors in this region involved in Baetzner's method. (He measured the velocity loss by the deflection of the particles in a magnetic field with low resolving power and the quantity of protons was determined by a gas counter with mica window.)

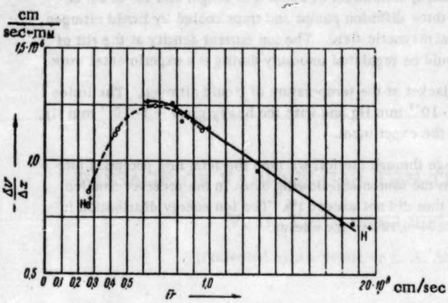

Fig. 3. Velocity losses of H^+ and He^+ ions in silver foil as a function of average ion velocity.

It follows from the measurements that with identical velocities of all the investigated atomic ions the velocity losses are alike within the limits of measurement and the energy losses are proportional to the ion mass. This indicates that the principal and determining factor in the mechanism of energy transfer is the velocity of the ions passing through the foil.

We also estimated the number of neutral particles emerging from the foil for H^+ and He^+ at $E \geq 25$ kev and at the threshold energies for the other ions. This was done through the secondary electron emission which is identical with neutral particles and ions (see [4]). This estimate is qualitative, as the secondary emission was evaluated with a nondegassed target with consequent possible errors in the determination of its emission coefficient.

Negative and doubly charged positive ions in our energy range do not comprise more than 5% [5, 6]; therefore these were not taken into account.

For protons the number of neutral particles equals the number of positive particles at an initial energy of 33-34 kev, which is in good agreement with [5] and supports the hypothesis regarding the determining significance of the last few (~ 5) atomic layers in the charge equilibrium ratios of particles passing through a foil.

For He^+, C^+, N^+, and O^+ ions in the investigated energy range neutral atoms predominate, comprising ~ 70 to 80% of the total number.

At angles greater than ± 4° there is scattering of only an insignificant part of the charged and neutral particles (~ 4-9 %).

LITERATURE CITED

[1] H.Baetzner, Ann. Physik(Series 5) 25, 233 (1936).

[2] P. M. Morozov and M. M. Butslov, J. Exptl.-Theoret. Phys. (USSR) 16, 8, 857 (1946).

[3] H. D. Keith, Proc. Phys. Soc., Sect. B, 69, part 2, No.434B, 180 (1956).

[4] V. G. Tel'kovskii, Doklady Akad. Nauk SSSR 108, 2, 444 (1956).

[5] J. A. Phillips, Phys. Rev. 97, 2, 404 (1955).

[6] G. A. Dissanaike, Phil. Mag. 44, 357, 1051 (1953).

Received November 5, 1956

STEADY TEMPERATURE OF A PLANE PLATE IN A REACTING GAS FLOW

E. P. Vaulin

(Presented by Academician N. N. Bogoliubov December 13, 1956)

We consider the problem of determining the steady temperature of a plane plate in a laminar gas flow within which the reaction $X_2 \rightarrow 2X$ is taking place. The desired temperature can be determined by solving the equations of the boundary layer. The complete set of boundary layer equations for this problem can be written as follows:

the diffusion equation for the initial reaction substance

$$\rho\left(u_1 \frac{\partial c_1}{\partial x_1} + u_2 \frac{\partial c_1}{\partial x_2}\right) = \frac{\partial}{\partial x_2}\left(\rho D \frac{\partial c_1}{\partial x_2}\right) - \rho Z_1; \qquad \text{(1a)}$$

the equation of continuity

$$\frac{\partial (\rho u_1)}{\partial x_1} + \frac{\partial (\rho u_2)}{\partial x_2} = 0; \qquad \text{(1b)}$$

the conservation of momentum

$$\rho\left(u_1 \frac{\partial u_1}{\partial x_1} + u_2 \frac{\partial u_1}{\partial x_2}\right) = \frac{\partial}{\partial x_2}\left(\eta \frac{\partial u_1}{\partial x_2}\right); \qquad \text{(1c)}$$

the conservation of energy

$$\rho\left(u_1 \frac{\partial (c_p\theta)}{\partial x_1} + u_2 \frac{\partial (c_p\theta)}{\partial x_2}\right) = \frac{\partial}{\partial x_2}\left(\lambda \frac{\partial T}{\partial x_2} + \eta u_1 \frac{\partial u_1}{\partial x_2} + q\rho D \frac{\partial c_1}{\partial x_2}\right); \qquad \text{(1d)}$$

$$c_1 + c_2 = 1; \qquad \text{(1e)}$$

$$p = R\rho T, \qquad \text{(1f)}$$

where

$$\theta = T + \frac{1}{2}\frac{u_1^2}{c_p} + \frac{q}{c_p} c_1; \qquad \text{(2)}$$

ρ is the density of the mixture; T is the temperature of the mixture, u_1 and u_2 are the velocity components of the flow in the boundary layer; $c_1 = \rho_1/\rho$ is the relative concentration of the initial reaction substance (ρ_1 is the density of component X_2); c_2 is the relative concentration of the reaction products, or if the flow contains an inert component c_3, is the sum of the relative concentration of the reaction products and the inert component (this can be done, for example, when the molecular weight of the reaction products is not very different from the molecular weight of the inert component [5]); D is the diffusion coefficient of component X_2; η is the coefficient of viscosity; λ is the coefficient of thermal conductivity; ρZ_1 is the reaction rate; q is the heat of reaction; c_p is the specific heat of the mixture at constant pressure; p is the pressure of the mixture.

If we assume that the thermal Prandtl number $\mathrm{Pr} = c_p\eta/\lambda$, the diffusion Prandtl number $\mathrm{Pr}_1 = \eta/\rho D$ and the specific heat c_p of the mixture are independent of the temperature the energy conservation Eq. (1d) becomes

$$\rho\left(u_1\frac{\partial\theta}{\partial x_1} + u_2\frac{\partial\theta}{\partial x_2}\right) = \frac{1}{\mathrm{Pr}}\frac{\partial}{\partial x_2}\left(\eta\frac{\partial\theta}{\partial x_2}\right) + \frac{\mathrm{Pr}-1}{\mathrm{Pr}}\frac{\partial}{\partial x_2}\left[\eta\frac{\partial}{\partial x_2}\left(\frac{u_1^2}{2c_p}\right)\right] + \frac{1}{\mathrm{Pr}}\left(\frac{\mathrm{Pr}}{\mathrm{Pr}_1} - 1\right)\frac{q}{c_p}\frac{\partial}{\partial x_2}\left(\eta\frac{\partial c_1}{\partial x_2}\right). \tag{3}$$

We consider the general case for the Prandtl numbers: $\mathrm{Pr} \neq 1$, $\mathrm{Pr}_1 \neq 1$, and $\mathrm{Pr} \neq \mathrm{Pr}_1$. For the temperature dependence of the viscosity we use the linear relation [1]

$$\eta = \eta_0\frac{T}{T_0}, \tag{4}$$

where η_0 and T_0 are constants.

As was shown by Chapman and Rubesin [2] the inaccuracy of this linear approximation for the viscosity vs temperature relation can be somewhat corrected because the Prandtl number differs from unity.

We consider a heterogeneous reaction in the diffusion region. Then the term ρZ_1 drops out of the diffusion Eq. (1a) and the energy conservation equation becomes

$$\rho\left(u_1\frac{\partial\theta}{\partial x_1} + u_2\frac{\partial\theta}{\partial x_2}\right) = \frac{1}{\mathrm{Pr}}\frac{\partial}{\partial x_2}\left(\eta\frac{\partial\theta}{\partial x_2}\right) + \frac{\mathrm{Pr}-1}{\mathrm{Pr}}\frac{\partial}{\partial x_2}\left[\eta\frac{\partial}{\partial x_2}\left(\frac{u_1^2}{2c_p}\right)\right], \tag{5}$$

where $\theta = T + \frac{1}{2}\frac{u_1^2}{c_p}$.

Using Dorodnitsyn's substitution [2], which involves replacing the coordinate x_1 with y_1:

$$y_1 = \int_0^{x_1}\frac{p}{p_0}\,dx_1, \tag{6}$$

and replacing x_2 with y_2:

$$y_2 = \int_0^{x_2}\frac{\rho}{\rho_0}\,dx_2 = \frac{p}{p_0}\int_0^{x_2}\frac{T_0}{T}\,dx_2, \tag{7}$$

the set of Eqs. (1) and the energy conservation equation in the form (5) become

$$v_1\frac{\partial c_1}{\partial y_1} + v_2\frac{\partial c_1}{\partial y_2} = D_0\frac{\partial^2 c_1}{\partial y_2^2}; \tag{8a}$$

$$\frac{\partial v_1}{\partial y_1} + \frac{\partial v_2}{\partial y_2} = 0; \tag{8b}$$

$$v_1\frac{\partial v_1}{\partial y_1} + v_2\frac{\partial v_1}{\partial y_2} = \nu_0\frac{\partial^2 v_1}{\partial y_2^2}; \tag{8c}$$

$$v_1\frac{\partial\theta}{\partial y_1} + v_2\frac{\partial\theta}{\partial y_2} = \frac{\nu_0}{\mathrm{Pr}}\frac{\partial^2\theta}{\partial y_2^2} + \frac{\mathrm{Pr}-1}{\mathrm{Pr}}\nu_0\frac{\partial^2}{\partial y_2^2}\left(\frac{v_1^2}{2c_p}\right), \tag{8d}$$

where $v_1 = u_1$; $v_2 = \frac{T_0}{T}u_2 + u_1\frac{p_0}{p}\frac{\partial y_2}{\partial x_1}$; $D_0, \nu_0 = \frac{\eta_0}{\rho_0}$ are constants.

We introduce the stream function ψ. Then by setting $v_1 = \frac{\partial\psi}{\partial y_2}$, $v_2 = -\frac{\partial\psi}{\partial y_1}$, we satisfy the continuity Eq. (8b).

Equations (8) will be solved subject to the following boundary conditions:

for $y_2 = 0$, $v_1 = v_2 = 0$ $$\left(\lambda \frac{\partial T}{\partial y_2}\right)_0 = -q\left(\rho D \frac{\partial c_1}{\partial y_2}\right)_0, \quad c_1 = 0; \tag{9}$$

for $y_2 = \infty$, $v_1 = u_\infty$ $$T = T_\infty, \quad c_1 = c_{1\infty} \quad \left(\theta = \theta_\infty = T_\infty + \frac{u_\infty^2}{2c_p}\right) \tag{10}$$

The solution will be sought in the form

$$\psi = \sqrt{\nu_0 u_\infty y_1} f(\tau), \quad \theta = \theta(\tau), \quad c_1 = c_1(\tau), \tag{11}$$

where $\tau = {}^1/_2\, y_2 \sqrt{u_\infty / \nu_0 y_1}$.

Substituting (11) in (8) we obtain

$$c_1'' + \mathrm{Pr}_1 f c_1' = 0; \tag{12}$$

$$f''' + ff'' = 0; \tag{13}$$

$$\theta'' + \mathrm{Pr}\, f\theta' = (1 - \mathrm{Pr}) \frac{u_\infty^2}{8c_p} \frac{d^2}{d\tau^2} (f'^2), \tag{14}$$

where the primes denote derivatives with respect to τ.

The solution of (13) is well known [1]. f is the Blasius function.

Equation (12) can easily be solved by two quadratures and the concentration profile is determined by

$$c_1 = c_{1\infty} \int_0^\tau (f'')^{\mathrm{Pr}_1} d\tau \Bigg/ \int_0^\infty (f'')^{\mathrm{Pr}_1} d\tau. \tag{15}$$

Equation (14) will be solved as the sum of the general solution of the homogeneous equation

$$M'' + \mathrm{Pr}\, f M' = 0 \tag{16}$$

under the boundary conditions:

$$\begin{aligned} &\text{for} \quad \tau = 0 \quad M' = -\frac{q}{c_p} \frac{\mathrm{Pr}}{\mathrm{Pr}_1} \left(\frac{dc_1}{d\tau}\right)_0, \\ &\text{for} \quad \tau = \infty \quad M = 0 \end{aligned} \tag{17}$$

and the particular solution $N(\tau)$ of the inhomogeneous equation

$$N'' + \mathrm{Pr}\, f N' = (1 - \mathrm{Pr}) \frac{u_\infty^2}{8c_p} \frac{d^2}{d\tau^2} (f'^2) \tag{18}$$

under the boundary conditions

$$\begin{aligned} &\text{for} \quad \tau = 0 \quad N' = 0, \\ &\text{for} \quad \tau = \infty \quad N = \theta_\infty. \end{aligned} \tag{19}$$

The solution of (16) is then

$$M(\tau) = \frac{q}{c_p} \frac{\mathrm{Pr}}{\mathrm{Pr}_1} \left(\frac{dc_1}{d\tau}\right)_0 \frac{\int_\tau^\infty (f'')^{\mathrm{Pr}} d\tau}{[f''(0)]^{\mathrm{Pr}}}, \tag{20}$$

where $\left(\frac{dc_1}{d\tau}\right)_0 = c_{1\infty} \frac{[f''(0)]^{\mathrm{Pr}_1}}{\int_0^\infty (f'')^{\mathrm{Pr}_1} d\tau}$.

The particular solution of the inhomogeneous Eq. (18) is obtained by the method of variation of constants, which gives [1]

$$N(\tau)=T_\infty+\frac{u_\infty^2}{2c_p}+(1-\mathrm{Pr})\frac{u_\infty^2}{8c_p}\int_\infty^\tau (f'')^{\mathrm{Pr}}\int_0^\tau (f'')^{-\mathrm{Pr}}\frac{d^3}{d\tau^3}(f'^2)\,d\tau\,d\tau. \tag{21}$$

Taking into account that the general solution of (14) is $\theta = M(\tau) + N(\tau)$ and that $\theta = T + u_1^2/2c_p$ we shall have the following expression for the temperature profile:

$$T=T_\infty+\frac{u_\infty^2}{2c_p}[1-a(\tau,\mathrm{Pr})]-\frac{u_\infty^2}{8c_p}f'^2+ \\ +\frac{qc_{1\infty}}{c_p}\frac{\mathrm{Pr}}{\mathrm{Pr}_1}\frac{[f''(0)]^{\mathrm{Pr}_1}\int\limits_\tau^\infty (f'')^{\mathrm{Pr}}\,d\tau}{[f''(0)]^{\mathrm{Pr}}\int\limits_0^\infty (f'')^{\mathrm{Pr}_1}\,d\tau}, \tag{22}$$

where

$$a(\tau,\mathrm{Pr})=\frac{1-\mathrm{Pr}}{4}\int_\tau^\infty (f'')^{\mathrm{Pr}}\int_0^\tau (f'')^{-\mathrm{Pr}}\frac{d^3}{d\tau^3}(f'^2)\,d\tau\,d\tau. \tag{23}$$

From (22) with $\tau = 0$ we obtain the desired formula for the steady temperature of the plane plate:

$$T_w=T_\infty+\frac{u_\infty^2}{2c_p}[1-a(\mathrm{Pr})]+\frac{qc_{1\infty}}{c_p}\frac{\mathrm{Pr}}{\mathrm{Pr}_1}\frac{b(\mathrm{Pr}_1)}{b(\mathrm{Pr})}; \tag{24}$$

where

$$a(\mathrm{Pr})=\frac{1-\mathrm{Pr}}{4}\int_0^\infty (f'')^{\mathrm{Pr}}\int_0^\tau (f'')^{-\mathrm{Pr}}\frac{d^3}{d\tau^3}(f'^2)\,d\tau\,d\tau; \tag{25}$$

$$b(\mathrm{Pr})=\frac{[f''(0)]^{\mathrm{Pr}}}{\int\limits_0^\infty (f'')^{\mathrm{Pr}}\,d\tau}; \tag{26}$$

$$b(\mathrm{Pr}_1)=\frac{[f''(0)]^{\mathrm{Pr}_1}}{\int\limits_0^\infty (f'')^{\mathrm{Pr}_1}\,d\tau}. \tag{27}$$

To a good degree of accuracy these functions can be represented by the expressions [3]

$$a(\mathrm{Pr})=1-\mathrm{Pr}^{1/2},\quad b(\mathrm{Pr})=\alpha\,\mathrm{Pr}^{1/3},\quad b(\mathrm{Pr}_1)=\alpha\,\mathrm{Pr}_1^{1/3}, \tag{28}$$

where α is the Blasius constant.

Substituting (28) into (24) we finally have

$$T_w=T_\infty+\frac{u_\infty^2}{2c_p}\mathrm{Pr}^{1/2}+\frac{qc_{1\infty}}{c_p}\left(\frac{\mathrm{Pr}}{\mathrm{Pr}_1}\right)^{2/3} \tag{29}$$

or in dimensionless form

$$\frac{T_w-T_\infty}{T_\infty}=\frac{\gamma-1}{2}M^2\,\mathrm{Pr}^{1/2}+W\left(\frac{\mathrm{Pr}}{\mathrm{Pr}_1}\right)^{2/3}, \tag{30}$$

where M is the Mach number; $W = qc_{1\infty}/c_pT_\infty$ is the ratio of the total chemical energy to the thermal energy of flow very far from the plate; γ is the ratio of the specific heats at constant pressure and at constant volume.

In the present paper by solving exactly the differential equations of the boundary layer of reacting gas mixtures with different physical properties we have obtained a formula for the steady temperature of a plane plate which can be used at high speeds or when the heat of friction is comparable with the heat evolved in the chemical reaction. For low Mach numbers (30) gives the result which D. A. Frank-Kamenetskii and N. Ia. Buben obtained [4, 5] from general considerations concerning the heat flow balance on the surface.

We have also obtained the concentration and temperature profiles for heterogeneous reactions in a region of diffusion.

In this work we have not taken account of thermal diffusion.

LITERATURE CITED

[1] N. E. Kochin, I. A. Kibel' and V. N. Roze, Theoretical Hydrodynamics 2 (1948).

[2] D. B. Chapman and M. W. Rubesin, J. Aer. Sci. 16, 9 (1949).

[3] H. Schlichting, Theory of the Boundary Layer (1956) (Russian translation).

[4] D. A. Frank-Kamenetskii, Diffusion and Heat Transfer in Chemical Kinetics (1947).

[5] N. Ia. Buben, Coll. of Articles on Physical Chemistry (1947) p. 148.

Received December 9, 1956

M. B. Lomonosov Moscow State University

THE TUNNEL EFFECT IN SULFIDE RECTIFIERS

Iu. M. Bolokobinskii

(Presented by Academician A. F. Ioffe December 19, 1956)

The theory of the tunnel effect [1-4] has not yet been confirmed by experiment. This results partly from the fact that the operation of ordinary commercial rectifiers (selenium, copper oxide, germanium, and silicon) are based on other processes. The phenomena which take place in sulfide rectifiers [5-6] and which are associated with the flow of electrons past a narrow potential barrier in the near-electrode layer are of interest as a verification of the tunnel effect theory.

The principal assumptions and deductions of the tunnel effect theory which can be verified experimentally to some extent are:

1. The contact is represented by a gap of about 10^{-7} cm. This gap can either be empty or filled by a dielectric medium. The gap produces a potential barrier of the same width as the gap, while its height is between 0.5 and 4 ev.

2. The current passes more easily from the metal into a p-type semiconductor than in the reverse direction.

3. The rectifying action is reduced by increased barrier width; thick barriers are opaque to electrons.

4. Rectification is reduced by increased concentration of carriers in the semiconductor.

5. The contact resistance between two metals separated by a gap must differ very little for the different current directions; the current I is related to the contact voltage V by the formula [1]

$$I = \alpha V + \beta V^2, \tag{1}$$

where α and β are constants. This same current-voltage relation must be valid for contact between a metal and a semiconductor of relatively high conductivity [2].

6. With rising temperature rectification is reduced and finally is reversed.

It is assumed that the applied voltage is lower than the barrier height; otherwise the theory becomes invalid.

The phenomena which will be described below take place in the contact between an aluminum (or magnesium) plate with a disk of (monovalent) cuprous sulfide of 3-4 mm thickness and 0.5 cm^2 area.

The pure cuprous sulfide $\beta\,Cu_2S$ had the following properties: specific gravity 5.52 g/cm^3 (6.1 g/cm^3 as calculated from x-ray data), resistivity at room temperature $2.5 \cdot 10^{-3}$ ohm-cm and Hall constant $+1.3 \cdot 10^{-22}$ cgse. The signs of the Hall constant and of the thermal emf represent p-type conductivity of the $\beta\,Cu_2S$. There is no ionic conductivity at temperatures below 200°. From these data a calculation gave the hole concentration $n = 5 \cdot 10^{20}\ cm^{-3}$ and hole mobility $\mu = 5\ cm^2/v\text{-sec}$.

To form a rectifier the disk is "welded" to the aluminum plate so that aluminum enters the near-electrode layer of the sulfide where its presence is detected by spectral analysis. The resistance of the sulfide, which depends strongly on a deficiency of metal ions [8-9] must be increased and the carrier concentration must be reduced. Variation of the sulfide properties prevents exact quantitative calculations; only a qualitative comparison can be made between experimental results and predictions of the tunnel effect theory.

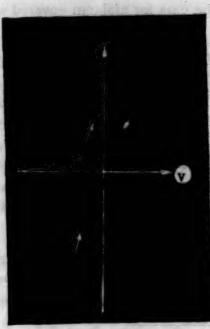

Fig. 1.

The processes in a sulfide cell depend strongly on the applied voltage. When the latter exceeds 0.7 v the near-electrode layer is saturated with aluminum (or magnesium) and the conditions for an n-p junction are probably created. The dynamic characteristics resemble the characteristics of selenium and other commerical rectifiers. The capacitance of the rectifier is 0.04μf when a cutoff voltage of 6 v is applied. If the dielectric constant of the layer with increased resistance is assumed to be 10 its thickness is about 10^{-5} cm.

When the voltage is reduced below 0.5 v the aluminum, which is in an unstable state in the near-electrode layer, apparently partly diffuses into the tablet and partly precipitates in the form of metallic grains and dendrites which penetrate the sulfide to a depth of a few hundred angstroms. Variation of the composition of the near-electrode layer with voltage is confirmed by measurements of the rectifier resistance as a function of time. After reduction of the voltage the resistance drops in a few minutes to an equilibrium value; when the voltage is increased the resistance rises. Below 0.5 v the near-electrode layer of the sulfide shows good conductivity and is separated from the aluminum by a thin oxide film of 20-30 A thickness. Thus the conditions for the theoretical tunnel effect are created. We give below a comparison of the experimental results and the previously mentioned theoretical assumptions.

1. Figure 1 is the dynamical current-voltage characteristic of a rectifier with an aluminum electrode at 22° which was photographed from the screen of a cathode-ray oscilloscope. The effective rectifier voltage was 0.4 v and the current $I_{eff} = 0.2$ amp. The coordinate axes are drawn according to the approximate calculation. Arrows show the direction of current change. Positive voltages are those for which the sulfide is positive, and positive currents flow from the sulfide to the aluminum. The looped shape of the characteristic shows that the capacity current is large. The capacitance of the rectifier calculated from the dynamic current-voltage characteristics for different voltages is about 0.005 f and is independent of the voltage from 0 to 0.4 v. At the same voltages the capacitance measured on a 50-cycle ac bridge was 0.007 f. This value is obtained for the capacitance if we assume that the thickness of the oxide layer is 20 A, that its dielectric constant is 10 and that the surface layer is 2000 cm² per unit area of the rectifier disk. The large area of the surface is not surprising considering that the dendrites can have a very large surface.

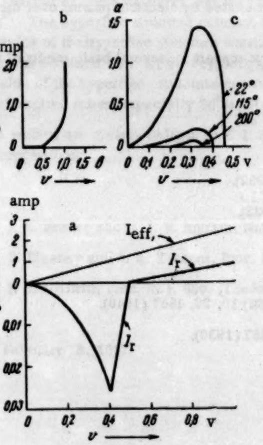

Fig. 2.

Assuming that the potential barrier is triangular and that its height is 0.7 ev we can obtain agreement between the currents calculated from the tunnel effect theory and the measurements.

2. The current flows more easily from the aluminum or magnesium to the sulfide.

3. The tunnel effect appears only when the insulating layers are thin. For example, when the aluminum is electrolytically coated with a stable oxide layer of about $5 \cdot 10^{-5}$ cm thickness the current flows more easily from the sulfide to the aluminum. Figure 2b shows the relation between the rectified current and the voltage for this case. The characteristic is seen to differ from that for a thin layer (see Fig. 2a). Rectification in the case of a thick layer is associated with the entrance of aluminum

into the sulfide. If this does not occur the current-voltage characteristic is symmetrical with respect to zero voltage; such is the case for niobium covered with a thick oxide layer.

4. When tantalum is used instead of aluminum, with its surface cleaned to remove oxides and impurities, metal ions do not enter the sulfide. With loose contact there is probably a gap of a few angstroms between the sulfide and the tantalum. The current-voltage relation generally follows Eq. (1) with the ratio β/α about 100 times smaller than for aluminum when the latter by entering the sulfide causes reduction of the hole concentration. Thus when the carrier concentration is increased the rectifying action is reduced. Since the width of the empty gap varies from experiment to experiment the magnitude of the current also varies. In experiments with tantalum electrodes the variation reached a factor of 2 to 3 at the same voltages.

5. Figure 2a gives the rectified current I_r and the effective current I_{eff} of a sulfide cell with an aluminum electrode as a function of the effective voltage at 22°. Similar characteristics are obtained with a magnesium electrode, as was known previously although the nature of the phenomenon was not understood [6-7]. The rectified current up to 0.4 v increases with the square of the voltage while the effective current increases linearly. Above 0.5 v the rectification is reversed and is associated with different processes.

Fig. 3.

6. Figure 2c shows the dependence of the rectified current on voltage at various temperatures for a cell with a magnesium electrode. At higher temperatures the rectifying action diminishes and above 200° is reversed. A cell with an aluminum electrode changes the direction of rectification at a temperature a little above 100°. With a tantalum electrode rectification is reversed at about 60°.

Figure 3 gives the interesting dynamic characteristic of a rectifier with a tantalum electrode which was first coated electrolytically with an oxide. This characteristic was photographed from the screen of an oscilloscope with effective rectifier voltage of 0.6 v at 22°. When a positive voltage is applied to the tantalum electrode the current increases in a stepped curve and decreases smoothly. This curve has not been explained. The cause may lie in electrons which pass over the potential barrier, as was suggested by Mott-Smith [10]. The relation is most clearly expressed for both current directions with a tantalum electrode. In this connection it is interesting to note that similar behavior has been observed during the study of emission from tantalum and tungsten cathodes [11]. Experiment shows the importance of the current generated by electrons passing over the potential barrier and of the capacity current.

The experimental findings presented here provide qualitative support for several basic results of the theory of the tunnel effect.

LITERATURE CITED

[1] J. Frenkel, Phys. Rev. 36, 1604 (1930).

[2] J. Frenkel and A. Ioffe, Physik Z. Sowjetunion 1, 60 (1932).

[3] A. H. Wilson, Proc. Roy. Soc. (London) A, 136, 487 (1932).

[4] L. Nordheim, Z. Physik 75, 434 (1932).

[5] A. Z. Levinzon, Semiconductor Rectifiers (1948).

[6] Iu. A. Dunaev and B. V. Kurchatov, J. Tech. Phys. (USSR) 10, 22, 1857 (1940).

[7] M. Bergstein, J. Rinke, and C. Gutheil, Phys. Rev. 36, 587 (1930).

[8] L. Eisenman, Ann. Physik 10, 129 (1952).

[9] I. Iokota, J. Phys. Soc. Japan 8, 595 (1953).

[10] H. M. Mott-Smith, Phys. Rev. 56, 668 (1939).

[11] D. Turnbull and T. E. Phipps, Phys. Rev. 56, 663 (1939).

Received November 1, 1956

NUCLEAR SPIN OF Fe^{57}

N. S. Garif'ianov, M. M. Zaripov, and B. M. Kozyrev

(Presented by Academician L. A. Artsimovich February 18, 1957)

We have measured paramagnetic resonance in fused borax containing iron. Cylindrical specimens were prepared by melting 5 mg $FeCl_3 \cdot 6H_2O$ and 4 g borax. Sample I contained iron enriched to 71.91% of Fe^{57}; the analogous sample II contained the ordinary unenriched isotope mixture. Measurements were performed at 77°K with the frequencies 115, 240, and 430 Mc using the grid current method and modulation of the constant magnetic field H.

The value of the effective *g* factor, the asymmetric shape of the χ'' (H) curves and the broadening of these curves at higher frequencies observed in the unenriched Specimen II indicate that the Fe^{+++} ion in vitrious borax is subject to the same conditions as in hemoglobin products. Evidently in the present instance because of the partially covalent character of the bond between Fe^{+++} and its surroundings the lower Kramers doublet ($M_s = \pm {}^1/_2$) is considerably separated from the other sublevels [1]. Then at the low frequencies which we used it can be expected that the absorption maximum will correspond to an effective *g* factor of ~ 4, which is just what is observed with Specimen II.

The χ''(H) curves for the enriched Specimen I were considerably broader at all three frequencies than the corresponding curves of II; in addition to the principal absorption maximum Specimen I showed an additional poorly resolved maximum in weaker fields H. The maximum observed for II lies between these.

An analysis of the data shows that they can be explained by assigning the value $I = {}^1/_2$ to the nuclear spin of Fe^{57}. The hyperfine structure constant is of the order of 10 gauss and is somewhat anisotropic. The observed value of the hyperfine structure constant is somewhat larger than would be expected from the data in [2], which was obtained from $K(Al, Fe)(SeO_4)_2 \cdot 12D_2O$, where the Fe^{+++} bonds are purely ionic. Such an increased value of the hyperfine structure constant is possible as the large initial splitting must be caused by the addition of excited states, especially $3d^34s$ [3].

The authors are greatly obliged to E. I. Semenova for preparing the specimens and to S. A. Al'tshuler for valuable suggestions.

LITERATURE CITED

[1] J. E. Bennet and D. J. E. Ingram, Nature 177, 275 (1956).

[2] B. Bleaney and R. S. Trenam, Proc. Roy. Soc. (London) A, 223, 1 (1953).

[3] J. S. Griffith, Proc. Roy. Soc. (London) A, 235, 23 (1956).

Received February 13, 1957

Physico-Technical Institute, Kazan Branch, Academy of Sciences USSR and V. I. Ul'ianov-Lenin Kazan State University

A HOMOGENEOUS FIELD BETA RAY SPECTROMETER WITH COMPENSATED SPHERICAL ABERRATION

K. A. Dolmatova and V. M. Kel'man

(Presented by Academician L. A. Artsimovich December 14, 1956)

We shall describe a beta ray spectrometer with a homogeneous longitudinal magnetic field, whose spherical aberration is compensated by a transverse magnetic field whose strength is given by $H = H_1/r$. The additional field was excited by a coil with turns of such shape that the electrons which were emitted by the source within a large solid angle formed a linear ring focus.•

There is no difficulty in calculating electron trajectories in the homogeneous field. In the region where the H_1/r field is superposed the differential equations of electron motion become quadratures [1] which can be written as

$$\frac{z - z_0}{r_0} = \int_1^\rho \frac{(\cos\psi_0 + K\ln\rho)\,d\rho}{\sqrt{1 - (\sin\psi_0\sin\varphi_0\rho)^2 - (\cos\psi_0 + K\ln\rho)^2}},$$

$$\varphi - \varphi_0 = \int_1^\rho \frac{\sin\varphi_0\sin\psi_0\,d\rho}{\sqrt{1 - (\sin\psi_0\sin\varphi_0\rho)^2 - (\cos\psi_0 + K\ln\rho)^2}}. \tag{1}$$

Here the cylindrical coordinates r, φ, z are used; the $\underline{z}$ axis coincides with the axis of the instrument and the origin is at the source. The direction $z = 0$, $\varphi = 0$ gives the projection of the velocity of an electron emitted by the source on the plane $z = 0$; $\rho = r/r_0$; r_0, φ_0, z_0 are the coordinates of the point of entry of the electron into the inhomogeneous field; ψ_0 is the angle between the velocity of the electron and the $\underline{z}$ axis at the instant of emission from the source; $K = -H_1/H\rho$, where $H\rho$ characterizes the electron momentum.

Since the compensating field was near the vertex of the trajectory it could be assumed that ρ in Eq. (1) changes relatively little so that we set $\rho = 1 + x$, where $x \ll 1$ and $\ln\rho = x - x^2/2$. Equation (1) can then be integrated:

$$\frac{z - z_0}{r_0} = \frac{1}{\sqrt{-c}}\left[\cos\psi_0 - \frac{bK}{2c} - \frac{K}{2}\left(\frac{3b^2}{8c^2} - \frac{a}{2c}\right)\right]\left(\arcsin\frac{b}{\sqrt{-\Delta}} - \arcsin\frac{2cx+b}{\sqrt{-\Delta}}\right) +$$

$$+ \frac{K}{c}\left[1 - \frac{1}{4}\left(x - \frac{3b}{2c}\right)\right]\sqrt{a + bx + cx^2} - \frac{K}{c}\left(1 + \frac{3b}{8c}\right)\sqrt{a},$$

$$\varphi - \varphi_0 = \sin\psi_0\sin\varphi_0\frac{1}{\sqrt{-c}}\left(\arcsin\frac{b}{\sqrt{-\Delta}} - \arcsin\frac{2cx+b}{\sqrt{-\Delta}}\right),$$

• Aberration also can be compensated by other types of longitudinal fields. Thus in 1955 when B. S. Dzhelepov learned of our instrument, which was then being assembled, he informed us that his laboratory was testing a beta ray spectrometer with a short magnetic lens in which the spherical aberration of the lens is compensated by a transverse field excited by a coil close to the source. This was later reported at the conference on beta spectroscopy in February 1956.

where $a = 1 - \sin^2\psi_0 \sin^2\varphi_0 - \cos^2\psi_0$; $b = -2\sin^2\psi_0 \sin^2\varphi_0 - 2K\cos\psi_0$; $c = -\sin^2\psi_0 \sin^2\varphi_0 - K^2 + \cos\psi_0 K$; $\Delta = 4ac - b^2$.

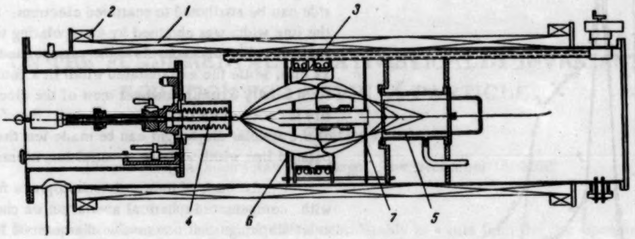

Fig. 1. Beta ray spectrometer with compensated spherical aberration.

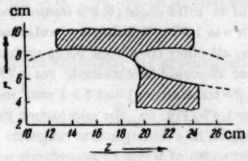

Fig. 2. Boundary of compensating magnetic field without account of the scattering field. The calculated boundary is indicated by the broken line.

From these formulas we obtained the shape of the boundary of the inhomogeneous field which insured an aberrationless ring focus from a point source that would coincide with a linear ring focus formed by an infinitely narrow electron beam emitted at an initial angle close to 30°. We calculated the electron trajectories for which the emission angle ψ_0 varies every 2° between 20° and 40°, with $K = -0.07$ and the homogeneous magnetic field H_0 characterized by the relation

$$K_0 = -\frac{H_0}{2\,(H\rho)} = -0.07.$$

The electron trajectories with $\psi_0 = 30°$ are then entirely within the homogeneous field.

The longitudinal field was excited by Coil 1 (Fig. 1) with 33 cm inside diameter and 110 cm length, which was wound on a copper tube that served as the spectrometer chamber. For improvement of field homogeneity we used correction coils 2. This arrangement insured longitudinal magnetic field homogeneity in the working space (50 cm long) with accuracy to 0.4%. Coil 3 which produced the compensating transverse field consisted of 30 turns of a 1 mm wire arranged symmetrically with respect to the axis. This was connected in series with coils 1 and 2. The shape of the turns agreed with the calculated field boundary shape everywhere except in those portions of the extra field that were traversed by trajectories of electrons emitted at 20° and 40° (Fig. 2).

The radioactive source adhered to holder 4 (Fig. 1) which was introduced into the chamber by means of a Wilson seal and vacuum stopcock without affecting the vacuum. The detector was a GM-5 end-window counter with a 90-mm window. The window was covered with a 17μ cellophane film which at 80 kev transmits about 50% of the electrons. The entrance slit 6 defined electrons in the solid angle $\Omega = 8.7\%$ of 4π (ψ_0 from 20° to 40°) or in the solid angle $\Omega = 7\%$ (ψ_0 from 25° to 40°). The transmission of the instrument was reduced by the fact that the inside correction coil screened about 15% of the beam. The annular diaphragm 7 was placed at the ring focus.

The characteristics of the instrument were first investigated with an electron gun and movable fluorescent screen perpendicular to the axis. It was shown that a compensating field reduces the width of the annular image by a factor of 2.5 compared with a homogeneous field.

Investigations were then carried out with a radioactive source (active ThB) measuring 1× 1 mm². In order to determine the position and size of the ring focus an x-ray film was placed in the path of the beta particles, to form the image of the ring focus that was produced by conversion electrons of the ThB F-line (148 kev). The position of the film for minimum image width was determined both for the homogeneous field (with the inside

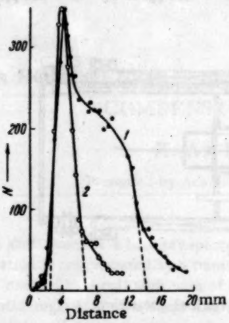

Fig. 3. Microphotograms of the annular image. 1) In a homogeneous field; 2) in a field with compensated spherical aberration. The horizontal axis gives the distance from the outer edge of the annular image; the vertical axis gives the intensity in arbitrary units.

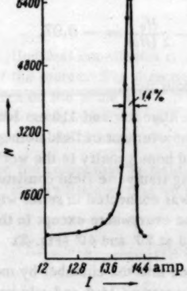

Fig. 4. Shape of line for 5.2 % transmission ($\Omega = 7\%$). The horizontal axis gives the current in the spectrometer coils.

coil switched off) and the corrected field. Figure 3 gives microphotograms of electron intensities in the annular image. The spreading of the annular image on its inner side can be attributed to scattered electrons; therefore the line width was obtained by extrapolating to the base line. In a homogeneous field the extrapolated width is 12 mm, while the extrapolated width in a compensated field is only 5 mm. However most of the electron intensity is concentrated in a narrower ring; therefore the width of the annular diaphragm can be made less than the extrapolated line width without essential loss of intensity.

On the basis of these microphotograms for a field with compensated spherical aberration we chose an annular diaphragm with an outside diameter of 108 mm and 3 mm slit width which transmitted about 88% of the electrons. With this diaphragm we tested the beta ray spectrometer in conjunction with a counter. For a 1×1 mm^2 source and 8.7 % of 4π solid angle (6.5% transmission) the line half width was 1.9%. By using a circular source of 5 mm diameter, all other conditions being unchanged, a line half width of 3% could be obtained. For a 7% of 4π solid angle (5.2% transmission) and 1×1 mm^2 source the half width was 1.4% (Fig. 4). For comparison the F-line was also measured in a homogeneous magnetic field with an annular slit width of 9 mm in accordance with the data obtained from the microphotograms. This diaphragm also transmitted about 88% of the radiation. With a 1×1 mm^2 source and 8.7 % solid angle (7.7% transmission) the half width was 5.7%. Thus for a 8.7% solid angle a compensating field increases the resolution by a factor of 3. But as already mentioned the presence of a compensating coil inside the instrument reduces the transmission. In a homogeneous field without inside coil the same transmission can be obtained with a smaller solid angle. For 6.5% transmission (equal to the solid angle in the ideal case) the theoretical half width in a homogeneous field is 3.6% [2], which is about 2 times worse than in a field with compensated spherical aberration for the same transmission.

LITERATURE CITED

[1] V. M. Kel'man and S. Ia. Iavor, J. Tech. Phys. (USSR) 24, 7, 1923 (1954).

[2] E. Persico, Rev. Sci. Instr. 20, 191 (1949).

Received October 1, 1956

Physico-Technical Institute, Academy of Sciences USSR

ON THE FUNDAMENTAL RELATIVISTICALLY INVARIANT EQUATION FOR A SPIN ½ PARTICLE

G. A. Zaitsev

(Presented by Academician N. N. Bogoliubov December 15, 1956)

Since the magnetic moment of a particle differs considerably as a rule from the corresponding magneton, with a small difference found only for the electron and positron, the Dirac equation cannot be used for all spin $^1/_2$ particles. We therefore consider once more the problem of obtaining a relativistically invariant equation for a particle of spin $^1/_2$, charge $\underline{e}$, mass m_0, and magnetic moment $\mu_0 = \dfrac{e\hbar}{2m_0c}(1+\delta)$ (where $\delta \neq 0$) in an external electromagnetic field.

In the nonrelativistic approximation the equation for a spin $^1/_2$ particle can be written as

$$\left[-i\hbar\frac{\partial}{\partial t}+\frac{1}{2m_0}\sum_{k=1}^{3}\left(-\hbar i\frac{\partial}{\partial x^k}-\frac{e}{c}A_k\right)^2+e\varphi\right]\xi_0-\frac{e\hbar}{2m_0c}(1+\delta)\sum_{k=1}^{3}H_k\sigma_k\xi_0=0 \tag{1}$$

(here ξ_0 is a first-order spinor; σ_k are the Pauli matrices; A_k are the components of the vector potential).

We know that when we study the behavior of a particle in a magnetic field Eq. (1) usually serves to determine the magnetic moment . For an electron, neglecting δ, Eq. (1) is the ordinary Pauli equation.

We shall begin by assuming that the state of a spin $^1/_2$ particle can be characterized by a single real spinor ψ, whose transformations are known for the complete Lorentz group [1, 2]. Both sides of the relations $-\hbar i\,(\partial\xi/\partial x^\alpha) = p_\alpha\xi$, or equivalently $-\hbar I(\partial\psi/\partial x^\alpha) = p_\alpha\psi$ (where in accordance with [1, 2] we assume $\xi \leftrightarrow \psi$, $i \leftrightarrow I$, $x^4 = ct$, $\alpha = 1, 2, 3, 4$) must be transformed in identical manner; the p_α are the components of a 4-vector. Therefore $\hbar$ must be regarded not as the usual scalar but as a pseudoscalar, which reverses its sign under space-time reversals and remains invariant under four-dimensional rotations, so that the numerical value of the Plank constant is the absolute value of the pseudoscalar, and the I matrix must equal ± J. Taking the positive sign for definiteness we find that the expressions for the R^α matrices are given by the first line in Table 1 of [2]. From these with the assumption $\xi_0 \leftrightarrow \psi$ we can rewrite (1) as

$$\begin{gathered}\left[-\hbar J\frac{\partial}{\partial t}+\frac{1}{2m_0}\sum_{k=1}^{3}\left(-\hbar J\frac{\partial}{\partial x^k}-\frac{e}{c}A_k\right)^2+e\varphi\right]\psi_0-\\ -\frac{e\hbar}{2m_0c}(1+\delta)R_4\sum_k R^kH_k\psi_0=0.\end{gathered} \tag{2}$$

In order to render Eq. (2) relativistically invariant we must replace the operator

$$-\hbar J\frac{\partial}{\partial t}-eA_4+\frac{1}{2m_0}\sum_k\left(\hbar J\frac{\partial}{\partial x^k}+\frac{e}{c}A_k\right)^2 \quad (A_4=-\varphi)$$

by

$$\frac{1}{2m_0}\left[-\left(\hbar J\frac{\partial}{\partial x^4}+\frac{e}{c}A_4\right)^2+\sum_{k=1}^{3}\left(\hbar J\frac{\partial}{\partial x^k}+\frac{e}{c}A_k\right)^2+m_0^2c^2\right],$$

and $R_4 \sum_k R^k H_k$ by

$$R_4 \sum_k R^k H_k - R \sum_k R^k E_k = -J \frac{1}{2} F_{\alpha\beta} R^\alpha R^\beta$$

($F_{\alpha\beta}$ are the components of the electromagnetic field tensor).

Then (2) becomes

$$\Big[-\Big(\hbar J \frac{\partial}{\partial x^4} + \frac{e}{c} A_4\Big)^2 + \sum_k \Big(\hbar J \frac{\partial}{\partial x^k} + \frac{e}{c} A_k\Big)^2 + m_0^2 c^2 + + \frac{e\hbar}{c}(1+\delta)\, J \frac{1}{2} F_{\alpha\beta} R^\alpha R^\beta\Big]\psi = 0 \tag{3}$$

(where ψ is a real spinor), and the invariance of this equation with respect to the complete Lorentz group follows directly from the properties of real spinors [2]. In order to obtain (2) from (3) we must set $\psi = \Big[\exp\Big(-J\frac{m_0 c^2 t}{\hbar}\Big)\Big]\psi_0$ and neglect the terms $\Big(\frac{m_0 \hbar^2}{2c^2}\Big)\Big(\frac{\partial^2 \psi_0}{\partial t^2}\Big), \Big(\frac{e^2 \varphi^2 m_0}{2c^2}\Big)\psi_0, \Big(\frac{m_0 e\hbar}{2c^2}\Big)\Big(J\frac{\partial}{\partial t}\varphi + J\varphi\frac{\partial}{\partial t}\Big)\psi_0$; we must also drop the term $\frac{e\hbar}{c}(1+\delta)\, J R_4 \Sigma R^k E_k$.

Let us consider the special case of (3) when $\mu_0 = \frac{2\hbar}{2m_0 c}$. For this case we denote ψ by $\psi_{(1)}$ and introduce a second real spinor $\psi_{(2)}$; with $\delta = 0$ we can then obtain (3) from a pair of first-order relativistically invariant differential equations:

$$R^\alpha \frac{\partial}{\partial x^\alpha}\psi_{(1)} + \frac{e}{\hbar c} J R^\alpha A_\alpha \psi_{(1)} = \frac{m_0 c}{\hbar}\psi_{(2)}, \tag{4}$$

$$R^\alpha \frac{\partial}{\partial x^\alpha}\psi_{(2)} - \frac{e}{\hbar c} J R^\alpha A_\alpha \psi_{(2)} = \frac{m_0 c}{\hbar}\psi_{(1)}. \tag{5}$$

For this purpose it is sufficient to multiply (4) on the left by the operator $R^\alpha\Big(\frac{\partial}{\partial x^\alpha}\Big) - \Big(\frac{e}{\hbar c}\Big) J R^\alpha A_\alpha$.

Introducing instead of $\psi_{(1)}$ and $\psi_{(2)}$ a column containing the complex elements

$$\tilde{\psi} = \frac{1}{\sqrt{2}}\left[(\psi_{(2)} + \psi_{(1)}) + iJ(\psi_{(2)} - \psi_{(1)})\right],$$

we can rewrite (4) and (5) as a single equation:

$$R^\alpha\Big(\frac{\partial}{\partial x^\alpha} - i\frac{e}{\hbar c}A_\alpha\Big)\tilde{\psi} = \frac{m_0 c}{\hbar}\tilde{\psi}. \tag{6}$$

This is the Dirac equation with the special matrices $\gamma_k = R^k$, $\gamma_4 = iR^4$ (where, however, because of the fact that $\hbar$ is a pseudoscalar, $\tilde{\psi}$ does not transform in exactly the usual way under reflection). Therefore all solutions of the Dirac equation with these matrices will also be solutions of (3) with $\delta = 0$.

From the present point of view the fundamental initial equation is (3) instead of the Dirac Eq. (6). The first-order differential equations are introduced only for convenience in solving the fundamental equation (like the factoring method [3]); they have no independent significance. In general with $\delta \neq 0$ (3) cannot be derived from a set of first-order equations.

In conclusion we shall write the fundamental equation (3) using complex quantities (assuming $\xi = \begin{pmatrix}\psi_1 + i\psi_3 \\ \psi_2 + i\psi_4\end{pmatrix}$, $i \leftrightarrow J$, etc.):

$$\left(\hbar i \frac{\partial}{\partial t} - e\varphi\right)^2 - c^2 \sum_k \left(\hbar i \frac{\partial}{\partial x^k} + \frac{e}{c} A_k\right)^2 - m_0^2 c^4 -$$

$$- e\hbar c\,(1+\delta)\left(-\sum_k H_k \sigma_k + i \sum_k E_k \sigma_k\right)\Big]\,\xi = 0. \qquad (7)$$

In this form it is especially simple and can be used to solve specific physical problems, whereas for a general study it is more suitable to use (3). In particular for $\delta = 0$ (7) appears much simpler than the second-order equation derived from the Dirac equation in the usual way. Another characteristic of (7) is that ξ is acted on from the left by an operator which is not Hermitian for $E_k \neq 0$, so that the quantum mechanical requirement of Hermitian operators must be regarded as only approximate. It is probable that the latter characteristic caused disregard of equations such as (7) in the attempts to generalize the Pauli equation.

We take this opportunity to thank Professor L. Infeld for his interest in this work.

LITERATURE CITED

[1] G. A. Zaitsev, J. Exptl.-Theoret. Phys. (USSR) 24, 653 (1953).

[2] G. A. Zaitsev, J. Exptl.-Theoret. Phys. (USSR) 25, 667 (1953).

[3] L. Infeld and T. E. Hull, Rev. Mod. Phys. 23, 21 (1951).

Received October 28, 1954

ON POSSIBLE DIPOLE TRANSITIONS OF Λ-PARTICLES

B. L. Ioffe and Associate Academician I. Ia. Pomeranchuk

We can regard it as experimentally established [1] that the system of two pions produced by θ^+-decay has spin 0 and positive parity, whereas the system of 3 pions created by τ^+-decay is in the state 0^-. If parity is to be conserved this would indicate that the θ and τ are different particles. For the purpose of explaining the existence of two K-mesons differing in parity but with very close masses it has been suggested [2] that in addition to the two types of K-mesons (θ and τ) two types of hyperons (Λ_θ and Λ_τ, Σ_θ and Σ_τ) also exist and that all except weak interactions are invariant with respect to the simultaneous interchanges $\theta \rightarrow \tau$ and $\Lambda_\theta \rightarrow \Lambda_\tau$, $\Sigma_\theta \rightarrow \Sigma_\tau$.

If this hypothesis is accepted the mass difference between Λ_θ and Λ_τ, which results only from weak interactions, is extremely small (of the order of 10^{-6} ev), so that the possibility of $\Lambda_\theta \rightleftharpoons \Lambda_\tau$ transitions arises in an external electromagnetic field.*

When the electromagnetic field is almost constant over the dimensions of a Λ-particle such transitions are effectively equivalent to the appearance of a transition dipole moment. It is clear that such a dipole moment **d** can only have the direction of the Λ-particle spin **s**, so that

$$\mathbf{d} = er_0\mathbf{s}C_p, \tag{1}$$

where r_0 is a constant with the dimension of length, which is determined by the size of the Λ-particle (hereinafter $\hbar = c = 1$)and C_p is the interchange operator of Λ_θ and Λ_τ [2]: $C_p = \left(\begin{smallmatrix}0&1\\1&0\end{smallmatrix}\right)$.

The existence of a dipole moment in the Λ-particle can lead to a number of the observed effects. Let us first consider the scattering of Λ-particles by a nuclear Coulomb field. The interaction energy is

$$U = -\frac{Ze^2r_0}{r^3}\mathbf{r}\mathbf{s}C_p. \tag{2}$$

In the Born approximation ** and assuming that the Λ-particle is nonrelativistic we obtain for the scattering amplitude

$$f_{\text{coul}} = 2iZe^2r_0m\frac{\mathbf{s}\mathbf{q}}{q^2}, \tag{3}$$

---

* We are following the most general hypothesis, to the effect that each of the θ- and τ-mesons interacts with both types of hyperons so that, for example, the simultaneous creation of both θ and Λ_θ and of θ and Λ_τ is possible.

** The validity of the Born approximation can be limited by the usual condition $|U| \ll v/r$. If r is the minimum distance (the nuclear radius R) we obtain from (2) the upper limit

$$E \gg {}^1/_8(Ze^2)^2\left(\frac{r_0}{R}\right)^2 m.$$

In the cases of interest this condition is well satisfied: thus with $Z = 30$ and $r_0 = 1/\mu_\pi$ it becomes $E \gg 0.5$ Mev.

where m is the mass of the Λ-particle; $q = 2p\sin(\theta/2)$ is the momentum transferred to the nucleus. If we assume spin $^1/_2$ for the Λ-particle the differential cross section is

$$d\sigma_{\text{coul}} = \frac{1}{4}\pi (Ze^2)^2 r_0^2 \frac{m}{E\sin^2(\theta/2)} \sin\theta \, d\theta. \tag{4}$$

Small angles contribute most to the total cross section. Therefore the total cross section can be obtained by integrating (4) over the range of angles corresponding to variation of the impact parameter from the nuclear radius R to the Born radius a. This gives

$$\sigma_{\text{coul}} = \pi (Ze^2)^2 r_0^2 \frac{m}{E} \ln \frac{a}{R}. \tag{5}$$

A numerical estimate shows that for $r_0 \sim 1/\mu_\pi = 1.4 \cdot 10^{-13}$ cm the Coulomb scattering cross section with the transition $\Lambda_\theta \rightarrow \Lambda_\tau$ at Λ-energies of the order of tens of Mev exceeds the nuclear cross section. Thus for $Z \sim 30$ and $E \sim 10$ Mev $\sigma_{\text{coul}}/\sigma_{\text{nuc}} \sim 5$. If Λ_θ and Λ_τ have very different lifetimes a strong Coulomb interaction could be observed by putting a thin plate of a substance with large Z in the path of the longer-lived Λ-particles and observing the increased number of Λ-decays.

It is interesting that because the Coulomb scattering amplitude (3) is spin-dependent and there is interference between the Coulomb and nuclear scattering the Λ-particles can be polarized in the plane perpendicular to the incident beam. The degree of polarization is determined by

$$\mathbf{P} = -\frac{\mathbf{q}}{q^2} \frac{2Ze^2 r_0 m \,\mathrm{Im}\, f_0}{|f_0|^2 + (Ze^2 r_0 m/q)^2}, \tag{6}$$

where f_0 is the nuclear scattering amplitude with the transition $\Lambda_\theta \rightarrow \Lambda_\tau$. Moreover, if the Λ-spin is greater than $^1/_2$, the term $\mathbf{sq}$ in (3) results in an "aligned" beam of Λ-particles, that is, when $s = {}^3/_2$ for example, after scattering the number of Λ-particles whose spin projections on $\mathbf{q}$ is $\pm{}^3/_2$ will be greater than the number whose spin projection is $\pm{}^1/_2$.

Another effect which can result from a dipole moment in Λ-particles is the appearance of levels in the Coulomb field of a nucleus. Indeed, since the potential energy is $U \sim Ze^2 r_0/r^2$, and the kinetic energy is $\sim 1/mr^2$, then when $Ze^2 r_0 m \gtrsim 1$ levels can be expected.

In this case the Schroedinger equation outside of the nucleus is

$$\left\{-\frac{1}{2m}\Delta - \frac{Ze^2 r_0}{2r^3}\mathbf{r}\vec{\sigma} C_P\right\}\psi = E\psi. \tag{7}$$

Instead of the two-component functions $\psi = \begin{Bmatrix} \psi_{\Lambda_\theta} \\ \psi_{\Lambda_\tau} \end{Bmatrix}$ it is convenient to introduce the functions $\varphi = {}^1/_2 (\psi_{\Lambda_\theta} - \psi_{\Lambda_\tau})$ and $\chi = {}^1/_2 (\chi_{\Lambda_\theta} + \psi_{\Lambda_\tau})$, for which (7) has the diagonal form

$$\left\{-\frac{1}{2m}\Delta + \frac{Ze^2 r_0}{2r^3}\mathbf{r}\vec{\sigma}\right\}\varphi = E\varphi \tag{8}$$

with a similar equation for χ. We shall limit ourselves to S-levels. The solution will be sought in the form

$$\varphi = \frac{1}{r}\left[u(r) + \frac{\sigma\vec{r}}{r} w(r)\right]. \tag{9}$$

The substitution of (9) in (8) leads to the following equations for the wave functions outside of the nucleus:

$$d^2u/dr^2 - \alpha w/r^2 = \varkappa^2 u, \tag{10a}$$

$$d^2w / dr^2 - 2w / r^2 - \alpha u / r^2 = \varkappa^2 w, \tag{10b}$$

where $\alpha = Ze^2r_0m$ and $\kappa^2 = 2m|E|$. Equations (10a) and (10b) can be solved by letting $w = Cu$, where C is a constant. The values of C are determined in such a way that (10a) agrees with (10b). This can be done if C satisfies

$$\alpha C = \alpha / C + 2, \tag{11}$$

whence

$$C_{1.2} = (1 \mp \sqrt{1 + \alpha^2}) / \alpha. \tag{12}$$

The general solution can then be written as $u = u_1 + u_2$, $w = C_1u_1 + C_2u_2$, where u_1 and u_2 obey

$$\dot{u}_{1.2} - \alpha C_{1.2} u_{1.2} / r^2 = \varkappa^2 u_{1.2}. \tag{13}$$

The solutions of (13) which vanish when $r \to \infty$ can be written as follows [3]:

$$u_1 = A\,\{J_{iq}(i\varkappa r) - e^{-\pi q} J_{-iq}(i\varkappa r)\}; \quad q = \sqrt{(\alpha^2 + 1)^{1/2} - {}^5/_4}, \tag{14a}$$

$$u_2 = B\,\{e^{i\pi p} J_{-p}(i\varkappa r) - J_p(i\varkappa r)\}; \quad p = \sqrt{(\alpha^2 + 1)^{1/2} + {}^5/_4}. \tag{14b}$$

We assume that inside the nucleus the interaction can be described by a potential well of depth V. The solutions of the corresponding equations for the region within the nucleus will be

$$u = A_1 \sin kr, \quad w = B_1\,[\sin kr / kr - \cos kr], \quad k^2 = 2m(V - |E|) \tag{15}$$

The solutions (14) and (15) must be joined smoothly at the nuclear edge R. We shall consider the levels for which $\kappa R \ll 1$, because only for these levels is the Λ-particle outside the nucleus with the energy level determined mainly by Coulomb forces. As we are interested in heavy nuclei we can assume $kR \gg 1$. By utilizing these two conditions and connecting the Solutions (14) and (15) at $r = R$, we arrive at the following equation to determine the eigenvalues of κ: *

$$\begin{gathered} kR = -\frac{1}{2} \frac{\alpha^2}{\sqrt{1+\alpha^2}\,(1+\sqrt{1+\alpha^2})} \left\{ \left[\operatorname{ctg} kR - \frac{(1+\sqrt{1+\alpha^2})^2}{\alpha^2} \operatorname{tg} kR \right] \times \right. \\ \left. \times \left[\frac{1}{2} + q \operatorname{ctg}\left(q \ln \frac{\varkappa R}{2} - \psi \right) \right] - \left(\frac{1}{2} - p \right) \left(- \frac{(1+\sqrt{1+\alpha^2})^2}{\alpha^2} \operatorname{ctg} kR + \operatorname{tg} kR \right) \right\}; \\ \psi = \frac{1}{2i} \ln \frac{\Gamma(iq+1)}{\Gamma(-iq+1)}. \end{gathered} \tag{16}$$

The left-hand side of (16) contains the large quantity kR. This makes it necessary that the quantity $\cot\left(q \ln \frac{\kappa R}{2} - \psi\right)$ in the right-hand side also be large. Hence we obtain for the energy of the n-th level

$$E_n = \frac{2}{mR^2} \exp\left\{ -2 \frac{n\pi - \psi}{\sqrt{(\alpha^2+1)^{1/2} - {}^5/_4}} \right\}. \tag{17}$$

It follows from (17) that bound states exist for $(\alpha^2 + 1)^{1/2} > {}^5/_4$, that is, for $Ze^2r_0m > {}^3/_4$. Equation (17) is valid for $n \geq 1$. If we assume $r_0 \sim 1/\mu_\pi$ then for a heavy nucleus ($Z \sim 80$) the first energy level will be of the order of 50 to 100 kev. The total number of levels is easily computed. The last levels must correspond to motion of the Λ-particle at distances of the order of the Bohr atomic radius a, i. e., $\sqrt{2mE_n}\,a \sim 1$. Thus the total number of levels is determined by

---

* ['ctg' ≡ 'cot'; 'tg' ≡ 'tan' – editor's note.]

$$\frac{n\pi - \psi}{\sqrt{(\alpha^2 + 1)^{1/2} - 5/4}} \sim \ln \frac{a}{R} \tag{18}$$

which when $r_0 \sim 1/\mu_\pi$ gives the number 7 for heavy nuclei.

We note that the spread of the levels associated with nuclear absorption of Λ-particles for $(kR)^{-1} \ll 1$ is small because, as follows from (16), in this case it is unimporant whether k is real or complex.

LITERATURE CITED

[1] J. Orear, G. Harris, and S. Taylor, Phys. Rev. 102, 1676 (1956).

[2] T. D. Lee and C. N. Yang, Phys. Rev. 102, 290 (1956).

[3] M. Morse and H. Feshbach, Methods of Theoretical Physics II (1953) p. 1665.

Received December 24, 1956

SIGNIFICANCE OF ABBREVIATIONS MOST FREQUENTLY ENCOUNTERED IN SOVIET PHYSICS PERIODICALS

AN SSSR	*Academy of Sciences, USSR*
FIAN	*Physics Institute, Academy of Sciences USSR*
GITI	*State Scientific and Technical Press*
GITTL	*State Press for Technical and Theoretical Literature*
GOI	*State Optical Institute*
GONTI	*State United Scientific and Technical Press*
Gosenergoizdat	*State Power Press*
Gosfizkhimizdat	*State Physical Chemistry Press*
Gozkhimizdat	*State Chemistry Press*
GOST	*All-Union State Standard*
Goztekhizdat	*State Technical Press*
GTTI	*State Technical and Theoretical Press*
GUPIAE	*State Office for Utilization of Atomic Energy*
IF KhI	*Institute of Physical Chemistry Research*
IFP	*Institute of Physical Problems*
IL	*Foreign Literature Press*
IPF	*Institute of Applied Physics*
IPM	*Institute of Applied Mathematics*
IREA	*Institute of Chemical Reagents*
ISN (Izd. Sov. Nauk)	*Soviet Science Press*
I YaP	*Institute of Nuclear Studies*
Izd	*Press (publishing house)*
KISO	*Solar Research Commission*
LETI	*Leningrad Electrotechnical Institute*
LFTI	*Leningrad Institute of Physics and Technology*
LIM	*Leningrad Institute of Metals*
LITMiO	*Leningrad Institute of Precision Instruments and Optics*
Mashgiz	*State Scientific-Technical Press for Machine Construction Literature*
MATI	*Moscow Aviation Technology Institute*
MGU	*Moscow State University*
Metallurgizdat	*Metallurgy Press*
MOPI	*Moscow Regional Institute of Physics*
NIAFIZ	*Scientific Research Association for Physics*
NIFI	*Scientific Research Institute of Physics*
NIIMM	*Scientific Research Institute of Mathematics and Mechanics*
NII ZVUKSZAPIOI	*Scientific Research Institute of Sound Recording*
NIKFI	*Scientific Institute of Motion Picture Photography*
OIYaI	*Joint Institute of Nuclear Studies*
ONTI	*United Scientific and Technical Press*
OTI	*Division of Technical Information*
OTN	*Division of Technical Science*
RIAN	*Radium Institute, Academy of Sciences of the USSR*
SPB	*All-Union Special Planning Office*
Stroĭizdat	*Construction Press*
URALFTI	*Ural Institute of Physics and Technology*

NOTE: Abbreviations not on this list and not explained in the translation have been transliterated, no further information about their significance being available to us.—*Publisher.*

The expanded program of the American Institute of Physics comprises translation of four leading Soviet physics journals, as listed below. These translations, by competent, qualified scientists, provide all research laboratories and libraries with accurate and up-to-date information of the results of research in the U.S.S.R.

Soviet Physics — Technical Physics

A translation of the "Journal of Technical Physics" of the Academy of Sciences of the U.S.S.R. The translation began with the 1956 issues, and is being continued. Twelve issues per year, approximately 3,000 Russian pages. Annually $90.00 domestic, $95.00 foreign.

Soviet Physics — Acoustics

A translation of the "Journal of Acoustics" of the Academy of Sciences of the U.S.S.R. The translation began with the 1955 issues. Four issues per year, approximately 400 Russian pages. Annual price, beginning with the 1957 issues, $12.00 domestic, $14.00 foreign. Prices for each volume prior to 1957, $20.00 domestic, $22.00 foreign.

Soviet Physics — "Doklady"

A translation of the "Physics Section" of the Proceedings of the Academy of Sciences of the U.S.S.R. The translation began with the 1956 issues. Six issues per year, approximately 900 Russian pages. Annually $25.00 domestic, $27.50 foreign.

Soviet Physics — JETP

A translation of the "Journal of Experimental and Theoretical Physics" of the Academy of Sciences of the U.S.S.R. Translation began with the 1955 issues. Twelve issues per year, approximately 4,000 Russian pages. Annual price, beginning with the 1957 issues, $75.00 domestic, $79.00 foreign. Prices for back volumes may be obtained from the American Institute of Physics upon request.

Subscriptions should be addressed to the American Institute of Physics, 335 East 45th Street, New York 17, N. Y.